Inhibition of Ectopic Mineralization with Mineral-Binding Peptide

by

Samantha J. McGoldrick

A dissertation submitted in partial fulfillment
of the requirements for the degree of
Doctor of Philosophy
(Biomedical Engineering)
in the University of Michigan
2024

Doctoral Committee:

Professor David H. Kohn, Chair
Associate Professor Carlos A. Aguilar
Associate Professor Benjamin Levi, University of Texas Southwestern
Professor Yuji Mishina

Samantha J. McGoldrick

smcgoldr@umich.edu

ORCID iD: 0000-0002-2615-621X

© Samantha J. McGoldrick 2024

Dedication

To Pip (my inspiration) and Meeko (my emotional support)

Acknowledgements

Although my name is on the front page of this thesis, there are many other people I would like to thank and acknowledge for their support over the past seven years. I would like to start by thanking my advisor, David Kohn. Thank you for trusting me to do good science, reminding me to focus on the big picture, and showing me how to focus my effort on the process instead of the output.

I would also like to thank my committee members, Yuji Mishina, Ben Levi, and Carlos Aguilar, for your support and scientific guidance. In particular, thank you to Yuji Mishina for your steady hands throughout our in vivo study and for showing me that mice are not intimidating. Thank you to Yuji Mishina and Haichun Pan, Benjamin Levi and Shuli Li for your assistance and expertise throughout our collaborative efforts, big and small.

Thank you to the core personnel and research staff who have been some of my most important teachers and colleagues: Michelle Lynch (UMSOD Micro-CT Core), Rob Goulet (ORL), Henriette Remmer (UM Peptides and Proteomics Core), Bo Wen (UM Pharmacokinetic and Mass Spectrometry Core), Owen Neill (EMAL), and Dalis Collins (ULAM). For all her help from recruitment weekend to graduation, I want to thank Maria Steele from BME; and for all their help with keeping our lab running smoothly, I want to thank Erin Semmens, Cherokee Taylor, Amy Jackson, and Tao Jin from Dental.

I would not have made it this far without the wonderful people of the Kohn Lab, with whom I have been able to celebrate every triumph, mourn every failed experiment, and navigate

this unique version of the PhD journey. To Genny – thank you for providing such a wonderful example of the type of scientist I aspire to be. To Tom – thank you for your steady reassurance and mentorship as this dissertation work (and my confidence as a scientist) has grown. To Eric – thank you for reminding me that science is fun and exciting, even when the day-to-day experiments are not. To Morgan – thank you for being a constant friend and calmly confident pacesetter as we grew and came into our own as scientists together. To Merjem – thank you for being my sounding board, my confidant, my editor, my co-conspirator, my fellow worrywart, and most importantly, my friend. To Carlos – thank you for being a source of joy, energy, optimism, and creativity, especially in the most frustrating moments. To Ben – thank you for gently coaching me to be more confident and reminding me to separate my success from my data. Thank you to my previous students – Kayla, Amy, and Victoria – for being patient as I learned how to be a mentor and for helping me make progress on the passion projects I would have had to set aside otherwise.

My friends have been a vital source of support for me throughout this challenging degree. To my Ann Arbor friends –Ciara, Raha, Lauren, and Kritika – I am so grateful to have grown alongside such brilliant, supportive, and strong women throughout the entirety of this process. To my Rochester friends – Abby, Christina, Emily, and Jacqueline – I cherish our girl council zoom nights for all the moments of joy, laughter, comfort, and connection (which were so especially important early in the pandemic). To my North Reading friends – Zoe and Kiera – I was able to share big parts of this journey with you and I am so grateful to have had two people who truly understood this experience.

Finally, I want to extend a massive thank you to my family for their love and support (and countless trips to Ann Arbor). To my parents Alycia and Michael, thank you for supporting

me in every possible sense for all these years, even as my educational pursuits have taken me farther from home. To my sister Leah, thank you for being with me and for me as we explore what it means to be adults – from navigating life's difficult moments to becoming great cat moms. To my aunt Teresa, thank you for showing me how to appreciate the fun parts of life while pursuing my research ambitions. To my partner (and good luck charm) Mike, thank you for standing beside me throughout the final stages of this journey, providing the gentle support and steady encouragement I so needed.

Table of Contents

Dedication ii

Acknowledgements iii

List of Figures xii

List of Tables xiv

Abstract xv

Chapter 1 Introduction 1

1.1 Background 1

1.1.1 Bone mineralization 1

1.1.2 Ectopic mineralization 2

1.1.3 Therapeutics in development for diseases involving EM 3

1.1.4 Mineral-binding peptide for inhibiting EM formation 4

1.2 Hypothesis and Specific Aims 6

1.2.1 Global Hypothesis 6

1.2.2 Specific Aims 6

1.3 Organization of Dissertation 8

1.4 References 10

Chapter 2 Phage Display to Augment Biomaterial Function 14

2.1 Introduction 14

2.1.1 Phage Display 15

2.1.2 In Vivo Phage Display 17

2.1.3 Processing Phage Display Data 18

2.1.4 Limitations and Improvements to Phage Display Technology 22
2.2 Phage Display and Biomaterials 24
2.2.1 Functional Molecules 25
2.3 Targeting Molecules 29
2.3.1 Locate Specific Cells or Tissue Types 29
2.3.2 Material Specific Binding 32
2.4 Phage Display for Dual-Functioning Peptides 34
2.5 Conclusions 36
2.6 Acknowledgements 36
2.7 Figures 38
2.8 References 45
Chapter 3 Mineral-Binding Peptide Inhibits Ectopic Mineralization due to BMP Stimulation 51
3.1 Introduction 51
3.2 Methods 52
3.2.1 Peptide synthesis 52
3.2.2 Cell culture and in vitro osteogenic differentiation 53
3.2.3 Staining for calcium and calcium phosphate deposition 54
3.2.4 Alkaline phosphatase activity 54
3.2.5 Protein quantification 54
3.2.6 Peptide stability testing 56
3.2.7 Animal care and subcutaneous implant surgeries 56
3.2.8 Micro-CT analysis 57
3.2.9 EM grading scheme 57
3.2.10 PLGA thin films 58
3.2.11 Modified simulated body fluid (mSBF, 1x) 58

3.2.12 Mineralizing thin films 59

3.2.13 Scanning electron microscopy (SEM) 59

3.2.14 Statistical analysis 59

3.3 Results 59

3.3.1 pVTK inhibits BMP-stimulated mineralization in vitro 59

3.3.2 pVTK affects BMP-stimulated osteogenic signaling differently at different stages of differentiation 60

3.3.3 pVTK inhibits ectopic mineral formation in vivo 61

3.3.4 pVTK disrupts spontaneous acellular mineralization 62

3.4 Discussion 62

3.4.1 pVTK inhibits BMP-stimulated mineralization in vitro 63

3.4.2 pVTK affects BMP-stimulated osteogenic activity differently at different stages of differentiation 64

3.4.3 pVTK inhibits ectopic mineralization in vivo 65

3.4.4 pVTK inhibits spontaneous, acellular mineralization 67

3.4.5 Limitations 68

3.5 Conclusion 69

3.6 Acknowledgements 70

3.7 Figures 71

3.8 References 78

Chapter 4 Mineral-Binding peptide Reduces Ectopic Mineralization in Conditional Alk2^{Q207D} Model of Heterotopic Ossification 81

4.1 Introduction 81

4.2 Methods 83

4.2.1 Animal model and care 83

4.2.2 HO induction 83

4.2.3 Peptide synthesis 84
4.2.4 Primary calvarial cell isolation 84
4.2.5 Cell culture 85
4.2.6 Staining 85
4.2.7 Calcium quantification 86
4.2.8 Alkaline phosphatase activity 86
4.2.9 Peptide administration in vivo 86
4.2.10 Micro-CT analysis 87
4.2.11 EM grading scheme 88
4.2.12 Histology 88
4.2.13 Statistical analysis 89
4.3 Results 89
4.3.1 pVTK reduced osteogenic activity and mineralization in vitro 89
4.3.2 pVTK reduced amount and severity of ectopic mineralization in vivo 89
4.3.3 pVTK fragmented ectopic mineral formation without altering density 90
4.4 Discussion 91
4.4.1 pVTK reduced osteogenic activity in vitro 91
4.4.2 pVTK reduced amount and severity of ectopic mineralization in vivo 92
4.4.3 pVTK fragmented ectopic mineral formation without altering density 94
4.4.4 Limitations and Future Directions 97
4.5 Conclusion 98
4.6 Acknowledgements 99
4.7 Figures 100
4.8 References 109
Chapter 5 Development of Drug Delivery Systems for Controlled Release of pVTK 112

5.1 Introduction 112
5.1.1 Drug delivery considerations for BMP therapies 112
5.1.2 Drug delivery considerations for HO/FOP 113
5.2 Methods 114
5.2.1 Peptide synthesis and fluorescent tagging 114
5.2.2 Hydrogel fabrication and model protein encapsulation 114
5.2.3 Particle synthesis 115
5.2.4 Scanning electron microscopy (SEM) 116
5.2.5 Encapsulation efficiency 116
5.2.6 Protein release quantification 117
5.2.7 Cell culture 117
5.2.8 Staining of deposited calcium/calcium phosphate and cell nuclei 118
5.2.9 Alizarin Red staining quantification 118
5.2.10 Staining of cell nuclei 118
5.2.11 Fluorescent imaging 119
5.2.12 Statistical analysis 119
5.3 Results 119
5.3.1 Injectable hydrogel for pVTK delivery to inhibit EM formation as an off-target effect of BMP therapies 119
5.3.2 Polymer particles for pVTK delivery to mitigate EM formation in HO/FOP 120
5.4 Discussion 121
5.4.1 Injectable hydrogel for pVTK delivery to inhibit EM formation as an off-target effect of BMP therapies 122
5.4.2 Polymer particles for pVTK delivery to mitigate EM formation in HO/FOP 123
5.4.3 Limitations 125
5.5 Conclusion 125

5.6 Acknowledgements 126
5.7 Figures and Tables 127
5.8 References 135
Chapter 6 Summary and Future Work 136
6.1 Summary of Dissertation 136
6.1.1 pVTK for inhibition of ectopic mineral (EM) formation 136
6.1.2 Mechanism of pVTK action 138
6.2 Future Directions 139
6.2.1 Drug delivery for prevention of EM formation 140
6.2.2 Mechanisms of pVTK function 141
6.2.3 Pharmacokinetics 144
6.2.4 Targeted drug delivery 144
6.2.5 Tissue engineering strategies 145
6.2.6 Broader Impacts 146
6.3 Concluding Remarks 148
6.4 References 149
6.5 Appendix A: Peptide Internalization Imaging 152
6.5.1 Methods 152
6.5.2 Figure 154
6.5.3 References 155
6.6 Appendix B: Mineralization Inhibition with Phosphorylated Peptide Variants 156
6.6.1 Methods 156
6.6.2 Figures 158

List of Figures

Figure 2.1 Schematic of panning stage of phage display 38

Figure 2.2 Endoscopy images demonstrating colon-targeting fluorescently labeled peptide 39

Figure 2.3 Schematic of the phage display process 40

Figure 2.4 Relationship of number of sequences with cost and time of phage sequencing 41

Figure 2.5 Fluorescent images of *S. aureus*-targeted peptide in lung tissue 42

Figure 2.6 Schematic of dual-functioning peptide 43

Figure 2.7 Dual-functional peptide for increasing cell adhesion to apatite substrates 44

Figure 3.1 pVTK inhibits BMP-stimulated mineralization in vitro 71

Figure 3.2 pVTK affects BMP-stimulated osteogenic activity differently throughout differentiation 72

Figure 3.3 pVTK significantly reduces ectopic mineral formation in vivo 73

Figure 3.4 pVTK treatment reduces severity of EM formation in subcutaneous implant 74

Figure 3.5 pVTK inhibits mineralization outside of cellular machinery 75

Figure 3.6S Development of EM grading scheme 76

Figure 3.7S Metabolic stability of pVTK in liver microsomes 77

Figure 4.1 Schematic for morphological analysis of ectopic mineral 100

Figure 4.2 pVTK reduces osteogenic activity and mineralization in primary calvarial cells in vitro 101

Figure 4.3 pVTK reduces in vivo EM formation in conditional Alk2^{Q207D} model 102

Figure 4.4 pVTK treatment reduces ectopic mineral severity but not tissue reorganization 103

Figure 4.5 pVTK treatment resulted in fragmentation of EM 104

Figure 4.6 pVTK treatment reduced size of EM network without altering overall connectivity 105

Figure 4.7S Compared distributions of human and caAlk2 mouse samples within EM grading schemes 106

Figure 4.8S Verification of in vitro induction of $Alk2^{Q207D}$ gene expression and maintenance through culture period 107

Figure 4.9S Visualization of mineralization patterns in caAlk2- and caAlk2+ cells 108

Figure 5.1 Effect of composition on hydrogel structure and protein release 130

Figure 5.2 Incorporation of FITC-pVTK into hydrogel compositions 3 and 4 for in vitro assessment 131

Figure 5.3 Effect of fabrication parameters on particle size and model protein release 132

Figure 5.4 Peptide release from PLGA particles 133

Figure 5.5 Effect of PLGA particles containing pVTK on MC3T3s undergoing osteogenic differentiation 134

Figure 6.1 Immunofluorescence images of Rab-5 labelled vesicles and FITC-tagged peptides 154

Figure 6.2 Alizarin Red staining of MC3T3s mineralized with different peptide variants 158

Figure 6.3 Quantification of Alizarin Red staining of MC3T3s mineralized with different peptide variants 159

List of Tables

Table 5.1 Engineering considerations for delivery of pVTK for prevention of EM due to BMP therapies 127

Table 5.2 Engineering considerations for delivery of pVTK for EM prevention in HO/FOP... 128

Table 5.3 Hydrogel composition descriptions..... 129

Abstract

Ectopic mineralization describes the formation of unwanted and non-physiological mineralization that primarily affects soft tissues and results in pain and dysfunction. Though ectopic mineralization is often one component of a larger disease state (e.g. coronary arterial calcification, kidney stones, calcific tendinitis, heterotopic ossification), intensifying ectopic mineralization is associated with worsening patient outcomes. However, the etiologies of most of these disease states are not fully known, complicating the search for disease-specific therapeutic approaches. Therefore, directly targeting and mitigating ectopic mineralization itself is proposed as an additional therapeutic strategy with broad potential application.

The work presented in this thesis investigates a phage display-derived mineral-binding peptide (pVTK, VTKHLNQI(p)SQ(p)SY, where p denotes phosphorylation of the serine residues) for the inhibition of ectopic mineralization. It was hypothesized that pVTK could inhibit ectopic mineralization regardless of disease state and that pVTK physically restricts mineral formation and growth to achieve inhibition. These hypotheses were tested in two disease states involving ectopic mineralization, one involving the off-target effects of an exogenous osteogenic promoter and the other involving downstream effects of a genetically modified osteogenic signaling pathway.

BMP2 (bone morphogenetic protein 2) is a major regulator of osteogenic differentiation and is FDA-approved for augmentation of bone regeneration in specific surgical applications. However, due to implant mishandling and off-label usage, there are major side effects, including

ectopic mineralization. In this thesis, pVTK was shown to inhibit BMP2-stimulated mineralization in vitro and in vivo. In culture, pVTK did not disrupt osteoblast recognition of exogenous BMP2, nor did pVTK compete with BMP2 for control over osteogenic differentiation. Since BMP2 therapies are designed to aid bone regeneration, it was important to demonstrate that pVTK would not decrease BMP2 efficiency by interfering with BMP2 signaling. In vivo, pVTK reduced ectopic mineral formation by 92%. Further, pVTK disrupted spontaneous mineral deposition in the absence of cells, demonstrating that pVTK does not rely on cell-mediated mineralization mechanisms for inhibition. Since pVTK's inhibition is not reliant on a specific cellular pathway, pVTK would not be considered disease-specific, and therefore broadly applicable for inhibiting ectopic mineralization.

Ectopic mineralization is the hallmark of heterotopic ossification (HO), a disease state involving endochondral ossification of soft tissue, and fibrodysplasia ossificans progressiva (FOP), a genetic disorder in which regulation of the osteogenic BMP pathway is impaired. In this thesis, pVTK was shown to reduce ectopic mineralization by 61% in an animal model of HO that utilizes an activatable genetic mutation inspired by FOP. pVTK treatment also resulted in more fragmented ectopic mineral with no change in overall density, supporting the hypothesis that pVTK acts directly on mineral assembly and formation to achieve inhibition. New micro computed tomography methods for assessing the morphology of ectopic mineral deposits were introduced, demonstrating alternative qualitative methods for evaluating amorphous 3D structures.

Altogether, this work demonstrated the potential for pVTK as a broadly applied therapeutic for ectopic mineralization. In addition, controlled release delivery systems were piloted for improving pVTK delivery in each disease state: an injectable collagen-alginate

hydrogel for delivery alongside BMP2-loaded implants and PLGA (poly-co-lactic-glycolic acid) particles for minimizing intramuscular injections in HO/FOP. Further, based on pVTK's high affinity for mineralized substrates and pVTK's unique ability to inhibit mineralization, pVTK could be applied to mineral-targeted drug delivery and musculoskeletal tissue engineering strategies.

Chapter 1 Introduction

1.1 Background

1.1.1 Bone mineralization

Bone is comprised of mineral (main inorganic component, 60% by weight), collagen (main organic component, 30% by weight), and water[1]. The type I collagen fibrils are highly organized, as in other load-bearing tissues, but the mineral component (in the form of carbonated hydroxyapatite) helps make bone uniquely strong[2].

Mineralization in bone occurs at all stages, from formation to repair to maintenance, yet the initiation of mineral deposition is not fully understood[3]. There is consensus that once there is a high enough concentration of ions in a defined space, they come together to form a nucleation point from which mineral crystal growth and organization proceeds spontaneously[4]. But it is not fully understood how the concentration of ions is controlled to establish a nucleation point. The main theories involve matrix-mediated mineralization and cell-mediated mineralization[3,5]. In matrix-mediated mineralization, it is thought that type I collagen itself may act as a nucleation point for mineralization with the aid of other extracellular matrix proteins[3]. In cell-mediated mineralization, it is thought that cells create matrix vesicles to concentrate ions and form crystals[3]. Once the crystals are large enough, matrix vesicle membranes are ruptured, and mineral crystals are deposited into the extracellular matrix. Additionally, there are many extracellular proteins that are known to regulate concentrations of ions, such as calcium and inorganic phosphate, to regulate calcification (deposition of calcium) or mineralization

(deposition of minerals like hydroxyapatite) in all tissue types, not just in bone[6]. These theories of mineralization/crystallization are not mutually exclusive, highlighting the fact that mineralization is a complex and dynamic process.

1.1.2 Ectopic mineralization

Ectopic mineral (EM) formation describes unwanted mineralization occurring in a non-physiological manner with regards to location, amount, and/or composition. Most commonly, EM forms in soft tissues (e.g. coronary artery calcification[7], kidney stones[8]) but EM also forms in tissues where some level of physiological mineralization is expected (e.g. osteoarthritis[9] and tendon/ligament calcification[10]). Many instances of EM are associated with an injury and inappropriate repair process, but EM formation also increases with age[11].

There is no one explanation for how or why ectopic mineralization occurs, as there is no singular explanation for how physiological mineralization occurs. Inflammation has been implicated in many cases of EM formation because signaling from recruited immune cells has been associated with a trans-differentiation of local stem-like cell populations into osteoblastic phenotypes, either resulting in or reacting to EM[12,13]. Further, immune cells have been shown to secrete matrix vesicles primed for calcification[14]. EM formation has also been attributed to imbalances of mineralization promoters and inhibitors due to genetic mutations[15]. Though specific genetic mutations have been characterized in animal studies and limited human studies, the actual disease mechanisms may not be fully characterized.

Though the mechanism of EM formation in various disease states is still not fully understood, EM formation has been directly linked with poorer patient outcomes. For example, in a 10-year follow-up study, increasing coronary arterial calcification scores were associated with increasing risks of mortality and future adverse cardiovascular events[7]. In a study of EM in

Werner syndrome, a genetic disorder that causes premature aging phenotypes (e.g. hair loss, cataracts, soft tissue atrophy and calcification), patients only complained of pain and ulcers in joints with calcification, not in unaffected joints[16]. Additionally, in an animal model, tendon mineralization due to injury progressed with time and resulted in deteriorating mechanical properties[17]. These examples demonstrate that unaddressed EM is a major contributor to the clinical burden of many disease states, as mineralization/calcification of soft tissues leads to impaired tissue function, pain, and life-threatening complications.

Current therapeutic approaches to manage diseases involving EM formation range widely from symptom management (e.g. non-steroidal anti-inflammatory drugs (NSAIDS) to regulate inflammation[18]) to modifying cell behavior (e.g. antibodies to block aberrant signaling[19]). Combinations of strategies are vital to curtail EM progression while also addressing the root cause of EM formation, if known. Managing EM formation itself may prevent the disease state from reaching severe levels at which soft tissue function is impaired. Furthermore, slowing or reducing EM progression buys clinicians time to evaluate disease-specific treatment options for each patient.

1.1.3 Therapeutics in development for diseases involving EM

For cases where the etiology of EM formation is understood, therapeutics can be developed to directly target the mechanism of action. For example, fibrodysplasia ossificans progressiva (FOP) is a rare genetic disorder involving the dysregulation of bone morphogenetic protein (BMP) signaling, leading to unregulated osteogenic signaling that causes EM formation in connective tissues with a median onset age of 5 years old[20]. Recently approved by the FDA for treatment of FOP, palovarotene reduces EM formation by inhibiting signal transduction downstream of leaky BMP channels[21]. However, since BMP signaling is required in

embryogenesis and throughout development, there are limitations for administering palovarotene to young patients who have not yet reached skeletal maturity (on average 25 years old)[21].

For cases where EM management is reactive rather than preventative, mineralization-targeting molecules and mineralization inhibitors are being investigated. For example, traumatic heterotopic ossification (HO) is an EM disease state where EM formation occurs in soft tissues subjected to major injuries or burns. In traumatic HO, EM formation occurs in 10-64% of patients, depending on the type and severity of the injury[22]. Since there is a lack of predictive factors for traumatic HO, a proposed therapeutic strategy was to use bisphosphonates to inhibit calcification since bisphosphonates are non-hydrolyzable analogs of pyrophosphate (a known regulator of calcification and mineralization)[23,24]. However, studies did not recommend bisphosphonates over NSAIDs for EM reduction, due to mixed results, high cost, and detrimental effects of bisphosphonates on physiological mineralization (e.g. osteonecrosis of the jaw)[25–27].

Currently, strategies for treating and managing EM are largely disease specific. Alternatively, therapeutic strategies could be aimed to focus the better-defined processes of EM formation such as nucleation and crystal growth. For example, patients on dialysis with coronary arterial calcification were successfully treated with the small molecule inhibitor SNF472 (phase II clinical trial)[28]. While SNF472 did inhibit calcification in vascular smooth muscle cells, likely by chelating free calcium ions, it had no effect on osteoblast mineralization[29]. This demonstrated that targeting the calcification itself was a valid strategy, but molecules may have to be tailored to the type of EM expected.

1.1.4 Mineral-binding peptide for inhibiting EM formation

Peptides bridge the gap between small molecule therapeutics and biologics (e.g. recombinant proteins or antibodies), balancing the need for bioactivity, high target specificity,

and biocompatibility with cost and customizability[30]. Currently, there are over 80 FDA-approved peptide therapeutics, 200 in clinical trials, and 600 in pre-clinical trials[31]. While peptides only make up about 5% of the overall drug market, peptide drug approvals are growing steadily, and revenue is expected to approach $80 billion by 2032[31]. In the 1980s, recombinant technology was adopted, allowing for efficient production of longer peptides. And in the 1990s, the advent of phage display technology allowed for massive libraries of peptides can be scanned for binding to specific targets for drug discovery. Since the introduction of these two technologies, the number of FDA-approved peptide therapeutics has doubled[30].

Phage display was used to identify the peptide VTK (VTKHLNQISQSY) with high affinity for hydroxyapatite and carbonated apatite, the synthetic versions of bone mineral[32]. Post-translational modification of the serine residues of VTK (pVTK, VTKHLNQIpSQpSY)[33] led to 2-fold higher adsorption to carbonated apatite and 10-fold higher adsorption to bone-like mineral (BLM), a biomimetic mineral substrate[33].

Though pVTK was initially identified for use in bone tissue engineering strategies, pVTK was also discovered to inhibit mineralization[34]. When added to osteogenic differentiation media, pVTK inhibited mineralization of MC3T3 cells, a pre-osteoblast cell line, whereas VTK did not[34]. In MC3T3s, mineralization begins to occur between days 9 and 12 of differentiation and it was necessary for pVTK to be present during days 7-12 (or during the entire culture) to achieve full inhibition[34]. Therefore, it is believed that pVTK inhibits mineralization by interacting directly with the mineralization rather than by altering osteogenic differentiation. This was supported by osteogenic gene expression of MC3T3s with and without pVTK during osteogenic differentiation. It was shown that mineralization promoter genes (*Runx2, BSP, TNAP*) were upregulated during later stages of osteogenic differentiation due to pVTK treatment while

mineralization inhibitor genes (*OPN, Ank, Enpp1*) were downregulated[34]. Additionally, another group showed that pVTK prevented the phase transition of calcium phosphate precipitates from amorphous to crystalline and pVTK reduced the number of nucleation clusters formed[35]. Though it is not understood how exactly pVTK inhibits mineralization, it is likely that pVTK is not reliant on typical cellular mineralization mechanisms to achieve inhibition.

1.2 Hypothesis and Specific Aims

There is a need for therapeutics to curtail EM formation in a variety of disease states. Since pVTK is known to inhibit physiological mineralization in an osteoblast cell line, the next step was to determine if pVTK can inhibit non-physiological mineralization in vitro and in vivo.

1.2.1 Global Hypothesis

pVTK can inhibit ectopic mineralization broadly because pVTK inhibits mineralization by interrupting the mineral growth.

1.2.2 Specific Aims

Aim 1. Evaluate pVTK as a therapeutic for EM formation due to exogenous osteogenic promoters

Bone morphogenetic protein 2 (BMP2) is vital for endochondral ossification and is FDA-approved for promoting bone regeneration in specific surgical applications[36]. To have an effect, BMP2 must be delivered at supraphysiological levels[37]. As a result, BMP2 therapies are known to result in off-target effects such as EM formation[37].

Hypothesis 1: Co-delivery of BMP2 with pVTK as a mineralization inhibitor would reduce EM formation without decreasing the therapeutic effect of BMP2 since pVTK acts directly on the mineral.

Sub-Aim 1.1: Assess the ability of pVTK to inhibit BMP-stimulated mineralization in osteoblasts

Using BMP2 to stimulate osteogenic activity of MC3T3s, pVTK will be administered to inhibit mineralization in vitro. Mineralization will be assessed via staining and ECM calcium quantification; osteogenic activity will be assessed via staining, protein activity assays, and Western blots. The concentration of pVTK to inhibit BMP-stimulated mineralization will be optimized as needed and an in vitro dose-response curve will be established.

Sub-Aim 1.2: Assess the ability of pVTK to reduce ectopic mineralization from a BMP-laden subcutaneous implant

After implanting collagen sponges with BMP2 subcutaneously in C5BL6/7 mice to induce ectopic mineralization, pVTK will be injected subcutaneously to inhibit mineralization in vivo. Mineralization will be assessed via micro-CT evaluation and histology.

Sub-Aim 1.3: Assess the ability of pVTK to inhibit acellular mineralization

Using simulated body fluid to spontaneously deposit mineral onto polymer thin films, pVTK will be administered to inhibit mineralization. Mineralization will be assessed via staining, free vs. deposited calcium and phosphate quantification, scanning electron microscopy, and Raman spectroscopy.

Aim 2. Evaluate pVTK as a therapeutic for EM formation due to genetic mutations

The conditional $Alk2^{Q207D}$ murine model combines a version of the genetic mutation in FOP with an inciting muscle injury to establish a clinically relevant model of HO with robust and reliable soft tissue mineralization[38]. Current HO management strategies are limited in cases with severe EM formation or cases requiring surgical excision which is preceded by a waiting period during which EM can progress[39].

Hypothesis 2: pVTK can reduce EM formation and EM severity in HO.

Sub-Aim 2.1: Assess the ability of pVTK to inhibit mineralization in primary conditional Alk2^{Q207D} cells

Using cells harvested from the conditional Alk2^{Q207D} murine model, pVTK will be administered to inhibit mineralization in vitro. Mineralization will be assessed via staining and ECM calcium quantification; mineralization activity will be assessed via protein activity assays. The concentration of pVTK to inhibit mineralization in mutant cells will be optimized as needed and an in vitro dose-response curve will be established.

Sub-Aim 2.2: Assess the ability of pVTK to reduce ectopic mineralization in the conditional Alk2^{Q207D} model

After inducing the mutation in the conditional Alk2^{Q207D} mice, pVTK will be injected intramuscularly to inhibit ectopic mineralization in vivo. Mineralization will be assessed via micro-CT evaluation and histology.

1.3 Organization of Dissertation

Chapter 1 provided background on physiological and pathological mineralization, setting the stage for the thesis work investigating the use of pVTK as a therapeutic for EM formation. In Chapter 2, the case for using peptides, especially dual-functional peptides, in tissue engineering and regenerative medicine is presented. In Chapter 3, pVTK is shown to inhibit EM formation associated with BMP2 therapy in vitro and in vivo. Additionally, experiments show that pVTK can inhibit mineralization without using cellular machinery, suggesting that pVTK can be applied broadly to prevent EM formation. Chapter 4 summarizes how pVTK reduced EM formation in a model of HO/FOP in which EM formation is much more robust and located within muscle tissue. In Chapter 5, considering the ultimate clinical application of pVTK, preliminary results from developmental projects for controlled drug delivery in each of the two

models of EM formation are presented. The final chapter of the thesis summarizes the presented work and introduces ideas for immediate continuation of this project and other ways in which pVTK can be leveraged for tissue engineering purposes.

1.4 References

1. Feng, X. Chemical and Biochemical Basis of Cell-Bone Matrix Interaction in Health and Disease. *Curr. Chem. Biol.* **2009**, *3* (2), 189–196. https://doi.org/10.2174/187231309788166398.

2. Murshed, M. Mechanism of Bone Mineralization. *Cold Spring Harb. Perspect. Med.* **2018**, *8* (12), 1–11. https://doi.org/10.1101/CSHPERSPECT.A031229.

3. Sharma, V.; Srinivasan, A.; Nikolajeff, F.; Kumar, S. Biomineralization Process in Hard Tissues: The Interaction Complexity within Protein and Inorganic Counterparts. *Acta Biomater.* **2021**, *120*, 20–37. https://doi.org/10.1016/j.actbio.2020.04.049.

4. Veis, A.; Dorvee, J. R. Biomineralization Mechanisms: A New Paradigm for Crystal Nucleation in Organic Matrices. *Calcif. Tissue Int.* **2013**, *93* (4), 307–315. https://doi.org/10.1007/s00223-012-9678-2.

5. Kirsch, T. Determinants of Pathological Mineralization. *Curr. Opin. Rheumatol.* **2006**, *18* (2), 174–180. https://doi.org/10.1097/01.bor.0000209431.59226.46.

6. Giachelli, C. M. Inducers and Inhibitors of Biomineralization: Lessons from Pathological Calcification. *Orthod. Craniofacial Res.* **2005**, *8* (4), 229–231. https://doi.org/10.1111/j.1601-6343.2005.00345.x.

7. Budoff, M. J.; Shaw, L. J.; Liu, S. T.; Weinstein, S. R.; Mosler, T. P.; Tseng, P. H.; Flores, F. R.; Callister, T. Q.; Raggi, P.; Berman, D. S. Long-Term Prognosis Associated With Coronary Calcification. Observations From a Registry of 25,253 Patients. *J. Am. Coll. Cardiol.* **2007**, *49* (18), 1860–1870. https://doi.org/10.1016/j.jacc.2006.10.079.

8. Wong, T. Y.; Wu, C. Y.; Martel, J.; Lin, C. W.; Hsu, F. Y.; Ojcius, D. M.; Lin, P. Y.; Young, J. D. Detection and Characterization of Mineralo-Organic Nanoparticles in Human Kidneys. *Sci. Rep.* **2015**, *5*, 1–13. https://doi.org/10.1038/srep15272.

9. Jarraya, M.; Guermazi, A.; Liew, J. W.; Tolstykh, I.; Lynch, J. A.; Aliabadi, P.; Felson, D. T.; Clancy, M.; Nevitt, M.; Lewis, C. E.; Torner, J.; Neogi, T. Prevalence of Intra-Articular Mineralization on Knee Computed Tomography: The Multicenter Osteoarthritis Study. *Osteoarthr. Cartil.* **2023**, *31* (8), 1111–1120. https://doi.org/10.1016/j.joca.2023.04.004.

10. Kraus, R.; Stahl, J. P.; Meyer, C.; Pavlidis, T.; Alt, V.; Horas, U.; Schnettler, R. Frequency and Effects of Intratendinous and Peritendinous Calcifications after Open Achilles Tendon Repair. *Foot Ankle Int.* **2004**, *25* (11), 827–832. https://doi.org/10.1177/107110070402501113.

11. Vilder, E. Y. De; Vanakker, O. M. From Variome to Phenome: Pathogenesis, Diagnosis and Management of Ectopic Mineralization Disorders. *World J. Clin. Cases* **2015**, *3* (7), 556. https://doi.org/10.12998/wjcc.v3.i7.556.

12. Cholok, D.; Chung, M. T.; Ranganathan, K.; Ucer, S.; Day, D.; Davis, T. A.; Mishina, Y.; Levi, B. Heterotopic Ossification and the Elucidation of Pathologic Differentiation. *Bone* **2018**, *109*, 12–21. https://doi.org/10.1016/j.bone.2017.09.019.

13. Kurozumi, A.; Nakano, K.; Yamagata, K.; Okada, Y.; Nakayamada, S.; Tanaka, Y. IL-6 and SIL-6R Induces STAT3-Dependent Differentiation of Human VSMCs into Osteoblast-like Cells through JMJD2B-Mediated Histone Demethylation of RUNX2. *Bone* **2019**, *124* (April), 53–61. https://doi.org/10.1016/j.bone.2019.04.006.

14. New, S. E. P.; Goettsch, C.; Aikawa, M.; Marchini, J. F.; Shibasaki, M.; Yabusaki, K.; Libby, P.; Shanahan, C. M.; Croce, K.; Aikawa, E. Macrophage-Derived Matrix Vesicles : An Alternative Novel Mechanism for Microcalcification in Atherosclerotic Plaques. *Circ. Res.* **2013**, *113* (1), 72–77. https://doi.org/10.1161/CIRCRESAHA.113.301036.

15. Li, Q.; van de Wetering, K.; Uitto, J. Pseudoxanthoma Elasticum as a Paradigm of Heritable Ectopic Mineralization Disorders: Pathomechanisms and Treatment Development. *Am. J. Pathol.* **2019**, *189* (2), 216–225. https://doi.org/10.1016/j.ajpath.2018.09.014.

16. Honjo, S.; Yokote, K.; Fujimoto, M.; Takemoto, M.; Kobayashi, K.; Maezawa, Y.; Shimoyama, T.; Satoh, S.; Koshizaka, M.; Takada, A.; Irisuna, H.; Saito, Y. Clinical Outcome and Mechanism of Soft Tissue Calcification in Werner Syndrome. *Rejuvenation Res.* **2008**, *11* (4), 809–819. https://doi.org/10.1089/rej.2007.0649.

17. Zhang, K.; Asai, S.; Hast, M. W.; Liu, M.; Usami, Y.; Iwamoto, M.; Soslowsky, L. J.; Enomoto-Iwamoto, M. Tendon Mineralization Is Progressive and Associated with Deterioration of Tendon Biomechanical Properties, and Requires BMP-Smad Signaling in the Mouse Achilles Tendon Injury Model. *Matrix Biol.* **2016**, *52–54*, 315–324. https://doi.org/10.1016/j.matbio.2016.01.015.

18. Joice, M.; Vasileiadis, G. I.; Amanatullah, D. F. Non-Steroidal Anti-Inflammatory Drugs for Heterotopic Ossification Prophylaxis after Total Hip Arthroplasty. *Bone Jt. J.* **2018**, *100B* (7), 915–922. https://doi.org/10.1302/0301-620X.100B7.BJJ-2017-1467.R1.

19. Di Rocco, M.; Forleo-Neto, E.; Pignolo, R. J.; Keen, R.; Orcel, P.; Funck-Brentano, T.; Roux, C.; Kolta, S.; Madeo, A.; Bubbear, J. S.; Tabarkiewicz, J.; Szczepanek, M.; Bachiller-Corral, J.; Cheung, A. M.; Dahir, K. M.; Botman, E.; Raijmakers, P. G.; Mukaddam, M. Al; Tile, L.; Portal-Celhay, C.; Sarkar, N.; Hou, P.; Musser, B. J.; Boyapati, A.; Mohammadi, K.; Mellis, S. J.; Rankin, A. J.; Economides, A. N.; Trotter, D. G.; Herman, G. A.; O'Meara, S. J.; DelGizzi, R.; Weinreich, D. M.; Yancopoulos, G. D.; Eekhoff, E. M. W.; Kaplan, F. S. Garetosmab in Fibrodysplasia Ossificans Progressiva: A Randomized, Double-Blind, Placebo-Controlled Phase 2 Trial. *Nat. Med.* **2023**, *29* (10), 2615–2624. https://doi.org/10.1038/s41591-023-02561-8.

20. Shore, E. M. Fibrodysplasia Ossificans Progressiva: A Human Genetic Disorder of Extraskeletal Bone Formation, or-How Does One Tissue Become Another? *Wiley Interdiscip. Rev. Dev. Biol.* **2012**, *1* (1), 153–165. https://doi.org/10.1002/wdev.9.

21. Pignolo, R. J.; Baujat, G.; Hsiao, E. C.; Keen, R.; Wilson, A.; Packman, J.; Strahs, A. L.; Grogan, D. R.; Kaplan, F. S. Palovarotene for Fibrodysplasia Ossificans Progressiva (FOP): Results of a Randomized, Placebo-Controlled, Double-Blind Phase 2 Trial. *J. Bone Miner. Res.* **2022**, *37* (10), 1891–1902. https://doi.org/10.1002/jbmr.4655.

22. Edwards, D. S.; Kuhn, K. M.; Potter, B. K.; Forsberg, J. A. Heterotopic Ossification: A Review of Current Understanding, Treatment, and Future. *J. Orthop. Trauma* **2016**, *30* (10), S27–S30. https://doi.org/10.1097/BOT.0000000000000666.

23. Fleisch, H.; Reszka, A.; Rodan, G.; Rogers, M. Bisphosphonates: Mechanisms of Action. *Princ. Bone Biol.* **2002**, 1361–XLIII. https://doi.org/10.1016/B978-012098652-1.50180-3.

24. Luo, H.; Li, Q.; Cao, Y.; Uitto, J. Therapeutics Development for Pseudoxanthoma Elasticum and Related Ectopic Mineralization Disorders: Update 2020. *J. Clin. Med.* **2021**, *10* (1), 1–16. https://doi.org/10.3390/jcm10010114.

25. Kennel, K. A.; Drake, M. T. Adverse Effects of Bisphosphonates: Implications for Osteoporosis Management. *Mayo Clin. Proc.* **2009**, *84* (7), 632–638. https://doi.org/10.4065/84.7.632.

26. Vasileiadis, G. I.; Sakellariou, V. I.; Kelekis, A.; Galanos, A.; Soucacos, P. N.; Papagelopoulos, P. J.; Babis, G. C. Prevention of Heterotopic Ossification in Cases of Hypertrophic Osteoarthritis Submitted to Total Hip Arthroplasty. Etidronate or Indomethacin? *J. Musculoskelet. Neuronal Interact.* **2010**, *10* (2), 159–165.

27. Haran, M. J.; Bhuta, T.; Lee, B. S. B. Pharmacological Interventions for Treating Acute Heterotopic Ossification. *Cochrane Database Syst. Rev.* **2010**, *2010* (5). https://doi.org/10.1002/14651858.cd003321.pub4.

28. Perelló, J.; Ferrer, M. D.; del Mar Pérez, M.; Kaesler, N.; Brandenburg, V. M.; Behets, G. J.; D'Haese, P. C.; Garg, R.; Isern, B.; Gold, A.; Wolf, M.; Salcedo, C. Mechanism of Action of SNF472, a Novel Calcification Inhibitor to Treat Vascular Calcification and Calciphylaxis. *Br. J. Pharmacol.* **2020**, *177* (19), 4400–4415. https://doi.org/10.1111/bph.15163.

29. Raggi, P.; Bellasi, A.; Bushinsky, D.; Bover, J.; Rodriguez, M.; Ketteler, M.; Sinha, S.; Salcedo, C.; Gillotti, K.; Padgett, C.; Garg, R.; Gold, A.; Perelló, J.; Chertow, G. M. Slowing Progression of Cardiovascular Calcification with SNF472 in Patients on Hemodialysis: Results of a Randomized Phase 2b Study. *Circulation* **2020**, *141* (9), 728–739. https://doi.org/10.1161/CIRCULATIONAHA.119.044195.

30. Muttenthaler, M.; King, G. F.; Adams, D. J.; Alewood, P. F. Trends in Peptide Drug Discovery. *Nat. Rev. Drug Discov.* **2021**, *20* (4), 309–325. https://doi.org/10.1038/s41573-020-00135-8.

31. Rossino, G.; Marchese, E.; Galli, G.; Verde, F.; Finizio, M.; Serra, M.; Linciano, P.; Collina, S. Peptides as Therapeutic Agents: Challenges and Opportunities in the Green Transition Era. *Molecules* **2023**, *28* (20). https://doi.org/10.3390/molecules28207165.

32. Segvich, S.; Biswas, S.; Becker, U.; Kohn, D. H. Identification of Peptides with Targeted Adhesion to Bone-Like Mineral via Phage Display and Computational Modeling. *Cells. Tissues. Organs* **2008**, *189* (1–4), 245. https://doi.org/10.1159/000151380.

33. Addison, W. N.; Miller, S. J.; Ramaswamy, J.; Mansouri, A.; Kohn, D. H.; McKee, M. D. Phosphorylation-Dependent Mineral-Type Specificity for Apatite-Binding Peptide Sequences. *Biomaterials* **2010**, *31* (36), 9422–9430. https://doi.org/10.1016/j.biomaterials.2010.08.064.

34. Ramaswamy, J.; Nam, H. K.; Ramaraju, H.; Hatch, N. E.; Kohn, D. H. Inhibition of Osteoblast Mineralization by Phosphorylated Phage-Derived Apatite-Specific Peptide. *Biomaterials* **2015**, *73*, 120–130. https://doi.org/10.1016/j.biomaterials.2015.09.021.

35. Ling, C.; Zhao, W.; Wang, Z.; Chen, J.; Ustriyana, P.; Gao, M.; Sahai, N. Structure-Activity Relationships of Hydroxyapatite-Binding Peptides. *Langmuir* **2020**, *36* (10), 2729–2739. https://doi.org/10.1021/acs.langmuir.9b03779.

36. McKay, W. F.; Peckham, S. M.; Badura, J. M. A Comprehensive Clinical Review of Recombinant Human Bone Morphogenetic Protein-2 (INFUSE® Bone Graft). *Int. Orthop.* **2007**, *31* (6), 729–734. https://doi.org/10.1007/s00264-007-0418-6.

37. James, A. W.; LaChaud, G.; Shen, J.; Asatrian, G.; Nguyen, V.; Zhang, X.; Ting, K.; Soo, C. A Review of the Clinical Side Effects of Bone Morphogenetic Protein-2. *Tissue Eng. - Part B Rev.* **2016**, *22* (4), 284–297. https://doi.org/10.1089/ten.teb.2015.0357.

38. Pan, H.; Fleming, N.; Hong, C. C.; Mishina, Y.; Perrien, D. S. Methods for the Reliable Induction of Heterotopic Ossification in the Conditional Alk2Q207D Mouse. *J. Musculoskelet. Neuronal Interact.* **2019**, 1–11.

39. Hwang, C. D.; Pagani, C. A.; Nunez, J. H.; Cherief, M.; Qin, Q.; Gomez-Salazar, M.; Kadaikal, B.; Kang, H.; Chowdary, A. R.; Patel, N.; James, A. W.; Levi, B. Contemporary Perspectives on Heterotopic Ossification. *JCI Insight* **2022**, *7* (14), 1–20. https://doi.org/10.1172/jci.insight.158996.

Chapter 2 Phage Display to Augment Biomaterial Function[1]

2.1 Introduction

Phage display is a selection technique used to identify amino acid sequences based on their affinity for a given substrate. Due to the random nature of phage libraries, phage display identifies known, but also new, non-obvious sequences that could not have been identified via protein engineering strategies. In general, the peptide sequences identified via phage display can be divided into targeting peptides and functional peptides. Targeting peptides have high affinity for a specific substrate, cell, or protein. Functional peptides modulate cell or protein activity upon binding to that cell or protein. Targeting peptides, functional peptides, or a combination of the two, can be implemented in biomaterial design for functionalization of materials with a goal of increasing the ability of the material to instruct cells.

Biomaterials require intelligent design to manipulate interactions between the biomaterial and the surrounding microenvironment. Phage display aids in the discovery of peptides with high affinity and specificity for a target, which can be used to guide interactions between the biomaterial and its environment. Functional molecules can elicit specific cellular behaviors upon interaction with the designed biomaterial. Targeting molecules can improve homing of biomaterials to specific cell types or add biological cues to a material that cells are unable to recognize. Dual-functional peptides add even greater versatility to biomaterials. For example,

[1] Published as Davidson TA, McGoldrick SJ, Kohn DH. Phage Display to Augment Biomaterial Function. Int J Mol Sci. 2020 Aug 20;21(17):5994. doi: 10.3390/ijms21175994.

combining a functional molecule and targeting molecule within a biomaterial can elicit a desired behavior from a specific cell type or cell subpopulation. Alternatively, combining two targeting molecules within a biomaterial can bridge two materials or recruit a specific cell type to a given material.

This review aims to show the potential for the use of peptides identified via phage display in the biomaterial engineering. First, we outline the general phage display technique and discuss technological limitations along with future advancements. Then, we highlight targeting versus functional peptides identified via phage display and describe how each can be utilized for the functionalization of biomaterials. Lastly, we describe the concept of dual-functionalized peptides for a modular approach to biomaterial design. In all, the reader should come away with an understanding of how phage display identifies previously unknown peptides with targeting or functional capabilities that can be used to augment and customize biomaterials for a vast array of biomedical applications.

2.1.1 Phage Display

Bacteriophage are viruses utilized to both encode and display a library of amino acid sequences. The sequence is encoded within the bacteriophage DNA via a mutation insertion sequence and is ultimately displayed on the outer coat of the bacteriophage which provides simultaneous genotypic and phenotypic expression of the peptide.

Two of the most common phage are the M13 and T7 bacteriophage. Phage display was first developed using the M13 bacteriophage, and the M13 bacteriophage is well characterized and easily engineered to express a variety of peptides and proteins[1,2]. Most commonly, the filamentous M13 bacteriophage is used to display up to 5 copies of an encoded peptide sequence (6-45 amino acids) on its pIII minor coat protein[3,4]. The M13 phage are replicated in E. coli, but

the release of the phage from the bacteria requires cooperation with the host secretory pathways[3]. This requirement limits the peptides that are actually displayed on the M13 phage to those that work within the host secretory pathways, despite the theoretical peptide diversity of the phage library[5,6]. To bypass this limitation, the T7 bacteriophage was adapted for phage display[5,6]. T7 bacteriophage also replicate using E. coli, but phage release upon lysis of the host cells[5,6]. This allows for phage display of all potential peptides in a given library, rather than only those that can be secreted by host bacteria[5,6]. T7 bacteriophage display peptide sequences (40-50 amino acids) or proteins (900-1200 amino acids) on protein 10, with up to 415 copies of smaller peptides and one or fewer copies of large proteins[5].

Phage libraries are created by introducing a mutation insertion sequence into the bacteriophage genome. This establishes a large set of phage (10^9-10^{12}) that display different amino acid sequences based on the general design of the insertion sequence. Depending on the design of the insertion sequence, the expressed peptides can be linear or cyclic and can range in size and composition.

Typically, phage display with a random peptide library consists of multiple rounds of biopanning, in which a phage library is exposed to the substrate of interest and the highest affinity binders are recovered (Figure 2.1)[7]. Care must be taken to wash the substrate thoroughly in each panning step to ensure that non-bound or weakly bound phage are removed. Once bound phage are eluted off the substrate, they are used to infect bacteria for amplification of the phage. Colonies can be harvested, and phage can be isolated for another round of panning and/or for sequencing. After multiple rounds of panning, the highest affinity binders can be identified, characterized, and tested for their specificity to the desired substrate in order to identify the top candidates.

The general phage display technique can be used to identify both functional peptide sequences and targeting peptide sequences. Phage display is ideally suited for identifying targeting peptide sequences through repeated rounds of panning against a specific substrate to isolate the highest affinity binders. However, using functional measures in combination with binding affinity, one can utilize phage display to identify functional peptide sequences that elicit a change in cellular or protein behavior upon binding.

2.1.2 In Vivo Phage Display

While phage display is largely performed in vitro, in vivo phage display expands the potential applications for peptide discovery and biomaterial customization. In vivo phage display involves local or systemic injection of the phage library into an animal. Then, both target and control tissues are harvested so that bound phage can be eluted, amplified, and analyzed. In vivo phage display provides the combination of positive and negative selection since phage can be identified for their binding to the target tissue and lack of binding to the control tissue in the same animal. In vivo phage display relies on high specificity of target-bound phage and efficient amplification of phage.

The first demonstration of in vivo phage display for organ-selective targeting identified the peptide sequence CLSSRLDAC for its affinity to brain tissue[8]. Advancement in technology has allowed for the use of in vivo phage display for the identification of peptides with higher selectivity for a specific tissue type. For example, one group sought to increase selectivity for xenografts of human prostate cancer in mice by performing multiple rounds of negative selection prior to in vivo phage display for a prostate cancer tissue homing peptide[9]. In each of three rounds of negative selection in mice and one subsequent round of negative selection in a cynomolgus monkeys, the phage library was injected into the bloodstream and non-bound phage

were harvested and identified[9]. This step eliminated phage with known in vivo targets from the library, so that in vivo phage display could be used to identify highly selective prostate cancer tissue homing peptides[9].

In addition, in vivo phage display advances have provided means for identifying peptides with greater targeting capacity for pathological tissues, even without known targets. For instance, in vivo phage display identified the peptide QPIHPNNM for its affinity and selectivity for adenomas over normal colon tissue[10]. Endoscopic monitoring of morphological changes in adenomas is used to manage colorectal cancer progression, but it could be improved with QPIHIPNNM-based targeting and labeling of adenomas over the current standard of qualitative observations (Figure 2.2)[10]. In vivo peptide phage display identified CSPGAKVRC (nicknamed UNO) for its affinity to tumor-associated macrophages (TAMs)[11]. UNO interacts with TAMs through CD206 and UNO can target solid tumors of different cancer types, making UNO a viable candidate for targeting CD206+ tumors for diagnosis, imaging, or drug delivery[11]. In vivo phage display was also used to identify the peptide CAQK for its affinity to brain tissue affected by a penetrating brain injury that allowed phage to cross the blood-brain barrier (BBB)[12]. In cases where the BBB has been disrupted due to injury, CAQK could be used to guide imaging or therapeutic molecules to the injury site, bypassing invasive delivery measures[12]. In both of these examples, in vivo phage display was used to identify peptides that could target specific types of pathological tissue to improve diagnostic and therapeutic strategies.

2.1.3 Processing Phage Display Data

After multiple rounds of biopanning and amplification, the number of potential peptide sequences will be reduced from ~10^9 to 10^2-10^3. The remaining candidates must be further

analyzed to determine the top candidates based on binding strength and selectivity for the desired target (Figure 2.3).

When phage are selected after biopanning and enrichment, they are sequenced in order to identify the peptide sequences encoded in the identified phage. Typically, Sanger sequencing is used to characterize <100 peptide sequences from multiple rounds of biopanning in order to find consensus sequences[13]. However, next-generation sequencing (NGS) offers the ability to sequence larger portions of the peptide library (e.g. Illumina sequencing can read over 10^7 sequences)[13]. Increased sample sizes for sequencing can lead to identification of peptide sequences that may have been under-represented by traditional biopanning and Sanger sequencing, due to poor amplification[13,14]. NGS identifies longer sequences than traditional Sanger sequencing[15]. NGS can also identify peptides based on metrics other than binding affinity, giving researchers more flexibility in utilizing peptides for biomaterial augmentation[14]. For example, one group used in vivo landscape phage display library in combination with NGS to identify a number of 3-mer consensus sequences, or elementary binding units (EBUs) based on peptide avidity, rather than peptide affinity[16]. The EBU motifs were categorized as unique to a single tissue type, common to multiple, similar tissue-types, or common to all tissue types[16]. This information was then used to discover a subset of EBUs unique to a tumor microenvironment, allowing for the directed evolution of the landscape phage display library for the identification of a tumor-specific peptide sequence[16]. In all, NGS is valuable for analyzing large peptide libraries, reducing costs and time with increasing magnitudes of sequences[15].

Once the number of selected peptides has been narrowed down by sequencing and identification of consensus sequences, binding assays are employed to quantify the peptides' binding strength and selectivity for the desired target. A combination of competitive and non-

competitive binding assays can quantify the association and dissociation constants of the peptides relative to their intended targets[17]. The enzyme-linked immunosorbent assay (ELISA) is a common tool utilized for the quantification of binding affinities of peptides to known targets and can be easily customized for the desired targets[18–23].

In the cases of cell or tissue targets, human biopsies can be used to assess peptide binding to validate the sequences identified via panning against in vitro or animal models of in vivo targets. Due to the variable nature of human biopsies, it is important to verify that the binding affinities and selectivities of peptides identified via phage display can translate to ex vivo human tissue. For example, a microarray of human prostate cancer tissues was used to validate binding of the peptide PC204 discovered via phage display against a prostate cancer cell line[19]. It was found that 74% of the tumor specimens exhibited positive binding to PC204, demonstrating that PC204 could recognize the majority of clinical specimens even though the cellular recognition motif had yet to be identified[19]. Additionally, after identifying multiple cervical cancer-specific targeting peptides (CSPs) via in vivo phage display, a microarray of human cervical cancer tissues was used to confirm selectivity for cervical cancer tissue over normal cervical tissue[24]. In this example, two different CSPs were identified for their selectivity to different presentations of cervical cancer: CSP-GD was found selectively bind to adenocarcinoma (82% of cases showed positive binding) over squamous cell carcinoma (8%) and normal cervical tissue (6%), while CSP-KQ was found to selectively bind to squamous cell carcinoma (80% of cases showed positive binding) over adenocarcinoma (7%) and normal cervical tissue (1%)[24].

For phage display against cells or tissues, the localization of the phage may provide additional information on the target and/or function of the displayed peptide. Phage could be sorted as membrane-bound or internalized by recovering phage before and after cell lysis[25].

Alternatively, imaging fluorescently tagged peptides can demonstrate whether or not the peptide is internalized by the target cell[22,26]. qPhage was developed for quantifying internalization of phage with RT-PCR of cells after exposure to a phage library[15]. qPhage requires a shorter incubation time than immunostaining and is more sensitive for the detection of internalized phage[15]. Another approach to identifying peptides with intracellular targets or functions is to use internalizing phage, rather than relying on sorting peptides by their internalization activity. An internalizing phage library (iPhage) is generated by adding a cell-penetrating peptide (CPP) to the coat protein to allow for simultaneous expression of the CPP and peptide library[27]. Using iPhage expands the application of phage display to internal cellular targets, such as organelles and intracellular signaling pathways, which are difficult to target[27]. Designing biomaterial systems based on peptides identified via the iPhage system would still require incorporation of an internalization mechanism or CPP since the peptides themselves are not necessarily internalized[27]. Taken together, phage display can be used to identify peptides that are naturally internalized by cells or have distinct intracellular targets, both of which are key for expanding the identification of functional peptides for biomaterials.

Based on the desired biomaterial application of the peptides identified via phage display, a combination of processing techniques may be required to verify the peptide's binding affinity and selectivity for a given target. For material targets, post-processing focuses on quantifying a peptide's affinity for and demonstrating a peptide's selectivity for the material. For cell- and tissue-based targets, processing focuses on quantifying a peptide's affinity for a given target, demonstrating a peptide's selectivity for that target, and probing the interaction mechanism between peptide and target. Post-processing techniques aim to bring the pool of candidate peptides down from 100+ sequences to <10 sequences.

2.1.4 Limitations and Improvements to Phage Display Technology

Though analysis of candidate sequences operates on the assumption that libraries are random and unbiased, there are limitations that conflict with that assumption. Due to preference for certain amino acids and early termination due to stop codons, libraries do not contain all possible peptide sequences and do not necessarily contain equal numbers of the same peptide sequences[28,29]. In addition, due to over- or under-representation of certain sequences, the isolation of the true highest affinity binders can be compromised[28,29]. Therefore, care must be taken to either create a truly unbiased, random amino acid library or to recognize inherent limitations to phage display technology and subsequent analysis. For instance, one group used 'deep panning' to sequence a random peptide library (7mer sequence of NNK codon where N = any nucleotide and K = G or T) and found over-representation of the UAG amber stop codon and a bias for glutamine[28]. In a subsequent experiment, neither of these outcomes occurred when the bacteria used to synthesize the peptide library were altered to suppress the translation of UAG, and the oligonucleotide mixtures were calibrated via mass spectroscopy[29]. As next generation sequencing becomes more widely used, phage libraries should be screened to ensure true randomness and lack of bias.

Another technical limitation of phage display is the identification of false positives due to peptides being recovered after binding to non-targets. However, sequences that bind to components other than the targets can be collected. For example, SAROTUP (Scanner And Reporter Of Target-Unrelated Peptides) is searchable online database for peptides known to bind to unintended targets, such as plastic or streptavadin[30,31]. Additionally, a microfluidic phage selection (MiPS) system, where the labor-intensive steps of incubation, washing, cell lysis, and lysate collection are fully automated, reduces human error, identification of nonspecific binders

due to improper washing, and the need for large numbers of adherent cells[32]. With the MiPS system, smaller, well-characterized populations of cells or even biopsies can be effectively used for phage display, expanding the potential use of phage display into the area of personalized medicine[32].

Phage display can be compromised by the prevalence of parasitic clones, or phage more easily amplified in bacteria. Parasitic clones become over-represented in the phage population, resulting in bias toward identification of the parasitic clones over other, potentially stronger binders. To demonstrate the negative effects of parasitic clones, Illumina deep-sequencing technology was used to analyze a portion of a phage display library before and after amplification in bacteria[13]. There was a significant decrease in diversity after a single round of amplification in bacteria that could not be observed with smaller-scale Sanger sequencing[13]. Illumina NGS could then be used to identify parasitic clones from the commonly used PhD7 Library and it was shown that performing amplification in an emulsion could also reduce amplification bias[33].

A significant limitation of phage display is the lack of post-translational modifications within the expressed peptides on the phage surface. Incorporation of post-translational modifications during phage display post-processing increases the naturally limited diversity of peptides made from 20 amino acids. Glycosylation, cyclized peptides, and phosphorylation may all affect the potency or specificity of the peptide ligand. For example, phosphorylation of two serine residues of the peptide VTKHLNQISQSY (VTK) identified for binding to bone-like mineral, a carbonated apatite with similar composition to the inorganic phase of bone, showed a 10-fold increase in adsorption compared to the unphosphorylated control[34]. Inclusions of these

post-translational modifications into phage display libraries could lead to identification of ligands that would otherwise not exist in purely linear peptide libraries.

While the general philosophy of phage display has remained the same over time, advances in automation of labor-intensive steps and integration with big data have enhanced computational analysis. NGS provides more data on the interactions between the peptide library and the desired substrate, making the application of the phage display process more flexible and akin to big data[15]. With NGS, one could identify peptides that may not necessarily be the highest affinity binders, but may be more infective, better at amplification, or have higher avidity[14,16]. Additionally, NGS can help identify consensus sequences faster than traditional methods and can help identify longer sequences than generally identified by traditional Sanger sequencing[15]. For example, one group used NGS after each round of traditional biopanning with a commercial phage display library against KS483 cells during different stages of osteoblastic differentiation[35]. They demonstrated that a single round of selection combined with NGS sufficiently enriched the phage population, suggesting that performing the first round of selection in duplicate or triplicate and sequencing with NGS may be a preferable method for identifying high affinity peptides via phage display[35]. Though costly, NGS can reduce labor time and overall costs when used to identify large numbers of sequences (Figure 2.4)[15].

2.2 Phage Display and Biomaterials

Biomaterials are materials designed to interface or interact with cells, tissues, or organs. Often, biomaterials are designed to mimic nature in order to elicit a specific biological response. However, not all biomaterials are made of natural or naturally inspired materials. Thus, functionalization of the material needs to be included in the design to enable direct interaction between biomaterial and organism.

Phage display provides an opportunity to identify peptides for functionalization of biomaterials. In general, peptides are better than proteins for functionalization because they are smaller, cheaper and easier to synthesize, less likely to lose function during conjugation, and more resilient to changes in the microenvironment, such as a change in pH. Depending on the intended use of a biomaterial, the design process could involve phage display for identification of different types of peptides. Targeting peptides can be used to functionalize a biomaterial based on the peptide's affinity for a specific substrate or cell type. Functional peptides can be used to functionalize a biomaterial based on the peptide's ability to elicit a desired cellular response. A dual-functional peptide can be used to functionalize a biomaterial for joining substrates and/or cell types or for eliciting a desired function from a specific cell type.

2.2.1 Functional Molecules

Functional peptides modulate protein activity or cellular behavior when bound to a protein or cell. When conjugated to a biomaterial, these peptides give the biomaterial greater control over the microenvironment. The presence of functional peptides on a biomaterial can prompt migration of desired cell populations to the material surface or differentiate stem cells down a specific lineage to induce tissue-specific regeneration. On the other hand, cell function antagonists can prevent less desirable responses, such as pathological calcification.

2.2.1.1 Adhesion and Migration

Many biomaterials take inspiration from extracellular matrix (ECM) proteins in order to add cell recognition motifs to enhance interactions with cells they would not recognize or mount an immune response against. For example, RGD is derived from the active domain of fibronectin and is one of the most common peptide sequences for promotion of adhesion via integrins. However, phage display reveals new amino acid sequences that also interact with ECM proteins

responsible for adhesion and/or migration. For example, phage display was used to identify the peptide sequence DPIYALSWSGMA (DPI) that increases adhesion strength and spreading of human marrow stromal cells (MSCs)[36]. While the mechanism of interaction has not been fully characterized, DPI interacts with MSCs via integrins[37]. DPI has been used to functionalize a biomaterial surface leading to increased specificity of MSC attachment over fibroblasts and osteoblasts and increase the magnitude of cell adhesion strength[36]. Another group used phage display to identify the peptide E7 for its affinity to bone marrow derived MSCs[38]. Then, to recruit MSCs for regeneration of irregularly shaped cartilage defects, particles of E7 and demineralized bone matrix (DBM) were added to a chitosan hydrogel[39]. The DBM-E7/CS scaffold improved chondrogenic differentiation of MSCs in vitro and yielded promising cartilage-like structures in vivo[39]. This strategy uses phage display to identify peptides for surface engineering of biomaterials to enable the recruitment of a local MSC population in-vivo to aid in tissue regeneration by bypassing the use of exogenous cells.

2.2.1.2 Differentiation

For the use of biomaterials in tissue engineering, one strategy is to design a biomaterial to present cues to local cell populations to initiate differentiation. Phage display can identify peptide sequences that have an affinity for different stem cell populations, with the goal of targeting sub-populations with greater differentiation. This approach requires panning against a well-characterized cell population, identifying the most promising binders, and evaluating the effects of the most promising binders on differentiation. For example, following phage display against a neuronal stem cell population, membrane-bound or internalized peptide sequences were separately characterized for effects on differentiation[25]. Peptides that directly interacted with membrane-bound proteins or peptides that were internalized by neuronal stem cells (NSCs) were

deemed more likely to modulate differentiation. When used to functionalize scaffolds designed to mimic the native stiffness of brain tissue, the identified sequences enhanced NSC binding and differentiation into three mature neural phenotypes[25]. This outcome demonstrates the potential use for peptides in surface engineering of biomaterials to direct local stem cell populations toward specific cell lineages for tissue engineering and regeneration.

As mentioned previously, another approach to facilitating differentiation of local stem-cell population would use peptides identified via phage display to recruit a stem cell population. Simply, one could use the peptide to recruit a stem cell population to a biomaterial containing known differentiation cues. This has been demonstrated in a number of studies aimed at identifying peptides specific to marrow stromal cells, with the ultimate goal to functionalize bone-promoting biomaterials for the recruitment of MSCs[36–40]. Alternatively, one could explore if and how the interaction of that peptide with the stem cell population impacts differentiation. For example, the peptide DPI, identified for its specificity to MSCs, was conjugated to an apatite-specific peptide and anchored to a biomimetic apatite substrate[36]. When MSCs were cultured on this peptide-coated apatite substrate, markers of both early- and late-stage osteogenic differentiation were upregulated, as compared to uncoated apatite substrate[36]. This indicated that DPI may play a part in both recruitment and osteogenic differentiation of MSCs[36]. Using either approach, the identified peptides could then be displayed on a biomaterial to provide cues for differentiation to a specific population of undifferentiated or partially differentiated stem cells in an effort to regenerate local, impaired tissue.

2.2.1.3 Inhibition of Cell Function

Phage display can also identify peptide sequences that interfere with known targets and unwanted functions. This strategy requires knowledge of the mechanism of action governing the

unwanted function since specific cells or proteins must be targeted. Alternatively, this strategy can elucidate mechanisms of action based on interactions of identified peptide sequences and specific cells or proteins. One group compiled a list of peptides identified via phage display for their affinity to a range of known enzymes[17]. They found that 13 of the 17 peptides tested inhibited the respective enzyme's activity through binding to functional sites rather than binding to random locations on the enzyme's surface[17]. In this case, the investigators were able to use phage display to identify peptides with high affinities for enzymes, but they needed to verify inhibitory activity levels of the peptides[17].

Phage display can also be used to identify peptide sequences for their affinity to a specific structure, composition or orientation on a substrate, inhibiting transformation upon binding. For example, the peptide sequence VTKHLNQISQSY was identified via phage display for its affinity to bone-like mineral[34]. Upon post-translational phosphorylation of the serine residues, the phosphorylated variant, pVTK, inhibited mineralization of osteoblasts[34]. It has been hypothesized that pVTK binds to early mineral deposits and inhibits crystal growth[34]. Therefore, biomaterials can incorporate pVTK for treatment of ectopic mineralization, taking advantage of the functional nature of pVTK for both targeting unwanted mineral in soft tissues and inhibiting further mineralization.

Together, these two examples establish how phage display is used to identify peptides that modify protein or cell functions based on known targets or known conformations. These examples also illustrate how phage display can also identify peptides with unanticipated effects on cell functions. In either case, the peptides identified can be used to functionalize materials to either promote or inhibit cellular responses to implanted or injected biomaterials.

2.3 Targeting Molecules

Targeting peptides have specific affinity for a given material or cell type. When conjugated to a biomaterial, these peptides confer the same affinity to the biomaterial. Peptide engineering of biomaterials surfaces thus allows for intelligent biomaterial design to home to specific targets.

2.3.1 Locate Specific Cells or Tissue Types

Phage display is suited for identifying peptides with high affinity for specific groups of cells and cell receptors, proteins, and compositional elements of the tissue extracellular matrix. This strategy relies on isolation and characterization of a given cell type or tissue feature. Alternatively, characterization of the cell population or tissue can be done after high affinity peptides have been identified. For instance, in vivo phage display[41] identified cells within the vascular system having different 'zip codes', or sets of receptors[41]. This strategy separates cell populations based on peptides that target different zip codes, allowing for subsequent characterization of these distinct cell populations[41].

2.3.1.1 Imaging and Diagnosis

Conjugation of imaging molecules to peptides with high affinity for specific cells or tissue constituents is a simple, modifiable approach for improved imaging of pathologies. This strategy can be employed to target areas of the body that are traditionally difficult to target. For instance, ovarian cancer is difficult to detect at early stages because it generally does not present with symptoms, but early detection of ovarian cancer leads to higher survival rates[42]. Using phage display against human ovarian cancer cells identified the peptide sequence pJ18, which could guide radiolabels to ovarian cancer cells for detection via SPECT/CT imaging[42]. The vast

potential for phage display to identify pathological targets is particularly suited for conjugation with imaging molecules for more accurate imaging and diagnosis of almost any pathology.

Peptides with high affinity for specific proteins or cells characteristic of a disease state can be utilized in the design of diagnostics. Many diseases rely on RT-PCR or antibody immunoassays, which require expensive equipment and are not suitable for efficient clinical testing. Phage display technology can be leveraged to identify peptides that will bind to proteins characteristic of certain disease states. Then, those peptides can be utilized in the design of microfluidic devices or biosensors to diagnose diseases based on small samples of bodily fluid. An electrochemical biosensor was designed for the detection of norovirus by using phage display to identify a peptide sequence with affinity for a recombinant norovirus capsid protein[18]. Then, the identified peptide was conjugated to a gold electrode to enable detection of positive binding between peptide and norovirus protein via quartz crystal microbalance (QCM) or electrochemical impedance spectroscopy (EIS)[20]. This example demonstrates the use of phage display to identify peptides for improved diagnosis, e.g. by increasing speed of clinical, bedside testing through the use of high affinity peptides in microfluidic devices.

2.3.1.2 Targeted Drug Delivery

Phage display is also suited for identifying peptide sequences that can be added onto drug delivery systems for spatial and biochemical targeting. Peptides can be directly conjugated to the drug in cases where conjugation would not affect the drug's activity and protection of the drug is not required. For instance, poor prognosis is associated with prostate cancer when the cancer is resistant to castration and/or when it metastasizes, but, at this point, treatment often needs to be halted due to poor systemic effects of currently available drugs[9]. One group used in vivo phage display to discover a peptide, C-TGTPARQ-C (LN1), with high affinity and selectivity for

prostate cancer tissue[9]. They conjugated LN1 to the peptide D(KLAKLAK)$_2$, which is known to induce apoptosis, to form a targeted anti-prostate cancer cell therapeutic, LN1-KLA[9]. They demonstrated that LN1-KLA inhibited prostate cancer cell proliferation in vitro and inhibited tumor growth in vivo[9]. This example demonstrates how homing peptides discovered via phage display can be directly conjugated to drugs for targeted delivery to a desired cell or tissue type.

Peptides can also be added to different drug delivery systems, such as nanoparticles, liposomes, or micelles, to guide the system without directly interacting with the delivered drug. Accurate targeting by drug delivery systems is critical to improve efficiency of drug dosing and reduce off-target effects. For example, when combating antibiotic-resistant bacteria, such as S. aureus, one must rely on strong antibiotics that have negative side effects due to the necessity for systemic administration[43]. Therefore, it would be desirable to design a system to target the delivery of antibiotics to the S. aureus bacteria and protect healthy cells[43]. One group used phage display to identify the peptide CARG for its affinity to S. aureus bacteria and demonstrated its in vivo homing and binding ability to infected lung tissue (Figure 2.5)[43]. A CARG-coated porous silicon nanoparticle (pSiNP) drug delivery system was also designed for vancomycin[43]. CARG is capable of guiding the pSiNPs to in vivo sites infected by S. aureus[43]. Another application for peptides identified via phage display is targeted delivery of chemotherapy drugs. The peptide SP204 has been identified for its high affinity to a number of human prostate cancer cell lines, with verification against a microarray of human prostate cancer tissues[19]. SP204 conjugated to liposomal nanoparticles for targeted delivery of doxorubicin against human prostate cancer cell xenografts in vivo shows no significant changes in body weight with administration of the drug-containing SP204-conjugated liposomes, which indicated no significant off-target toxicity upon systemic delivery of the targeted nanoparticles[19]. These are both examples of how peptides

identified via phage display can be used for homing drug delivery systems to specific types of pathological tissue, regardless of a known tissue-specific target.

2.3.2 Material Specific Binding

Phage display is also useful for detecting peptides with affinity towards inorganic and organic synthetic substrates. This technique has been used to isolate peptide sequences with attraction towards titanium[44], silver[45], palladium[46], platinum[47], and carbon nanotubes[32,48]. More recently it has been used to find sequences with specific affinity for specific synthetic substrate chemistries.

2.3.2.1 Silicon

Silicon is a commonly used semiconductor material in both micro- and nanoelectronics. Attaching biomolecules such as peptides to act as molecular crosslinkers to silicon- based materials, can increase sensitivity in biosensing applications. Phage display identified two peptides with high affinity for porous silicon films, SPGLSLVSHMQT and LLADTTHHRPWT. When a biotin molecule was conjugated to SPGLSLVSHMQT the detection limit for streptavidin was decreased 21-fold[49].

2.3.2.2 Platinum and Palladium

Nanomaterial physical and chemical properties are regulated by its shape. Customizable, programmable crystal synthesis with predictable properties in nanomaterials can produce desired functions. Crystal growth is largely controlled by the surface energy of the facets where low-energy facets tend to persist and high-energy facets disappear resulting in the shape enclosure by low-energy facets. Biomolecules such as peptides can be chosen for their affinity to specific facets, leading to a desired shape. Two peptides (TLTTLTN and SSFPQPN) bind specific

platinum facets (Pt-{100} and Pt-{111} respectively) and shift crystal formation towards nanocube or nano-octahedrons respectively[47]. Likewise, two peptides (LSNNNLR and SPSTHWK) have affinity for Pd-{100}[46].

Peptides can be controlled with external stimuli such as pH, temperature, and light. pH changes can release peptides from a surface, allowing control of peptide density on the surface. When palladium nanocubes are capped with the LSNNNLR peptide at pH 7.5, the shape remained stable[46]; however when pH is lowered to 2.2, the peptide was released leading to a new surface-energy profile allowing previously protected Pd atoms to be released and form a concave structure on the Pd-{100} facets[46]. This pH-dependent control of surface composition indicates peptides might be used as a "smart-cap" for structural control of nanomaterials[46].

2.3.2.3 Apatite

Hydroxyapatite (HA) is a versatile biomaterial that accelerates osteointegration and is used as a bone defect filling material. HA can also be designed to have osteoinductive properties via attachment of biological factors such as growth factors. Standard processing conditions (sintering at >1000°C) cause biological factors to denature. Bone-like mineral (BLM), a biomimetic formation of carbonated apatite, provides an alternative to increase osteogenesis in vivo. Since BLM is formed under STP conditions, it is amenable to sequestering biological molecules[50]. The use of BLM in concert with exogenous factors can spatiotemporally regulate bone formation. Regarding surface engineering of HA and BLM, these chemistries cannot be readily modified to attach carboxyl, hydroxyl, or amine functional groups. Phage display identified several peptides with binding specificity to BLM such as VTK[51]. Since these peptides show preferential adsorption to apatite present in a variety of tissues, including bone, dentin, and enamel, they can be used for tissue engineering by attaching a second peptide such as a growth

factor to create a dual-functioning peptide to generate the desired effect as well as possibly in injury repair for tendon and ligament by creating a dual-functioning peptide adhesive with affinity for bone on one end and tendon/ligament on the other.

2.4 Phage Display for Dual-Functioning Peptides

A benefit of using peptides is the ease with which they can be combined. Many ECM proteins have multifunctional domains that work concurrently to allow cell adhesion as well as provide directions for other cell functions. Typically, bi-functional or dual-functioning peptides are equipped with one targeting peptide conjugated to another targeting peptide or a functional peptide. Fusion of two peptides to create a dual-functioning peptide can mimic the multifunctional domains of native proteins (Figure 2.6). Since load-bearing biomaterials are typically selected for their mechanical and chemical properties rather than biointeractive properties, dual functioning peptides provide a way to spatially control function of the adjacent cells or integration into the surrounding tissue as well as provide biological or chemical cues.

Often, implanted devices do not have the molecular structure to control the surrounding cells to generate ideal integration in vivo. Metal implants, including those used in orthopedic procedures such as hip replacements, or cardiovascular therapies such as stents, are chosen due to their mechanical strength and durability as well as their inertness. While materials like titanium are often favored for implants, a lack of integration with the surrounding tissue can lead to negative outcomes such as restenosis[52]. A titanium binding peptide identified via phage display and attached to the integrin binding peptide, RGD, increases cell retention to the titanium surface[44]. Such a modular design was also used to create a PEGylated peptide with four of the titanium binding peptides that prevents bacterial colonization and biofilm formation[53].

Polypyrole (PPy) is a conducting polymer with applications in drug delivery, nerve regeneration, and biosensors. Different dopants alter the conductivity or topography of PPy. One of these dopants is chlorine, to create PPyCl. T59 (THRTSTLDYFVI) binds to PPyCl and stabilizes in serum[54]. When combined with RGD, T59-RGD increases adhesion to PC12 cells (a rat pheochromacytoma cell line)[54]. PPyCL specific binding peptides attached to cell binding peptides can be applied to uses in drug delivery vehicles and neural probe coatings.

Similar experiments have been done on polystyrene for drug-eluting stents that prevent restenosis (poly(styrene-b-isobutylene-b- styrene)[55]. The dual-functioning peptide FFSFFFPASAWGSSGSSGK(biotin)CRRETAWAC binds to polystyrene as well as endothelial cells and reduces platelet binding to the surface[55]. Inclusion of the peptide RRETAWA allows for binding of the α5β1 integrin present in endothelial cells and lacking in platelets[55].

Cell adhesion is an important objective in modifying biomaterials for tissue engineering purposes. Increasing specificity of cell adhesion can increase the efficiency of cell-based therapies. When considering large tissue defects or clinically relevant applications of tissue engineering, promoting cell differentiation and the formation of functional ECM is important. The group responsible for identification of the VTK apatite binding peptide and the phosphorylated variants[51] also identified a peptide with affinity for human bone-marrow stromal cells, (DPIYALSWSGMA, DPI)[56]. These two peptides were combined to form DPI-VTK which exhibited greater binding affinity for apatite surfaces than VTK, pVTK, and VTK-RGD[56]. Additionally, DPI-VTK increased adhesion strength of hBMSCs and iPS derived MSCs with minimal adhesion of osteoblasts and fibroblasts compared to VTK-RGD[56]. Interestingly, the DPI domain was not only specific for MSCs, but also led to an increase in cell spreading, proliferation, and differentiation, all of which are necessary for tissue regeneration (Figure 2.7)[56].

2.5 Conclusions

Phage display derived peptides can be used in a wide array of applications from imaging to tissue engineering to drug targeting. Phage display takes advantage of nature's randomness to find a peptide that can provide a specific function without full understanding of the substrate structure. Phage display is used to identify peptides that: 1) target a particular cell type, 2) attach preferentially to an inorganic or organic synthetic material and 3) elicit a precise cellular response. While awaiting the results from the multitude of studies about COVID-19, it may be useful to find a peptide that can specifically target the outer shell of the virus or a peptide that can interfere with some portion of its viral behavior, or both. This review demonstrates the usefulness of phage display and suggests new opportunities to take advantage of more than one type of phage display derived peptides (i.e. peptides combining targeting-functional or targeting-targeting sequences) to engineer peptides with broader applications. As the number of targeting and functional peptides identified by phage display continues to grow, the number of studies focusing on dual-functioning peptides at the interface between biomaterials and tissue will continue to grow as well. By using dual functioning peptides, cell functions can be specifically and spatially controlled in a well-defined manner. The modular design of most dual-functioning peptides lends itself to switching out the targeting or functional peptide based on the specific requirements of the material or desired cell-type/function.

2.6 Acknowledgements

Author Contributions: Thomas Davidson contributed to conception, drafting, and editing of the manuscript. Samantha McGoldrick contributed to conception, drafting, and editing of the manuscript. David Kohn contributed to conception and critically editing of the manuscript. All authors have read and agreed to the published version of this manuscript.

Funding: NIH R01 DE026116

Conflicts of Interest: The authors declare no conflict of interest.

2.7 Figures

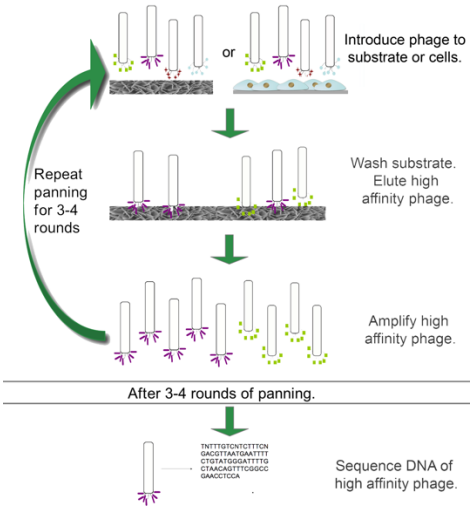


Figure 2.1 Schematic of panning stage of phage display

Phage are introduced to either a substrate or specific cell population followed by washing away nonadherent phage and eluting high affinity phage. High affinity phage are amplified and the process is repeated at least 3 times to reach a consensus sequence. (Used with permission from Springer)

	Adenomas	QPIHPNNM	GGGAGGGA
A	+++	+	-
B	+	+	-
C	+++	-	+
D	-	+	-

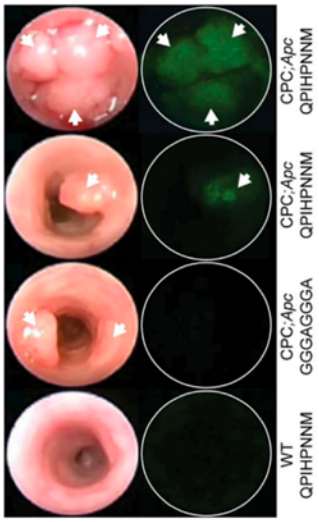


Figure 2.2 Endoscopy images demonstrating colon-targeting fluorescently labeled peptide

[Modified from Ref 10]. Wide-field endoscopy images acquired after in vivo incubation (5 minutes) of fluorescently labeled peptide QPIHPNNM in a genetic mouse model of adenoma formation in the colon. The left column shows white light images and the right column shows fluorescence images for binding of (a) QPIHPNNM to colon tissue with multiple adenomas, (b) QPIHPNNM to colon tissue with one adenoma, (c) control peptide GGGAGGGA to colon tissue with multiple adenomas, and (d) QPIHPNNM to lumen of colon tissue of a WT mouse. (Used with permission from PLoS One)

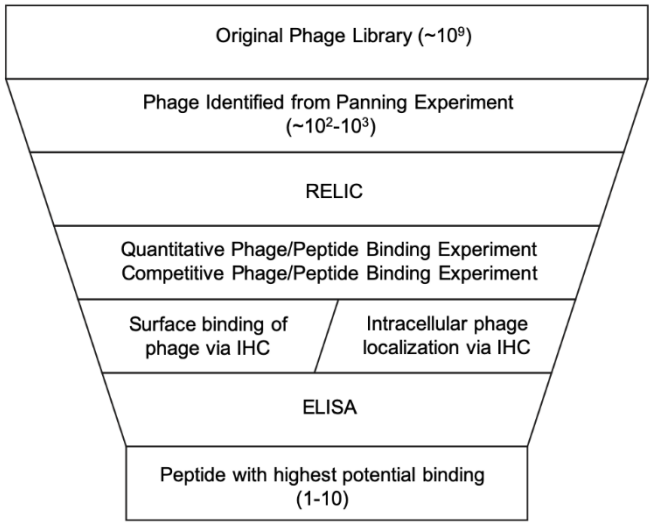


Figure 2.3 Schematic of the phage display process

[Modified from Ref 7]. Representation of steps in the phage display process to narrow the phage library down to only peptides with high affinity to the target substrate or cell population. (Used with permission from Springer)

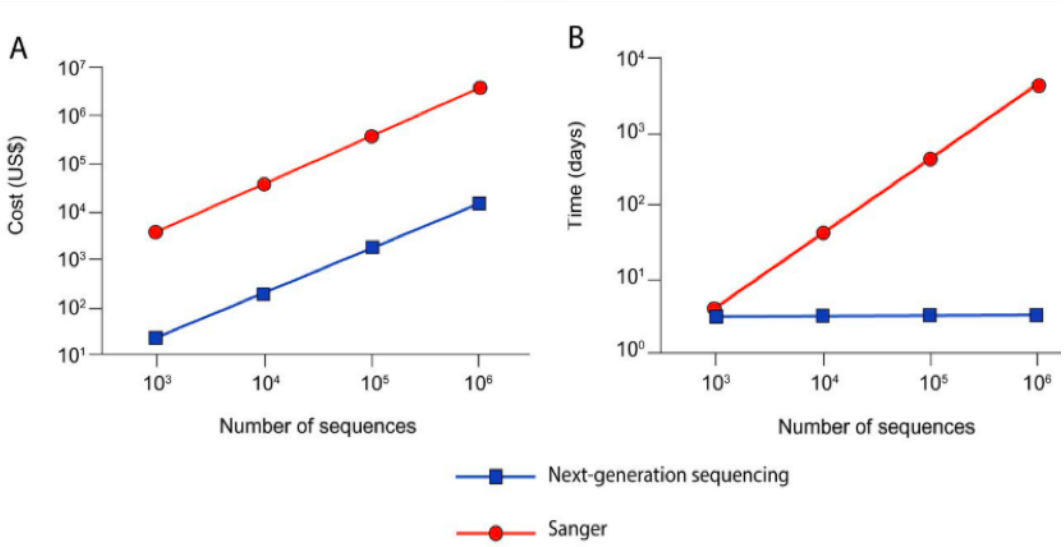


Figure 2.4 Relationship of number of sequences with cost and time of phage sequencing

These graphs demonstrate how (a) cost and (b) time necessary for phage sequencing decreases when using next-generation-sequencing (blue) over traditional Sanger sequencing (red) for increasing numbers of sequences. (Used with permission from PLoS One)

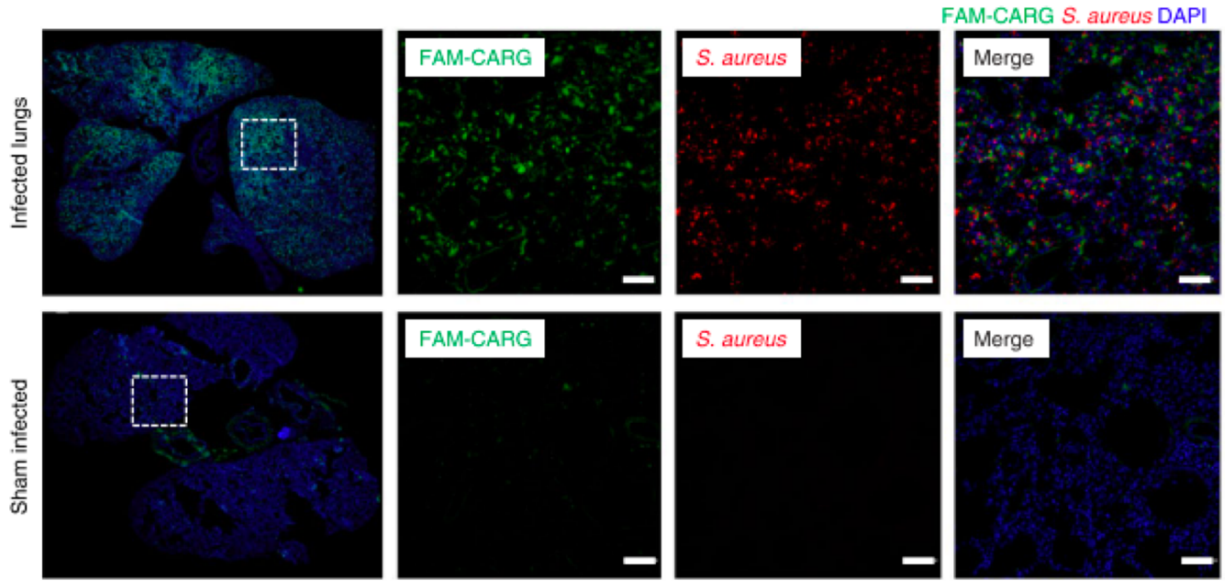


Figure 2.5 Fluorescent images of *S. aureus*-targeted peptide in lung tissue

[Modified from Ref 43]. Representative immunofluorescence images of fluorescently labeled peptide CARG (FAM-CARG, green) homing and binding to lungs infected with S. aureus (red) lungs (top row) and sham-infected lungs (bottom row). FAM-CARG was intravenously injected into tails of infected mice and allowed to circulate for 30 minutes prior to sacrifice and histological examination (n= 3-5 mice per group with 5 histological samples examined per lung). (Used with permission from Nature Biomedical Engineering)

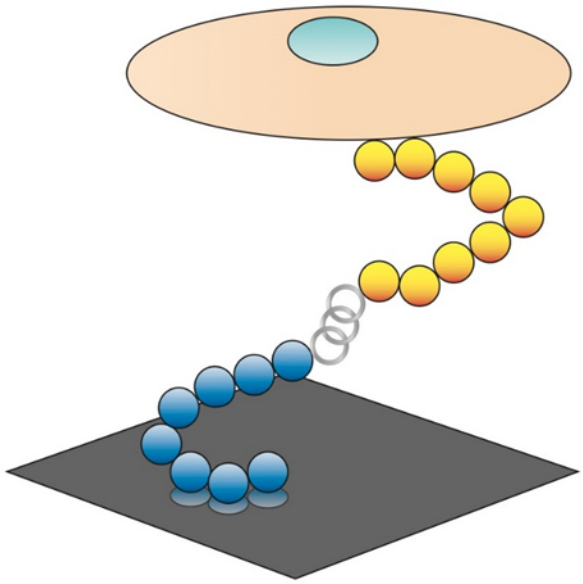


Figure 2.6 Schematic of dual-functioning peptide

[Modified from Ref 44]. Dual functioning peptide schematic with targeting peptide (blue) attached to a substrate (dark grey) connected to a functional or specific cell targeting peptide (yellow) via spacer amino acids (light grey). (Used with permission from Advanced Materials)

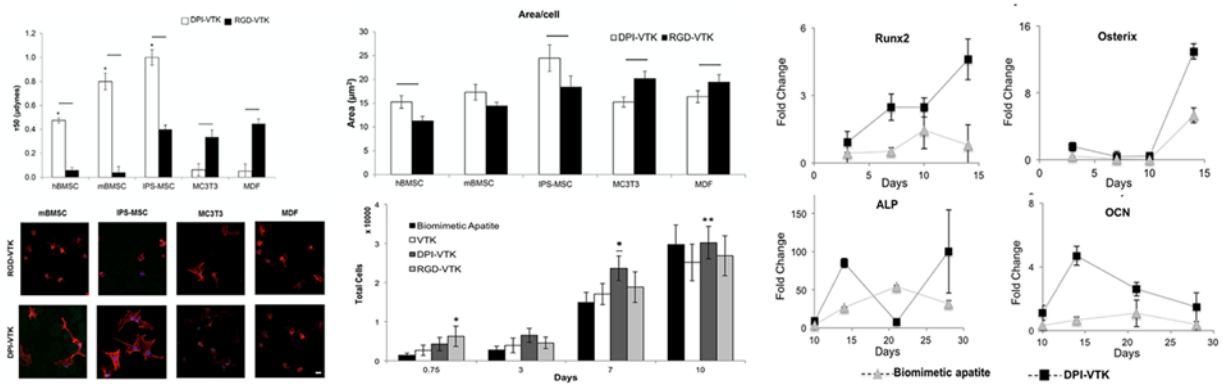


Figure 2.7 Dual-functional peptide for increasing cell adhesion to apatite substrates

(a) Half-cell detachment force (τ50) measured from peptide coated apatite films of human bone marrow stem cells, murine bone marrow stem cells, IPS derived MSCs, pre-osteoblastic MCTC3s, and murine dermal fibroblasts (MDFs). (b) Confocal microscopy images taken at 40x show increased spreading of mBMSCs and IPS-MSCs on DPI-VTK coated apatite films and increased spreading of MCTC3 and MDFs on RGD-VTK coated apatite films. (c) Quantitative analysis of cell spreading via ImageJ on peptide coated apatite films. (d) Total number of cells over time, reaching saturation at day 10. * denotes significance compared to apatite control and TCPS. * denotes significance compared to apatite control. ** denotes significance compared to VTK. (e-h) Relative gene expression of osteogenic markers (Runx2, OSX, ALP, and OCN) normalized to day 0 and GAPDH. (Used with permission from Taylor & Francis)

2.8 References

1. Smith, G. P. Filamentous Fusion Phage: Novel Expression Vectors That Display Cloned Antigens on the Virion Surface. Science (80-.). 1985, 228 (4705), 1315–1317. https://doi.org/10.1126/science.4001944.

2. Sidhu, S. S. Phage Display in Pharmaceutical Biotechnology. Current Opinion in Biotechnology. Elsevier Ltd December 1, 2000, pp 610–616. https://doi.org/10.1016/S0958-1669(00)00152-X.

3. Kehoe, J. W.; Kay, B. K. Filamentous Phage Display in the New Millennium. Chemical Reviews. American Chemical Society November 2005, pp 4056–4072. https://doi.org/10.1021/cr000261r.

4. Newton, J. R.; Deutscher, S. L. In Vivo Bacteriophage Display for the Discovery of Novel Peptide-Based Tumor-Targeting Agents. Methods Mol. Biol. 2009, 504, 275–290. https://doi.org/10.1007/978-1-60327-569-9_17.

5. Rosenberg, A.; Griffin, K.; Studier, E. W.; Mccormick, M.; Berg, J.; Novy, R.; Mierendorf, R. T7Select Phage Display System: A Powerful New Protein Display System Based on Bacteriophage T7. Innovations 1996, No. 6, 1–6.

6. Krumpe, L. R. H.; Atkinson, A. J.; Smythers, G. W.; Kandel, A.; Schumacher, K. M.; McMahon, J. B.; Makowski, L.; Mori, T. T7 Lytic Phage-Displayed Peptide Libraries Exhibit Less Sequence Bias than M13 Filamentous Phage-Displayed Peptide Libraries. Proteomics 2006, 6 (15), 4210–4222. https://doi.org/10.1002/pmic.200500606.

7. Segvich, S.; Kohn, D. H. Phage Display as a Strategy for Designing Organic/Inorganic Biomaterials. In Biological Interactions on Materials Surfaces; Springer US, 2009; pp 115–132. https://doi.org/10.1007/978-0-387-98161-1_6.

8. Pasqualini, R.; Ruoslahti, E. Organ Targeting in Vivo Using Phage Display Peptide Libraries. Nature 1996, 380 (6572), 364–366. https://doi.org/10.1038/380364a0.

9. Wada, A.; Terashima, T.; Kageyama, S.; Yoshida, T.; Narita, M.; Kawauchi, A.; Kojima, H. Efficient Prostate Cancer Therapy with Tissue-Specific Homing Peptides Identified by Advanced Phage Display Technology. Mol. Ther. - Oncolytics 2019, 12, 138–146. https://doi.org/10.1016/j.omto.2019.01.001.

10. Miller, S. J.; Joshi, B. P.; Feng, Y.; Gaustad, A.; Fearon, E. R. In Vivo Fluorescence-Based Endoscopic Detection of Colon Dysplasia in the Mouse Using a Novel Peptide Probe. PLoS One 2011, 6 (3), 17384. https://doi.org/10.1371/journal.pone.0017384.

11. Scodeller, P.; Simón-Gracia, L.; Kopanchuk, S.; Tobi, A.; Kilk, K.; Säälik, P.; Kurm, K.; Squadrito, M. L.; Kotamraju, V. R.; Rinken, A.; De Palma, M.; Ruoslahti, E.; Teesalu, T. Precision Targeting of Tumor Macrophages with a CD206 Binding Peptide. Sci. Rep. 2017, 7 (1). https://doi.org/10.1038/s41598-017-14709-x.

12. Mann, A. P.; Scodeller, P.; Hussain, S.; Joo, J.; Kwon, E.; Braun, G. B.; Mölder, T.; She, Z. G.; Kotamraju, V. R.; Ranscht, B.; Krajewski, S.; Teesalu, T.; Bhatia, S.; Sailor, M. J.; Ruoslahti, E. A Peptide for Targeted, Systemic Delivery of Imaging and Therapeutic Compounds into Acute Brain Injuries. Nat. Commun. 2016, 7 (1), 1–11. https://doi.org/10.1038/ncomms11980.

13. Matochko, W. L.; Chu, K.; Jin, B.; Lee, S. W.; Whitesides, G. M.; Derda, R. Deep Sequencing Analysis of Phage Libraries Using Illumina Platform. Methods 2012, 58 (1), 47–55. https://doi.org/10.1016/j.ymeth.2012.07.006.

14. Newman, M. R.; Benoit, D. S. W. In Vivo Translation of Peptide-Targeted Drug Delivery Systems Discovered by Phage Display. Bioconjugate Chemistry. American Chemical Society July 18, 2018, pp 2161–2169. https://doi.org/10.1021/acs.bioconjchem.8b00285.

15. Dias-Neto, E.; Nunes, D. N.; Giordano, R. J.; Sun, J.; Botz, G. H.; Yang, K.; Setubal, J. C.; Pasqualini, R.; Arap, W. Next-Generation Phage Display: Integrating and Comparing Available Molecular Tools to Enable Costeffective High-Throughput Analysis. PLoS One 2009, 4 (12). https://doi.org/10.1371/journal.pone.0008338.

16. Gillespie, J. W.; Yang, L.; De Plano, L. M.; Stackhouse, M. A.; Petrenko, V. A. Evolution of a Landscape Phage Library in a Mouse Xenograft Model of Human Breast Cancer. Viruses 2019, 11 (11). https://doi.org/10.3390/v11110988.

17. Hyde-Deruyscher, R.; Paige, L. A.; Christensen, D. J.; Hyde-Deruyscher, N.; Lim, A.; Fredericks, Z. L.; Kranz, J.; Gallant, P.; Zhang, J.; Rocklage, S. M.; Fowlkes, D. M.; Wendler, P. A.; Hamilton, P. T. Detection of Small-Molecule Enzyme Inhibitors with Peptides Isolated from Phage-Displayed Combinatorial Peptide Libraries. Chem. Biol. 2000, 7 (1), 17–25. https://doi.org/10.1016/S1074-5521(00)00062-4.

18. Hwang, H. J.; Ryu, M. Y.; Park, J. P. Identification of High Affinity Peptides for Capturing Norovirus Capsid Proteins. RSC Adv. 2015, 5 (68), 55300–55302. https://doi.org/10.1039/c5ra09655c.

19. Yeh, C. Y.; Hsiao, J. K.; Wang, Y. P.; Lan, C. H.; Wu, H. C. Peptide-Conjugated Nanoparticles for Targeted Imaging and Therapy of Prostate Cancer. Biomaterials 2016, 99, 1–15. https://doi.org/10.1016/j.biomaterials.2016.05.015.

20. Hwang, H. J.; Ryu, M. Y.; Park, C. Y.; Ahn, J.; Park, H. G.; Choi, C.; Ha, S. Do; Park, T. J.; Park, J. P. High Sensitive and Selective Electrochemical Biosensor: Label-Free Detection of Human Norovirus Using Affinity Peptide as Molecular Binder. Biosens. Bioelectron. 2017, 87, 164–170. https://doi.org/10.1016/j.bios.2016.08.031.

21. Huang, X.; Zauscher, S.; Klitzman, B.; Truskey, G. A.; Reichert, W. M.; Kenan, D. J.; Grinstaff, M. W. Peptide Interfacial Biomaterials Improve Endothelial Cell Adhesion and Spreading on Synthetic Polyglycolic Acid Materials. Ann. Biomed. Eng. 2010, 38 (6), 1965–1976. https://doi.org/10.1007/s10439-010-9986-5.

22. Xing, L.; Xu, Y.; Sun, K.; Wang, H.; Zhang, F.; Zhou, Z.; Zhang, J.; Zhang, F.; Caliskan, B.; Qiu, Z.; Wang, M. Identification of a Peptide for Folate Receptor Alpha by Phage Display and Its Tumor Targeting Activity in Ovary Cancer Xenograft. Sci. Rep. 2018, 8 (1), 1–13. https://doi.org/10.1038/s41598-018-26683-z.

23. Segvich, S.; Biswas, S.; Becker, U.; Kohn, D. H. Identification of Peptides with Targeted Adhesion to Bone-like Mineral via Phage Display and Computational Modeling. In Cells Tissues Organs; Cells Tissues Organs, 2008; Vol. 189, pp 245–251. https://doi.org/10.1159/000151380.

24. Liu, X.; Peng, J.; He, J.; Li, Q.; Zhou, J.; Liang, X.; Tang, S. Selection and Identification of Novel Peptides Specifically Targeting Human Cervical Cancer. Amino Acids 2018, 50 (5), 577–592. https://doi.org/10.1007/s00726-018-2539-1.

25. Caprini, A.; Silva, D.; Zanoni, I.; Cunha, C.; Volontè, C.; Vescovi, A.; Gelain, F. A Novel Bioactive Peptide: Assessing Its Activity over Murine Neural Stem Cells and Its Potential for Neural Tissue Engineering. N. Biotechnol. 2013, 00. https://doi.org/10.1016/j.nbt.2013.03.005.

26. Ramaswamy, J.; Nam, H. K.; Ramaraju, H.; Hatch, N. E.; Kohn, D. H. Inhibition of Osteoblast Mineralization by Phosphorylated Phage-Derived Apatite-Specific Peptide. Biomaterials 2015, 73, 120–130. https://doi.org/10.1016/j.biomaterials.2015.09.021.

27. Rangel, R.; Guzman-Rojas, L.; Le Roux, L. G.; Staquicini, F. I.; Hosoya, H.; Barbu, E. M.; Ozawa, M. G.; Nie, J.; Dunner, K.; Langley, R. R.; Sage, E. H.; Koivunen, E.; Gelovani, J. G.; Lobb, R. R.; Sidman, R. L.; Pasqualini, R.; Arap, W. Combinatorial Targeting and Discovery of Ligand-Receptors in Organelles of Mammalian Cells. Nat. Commun. 2012, 3 (1), 1–10. https://doi.org/10.1038/ncomms1773.

28. Ryvkin, A.; Ashkenazy, H.; Smelyanski, L.; Kaplan, G.; Penn, O.; Weiss-Ottolenghi, Y.; Privman, E.; Ngam, P. B.; Woodward, J. E.; May, G. D.; Bell, C.; Pupko, T.; Gershoni, J. M. Deep Panning: Steps towards Probing the IgOme. PLoS One 2012, 7 (8), e41469. https://doi.org/10.1371/journal.pone.0041469.

29. Ryvkin, A.; Ashkenazy, H.; Weiss-Ottolenghi, Y.; Piller, C.; Pupko, T.; Gershoni, J. M. Phage Display Peptide Libraries: Deviations from Randomness and Correctives. Nucleic Acids Res. 2018, 46 (9). https://doi.org/10.1093/nar/gky077.

30. Huang, J.; Ru, B.; Li, S.; … H. L.-B. R.; 2010, undefined. SAROTUP: Scanner and Reporter of Target-Unrelated Peptides. downloads.hindawi.com.

31. He, B.; Chen, H.; Li, N.; Huang, J. Sarotup: A Suite of Tools for Finding Potential Target-Unrelated Peptides from Phage Display Data. Int. J. Biol. Sci. 2019, 15 (7), 1452–1459. https://doi.org/10.7150/ijbs.31957.

32. Wang, J.; Liu, Y.; Teesalu, T.; Sugahara, K. N.; Kotamrajua, V. R.; Adams, J. D.; Ferguson, B. S.; Gong, Q.; Oh, S. S.; Csordas, A. T.; Cho, M.; Ruoslahti, E.; Xiao, Y.; Soh, H. T. Selection of Phage-Displayed Peptides on Live Adherent Cells in Microfluidic

Channels. Proc. Natl. Acad. Sci. U. S. A. 2011, 108 (17), 6909–6914. https://doi.org/10.1073/pnas.1014753108.

33. Matochko, W. L.; Cory Li, S.; Tang, S. K. Y.; Derda, R. Prospective Identification of Parasitic Sequences in Phage Display Screens. Nucleic Acids Res. 2014, 42 (3), 1784–1798. https://doi.org/10.1093/nar/gkt1104.

34. Addison, W. N.; Miller, S. J.; Ramaswamy, J.; Mansouri, A.; Kohn, D. H.; McKee, M. D. Phosphorylation-Dependent Mineral-Type Specificity for Apatite-Binding Peptide Sequences. Biomaterials 2010, 31 (36), 9422–9430. https://doi.org/10.1016/j.biomaterials.2010.08.064.

35. 'T Hoen, P. A. C.; Jirka, S. M. G.; Ten Broeke, B. R.; Schultes, E. A.; Aguilera, B.; Pang, K. H.; Heemskerk, H.; Aartsma-Rus, A.; Van Ommen, G. J.; Den Dunnen, J. T. Phage Display Screening without Repetitious Selection Rounds. Anal. Biochem. 2012, 421 (2), 622–631. https://doi.org/10.1016/j.ab.2011.11.005.

36. Ramaraju, H.; Miller, S. J.; Kohn, D. H. Dual-Functioning Peptides Discovered by Phage Display Increase the Magnitude and Specificity of BMSC Attachment to Mineralized Biomaterials. Biomaterials 2017, 134, 1–12. https://doi.org/10.1016/j.biomaterials.2017.04.034.

37. Ramaraju, H.; Kohn, D. H. Cell and Material-Specific Phage Display Peptides Increase IPS-MSC Mediated Bone and Vasculature Formation In Vivo. Adv. Healthc. Mater. 2019, 8 (9). https://doi.org/10.1002/adhm.201801356.

38. Shao, Z.; Zhang, X.; Pi, Y.; Wang, X.; Jia, Z.; Zhu, J.; Dai, L.; Chen, W.; Yin, L.; Chen, H.; Zhou, C.; Ao, Y. Polycaprolactone Electrospun Mesh Conjugated with an MSC Affinity Peptide for MSC Homing in Vivo. Biomaterials 2012, 33 (12), 3375–3387. https://doi.org/10.1016/j.biomaterials.2012.01.033.

39. Meng, Q.; Man, Z.; Dai, L.; Huang, H.; Zhang, X.; Hu, X.; Shao, Z.; Zhu, J.; Zhang, J.; Fu, X.; Duan, X.; Ao, Y. A Composite Scaffold of MSC Affinity Peptide-Modified Demineralized Bone Matrix Particles and Chitosan Hydrogel for Cartilage Regeneration. Sci. Rep. 2015, 5 (1), 1–14. https://doi.org/10.1038/srep17802.

40. Wang, G.; Man, Z.; Zhang, N.; Xin, H.; Li, Y.; Sun, T.; Sun, S. Biopanning of Mouse Bone Marrow Mesenchymal Stem Cell Affinity for Cyclic Peptides. Mol. Med. Rep. 2019, 19 (1), 407–413. https://doi.org/10.3892/mmr.2018.9626.

41. Teesalu, T.; Sugahara, K. N.; Ruoslahti, E. Mapping of Vascular ZIP Codes by Phage Display. In Methods in Enzymology; Academic Press Inc., 2012; Vol. 503, pp 35–56. https://doi.org/10.1016/B978-0-12-396962-0.00002-1.

42. Soendergaard, M.; Newton-Northup, J. R.; Deutscher, S. L. In Vivo Phage Display Selection of an Ovarian Cancer Targeting Peptide for SPECT/CT Imaging. Am. J. Nucl. Med. Mol. Imaging 2014, 4 (6), 561–570.

43. Hussain, S.; Joo, J.; Kang, J.; Kim, B.; Braun, G. B.; She, Z. G.; Kim, D.; Mann, A. P.; Mölder, T.; Teesalu, T.; Carnazza, S.; Guglielmino, S.; Sailor, M. J.; Ruoslahti, E. Antibiotic-Loaded Nanoparticles Targeted to the Site of Infection Enhance Antibacterial Efficacy. Nat. Biomed. Eng. 2018, 2 (2), 95–103. https://doi.org/10.1038/s41551-017-0187-5.

44. Meyers, S. R.; Hamilton, P. T.; Walsh, E. B.; Kenan, D. J.; Grinstaff, M. W. Endothelialization of Titanium Surfaces. Adv. Mater. 2007, 19 (18), 2492–2498. https://doi.org/10.1002/adma.200700029.

45. Naik, R. R.; Stringer, S. J.; Agarwal, G.; Jones, S. E.; Stone, M. O. Biomimetic Synthesis and Patterning of Silver Nanoparticles. Nat. Mater. 2002, 1, 169–172. https://doi.org/10.1038/nmat758.

46. Wei, Z.; Maeda, Y.; Kanetsuki, Y.; Shi, M.; Matsui, H. Screening of Oligopeptides That Recognize Inorganic Crystalline Facets of Metal Nanoparticles. Isr J. Chem 2019, 55 (6–7), 749–755. https://doi.org/10.1016/j.physbeh.2017.03.040.

47. Chiu, C. Y.; Li, Y.; Ruan, L.; Ye, X.; Murray, C. B.; Huang, Y. Platinum Nanocrystals Selectively Shaped Using Facet-Specific Peptide Sequences. Nat. Chem. 2011, 3 (5), 393–399. https://doi.org/10.1038/nchem.1025.

48. Kase, D.; Kulp, J. L.; Yudasaka, M.; Evans, J. S.; Iijima, S.; Shiba, K. Affinity Selection of Peptide Phage Libraries against Single-Wall Carbon Nanohorns Identifies a Peptide Aptamer with Conformational Variability. Langmuir 2004, 20 (20), 8939–8941. https://doi.org/10.1021/la048968m.

49. Estephan, E.; Saab, M.-B.; Agarwal, V.; Cuisinier, F. J. G.; Larroque, C.; Gergely, C. Peptides for the Biofunctionalization of Silicon for Use in Optical Sensing with Porous Silicon Microcavities. Adv. Funct. Mater. 2011, 21 (11), 2003–2011. https://doi.org/10.1002/adfm.201002742.

50. Luong, L. N.; Hong, S. I.; Patel, R. J.; Outslay, M. E.; Kohn, D. H. Spatial Control of Protein within Biomimetically Nucleated Mineral. Biomaterials 2006, 27 (7), 1175–1186. https://doi.org/10.1016/j.biomaterials.2005.07.043.

51. Segvich, S. J.; Smith, H. C.; Kohn, D. H. The Adsorption of Preferential Binding Peptides to Apatite-Based Materials. Biomaterials 2009, 30 (7), 1287–1298. https://doi.org/10.1016/j.biomaterials.2008.11.008.

52. Wu, P.; Grainger, D. W. Drug/Device Combinations for Local Drug Therapies and Infection Prophylaxis. Biomaterials 2006, 27, 2450–2467. https://doi.org/10.1016/j.biomaterials.2005.11.031.

53. Khoo, X.; O'Toole, G. A.; Nair, S. A.; Snyder, B. D.; Kenan, D. J.; Grinstaff, M. W. Staphylococcus Aureus Resistance on Titanium Coated with Multivalent PEGylated-Peptides. Biomaterials 2010, 31 (35), 9285–9292. https://doi.org/10.1016/j.biomaterials.2010.08.031.

54. Sanghvi, A. B.; Miller, K. P. H.; Belcher, A. M.; Schmidt, C. E. Biomaterials Functionalization Using a Novel Peptide That Selectively Binds to a Conducting Polymer. Nat. Mater. 2005, 4 (6), 496–502. https://doi.org/10.1038/nmat1397.

55. Meyers, S. R.; Kenan, D. J.; Khoo, X.; Mark W. Grinstaff. A Bioactive Stent Surface Coating That Promotes Endothelialization While Preventing Platelet Adhesion. Biomacromolecules 2011, 12 (3), 533–539. https://doi.org/10.1021/bm101212k.A.

56. Ramaraju, H.; Miller, S. J.; Kohn, D. H. Dual-Functioning Phage-Derived Peptides Encourage Human Bone Marrow Cell-Specific Attachment to Mineralized Biomaterials. In Connective Tissue Research; Informa Healthcare, 2014; Vol. 55, pp 160–163. https://doi.org/10.3109/03008207.2014.923868.

Chapter 3 Mineral-Binding Peptide Inhibits Ectopic Mineralization due to BMP Stimulation

3.1 Introduction

Bone morphogenetic proteins (BMPs) are drivers of osteogenic pathways and BMP2 is an FDA-approved therapeutic for enhancing bone regeneration[1]. BMPs are delivered at supraphysiological levels via sponge at load-bearing sites, and leakage (due to implant handling) can result in complications and off-target effects, especially when employed in off-label surgical applications[2,3]. The most severe off-target complications are swelling and ectopic mineralization which, near the upper spine, could cause airway obstruction or neurological impairment[4]. Approaches to mitigating these off-target effects include co-delivery of BMP2 with drugs to reduce inflammation (e.g. NSAIDs), enhance osteogenic activity to reduce the amount of delivered BMP (e.g. VEGF to promote angiogenesis for bone regeneration), or promote osteoclastic activity (e.g. bisphosphonates)[3]. However, both pro-osteogenic and pro-osteoclastic molecules increase the severity of ectopic mineralization[5,6]. Therefore, there is a need for improvements to BMP therapies to better control osteogenesis and reduce side effects, enabling expanded use of BMP therapies without causing life-threatening complications.

Alternatively, strategies could directly target mineral formation rather than intervene with highly interconnected signaling pathways during bone regeneration and recovery from surgery. To combat ectopic mineralization due to BMP2, co-delivery of BMP2 with a mineral-binding peptide, pVTK was proposed. pVTK is the phosphorylated variant of mineral-binding peptide VTK (VTKHLNQI(p)SQ(p)SY, where p denotes phosphorylation of the serine residues),

identified via phage display for its high and preferential affinity for apatite-based substrates[7,8]. Post-translational phosphorylation of VTK's serine residues established pVTK and resulted in increased affinity for mineralized substrates compared to VTK[9]. Further, pVTK inhibits mineralization in murine calvarial pre-osteoblasts throughout osteogenic differentiation without causing cell death[9]. pVTK treatment was associated with increases in pro-osteogenic markers and decreases in anti-osteogenic markers, trends attributed to a compensatory response by osteogenic cells in the absence of matrix mineral[10]. Though it is not understood how pVTK inhibits mineralization, pVTK does not disrupt cellular response to osteogenic cues. In solution, pVTK inhibits calcium phosphate nucleation, disrupts the phase transition from amorphous to crystalline, and slows crystal growth[11]. Therefore, it is believed that pVTK inhibits mineralization by binding to early mineral clusters and disrupting nucleation and crystallization. Based on the evidence that pVTK directly targets mineral formation, pVTK is presented as a complement for BMP2 therapies, as pVTK is hypothesized to inhibit ectopic mineral (EM) formation without disrupting osteogenic cell signaling.

This study investigated if pVTK inhibited EM formation of BMP-stimulated osteoblasts in vitro and BMP-containing subcutaneous implants in vivo. The subcutaneous BMP implant model was chosen to isolate the off-target effects of BMP2 therapies and the effects on cells that are not naturally osteogenic. To investigate whether pVTK's inhibition of EM formation would rely on cellular machinery, an acellular model of spontaneous mineral formation was used as well. Taken together, data presented in this paper demonstrate that pVTK could be co-delivered with BMP2 to prevent ectopic mineralization.

3.2 Methods

3.2.1 Peptide synthesis

Peptide synthesis of pVTK (VTKHNLQI(pS)Q(pS)Y; pS = phosphoserine) and scram-pVTK (IYQ(pS)KHTL(pS)NQV) was performed by the University of Michigan's Proteomics and Peptide Synthesis Core. Peptides were synthesized using solid phase synthesis (purity ≥ 90% by HPLC). Post-translational phosphorylation of serine residues utilized preformed, protected phosphoserine amino acids. For in vitro experiments, pVTK was dissolved in a carbonate-bicarbonate buffer (pH 9) (10mM, sterile-filtered) and stored at -20℃ for up to one month. For in vivo experiments, pVTK was dissolved in PBS (2mM), sterile filtered, and stored at -20℃.

3.2.2 Cell culture and in vitro osteogenic differentiation

MC3T3 (subclone 14) cells, murine calvarial pre-osteoblasts, were used for all in vitro studies. MC3T3s were maintained in growth media: alpha-MEM (Gibco 12561-056) with 10% FBS (Gibco 10082147, Reserve 77813196) and 1% penicillin-streptomycin (Gibco, 15140-122).

For osteogenic differentiation studies, MC3T3s were plated at 50,000 cells/cm^2 and allowed to reach confluence before switching to osteogenic differentiation media: growth media plus β-glycerophosphate (10mM, Sigma-Aldrich) and ascorbic acid (50μg/mL, Sigma-Aldrich). pVTK (in carbonate-bicarbonate buffer) and BMP2 (recombinant human/mouse/rat BMP2 from, R&D Systems) (in 4mM HCl with 0.1% human serum albumin from Sigma-Aldrich) were added to culture for up to 12 days.

To evaluate the effect of pVTK on BMP2-stimulated mineralization, MC3T3s (n = 3) were cultured in osteogenic media plus pVTK (0, 200, 300, or 400μM) and BMP2 (50 or 100ng/mL) for 12 days. To evaluate effect of pVTK on BMP2-stimulated osteogenic activity, MC3T3s (n = 3) were cultured in osteogenic media plus pVTK (0 or 300μM) and/or BMP2 (0 or 50ng/mL) for 1 hour, 6 days, or 12 days.

3.2.3 Staining for calcium and calcium phosphate deposition

Mineralized cell monolayers were fixed in 10% neutral-buffered formalin for 10 minutes, then washed with deionized water. To visualize calcium phosphate deposits, von Kossa staining (5% silver nitrate solution, Sigma-Aldrich) was performed by incubating fixed monolayers with the staining solution for one hour under UV light. To visualize calcium deposits, Alizarin Red staining was performed by incubating fixed monolayers with a 2% (w/v) Alizarin Red S solution (pH 4.2, Sigma-Aldrich) for 45 minutes protected from light. Following both stains, monolayers were washed with deionized water until the wash solution ran clear.

3.2.4 Alkaline phosphatase activity

After 6 or 12 days of osteogenic differentiation with pVTK (0 or 300μM) and BMP2 (0 or 50ng/mL), MC3T3 lysates were collected for alkaline phosphatase (ALP) activity via p-nitrophenyl phosphate assay method (Colorimetric Alkaline Phosphatase Activity Assay, Abcam) with normalization to DNA content (Quant-iT PicoGreen dsDNA Assay, Invitrogen). Briefly, lysates were harvested in assay buffer after one freeze/thaw cycle at -20℃, sonicated for 5 minutes on ice, and centrifuged at 13,000 rpm for 5 minutes at 4℃. Then, supernatant was collected and used for ALP activity quantification and DNA quantification. Three biological replicates for each experimental group were assayed in duplicate at each timepoint.

3.2.5 Protein quantification

Cells were harvested after 1 hour, 6 days, or 12 days of BMP2 (0 or 50ng/mL) and/or pVTK (0 or 300μM) in lysis buffer (RIPA buffer with 1mM sodium orthovanadate, 10mM sodium fluoride, 1mM poly-methylsulfonylfluoride, and protease inhibitor cocktail (Thermo Scientific)). For the 1-hour timepoint, cells were serum-starved for 24 hours prior to pVTK

and/or BMP2 administration. For the 1-hour timepoint, biological replicates (n = 3) were run individually; for the 6-day and 12-day timepoints, biological replicates (n = 3) were pooled for representative protein bands.

Cell lysates were collected and homogenized in an ultrasonic bath for 5 minutes in ice water. Homogenized cell lysates were centrifuged at 13,000rpm for 5 minutes at 4°C. Lysate supernatant was used to quantify sample protein concentration using BCA assay (Pierce). Samples were prepared at a normalized concentration of 20ug in 40uL of loading buffer (1:1 Laemmli: RIPA buffer) with 5% B-mercaptoethanol (Sigma-Aldrich) and heated at 95°C for 5 minutes. Electrophoresis was performed in Novex Tris-Glycine (4-20%) gradient gels (Invitrogen), run at 225V for 40 minutes. Protein transfer to poly-vinylidene fluoride (PVDF, Millipore-Sigma) membranes was run at 50V for 75 minutes. Membranes were blocked for 1 hour at room temperature in 3% bovine serum albumin (BSA, Fisher). Membranes were incubated with primary antibodies in 3% BSA overnight at 4°C, followed by 3 5-minute washes in TBST. Membranes were then incubated with the secondary antibody in 3% BSA for 2 hours at room temperature, followed by TBST washes. Membranes were developed with SuperSignal™ West Pico PLUS Chemiluminescent Substrate (ThermoFisher) and imaged with the ChemiDoc (Bio-Rad). Band quantification was performed with ImageLab software (Bio-Rad) with all protein levels being normalized to β-actin loading control. Primary antibodies used were pSmad (Cell Signaling Technologies #13820, rabbit monoclonal), Smad (Cell Signaling Technologies #6944, rabbit monoclonal), Runx2 (Cell Signaling Technologies #12556, rabbit monoclonal), TNAP (abcam ab203106, rabbit polyclonal), and B-actin (Cell Signaling Technologies #4970, rabbit monoclonal). The secondary antibody used was anti-rabbit IgG, HRP-linked (Cell Signaling Technologies, #7074).

3.2.6 Peptide stability testing

Predicted in vivo stability testing was performed by the Pharmacokinetic and Mass Spectrometry Core at the University of Michigan. For plasma stability testing, pVTK and Benfluorex (positive control) were incubated in pooled mouse plasma for up to 120 minutes. For liver microsomal stability testing, pVTK and Verapamil (positive control) were incubated in pooled mouse microsomes isolated from liver tissue for up to 60 minutes after reaction activation with NADPH. Aliquots were removed at specified timepoints (0, 5, 10, 15, 30, 45, 60, and 120 minutes) and acetonitrile with 100ng/mL internal standard (ERD1233A) was added to quench the reactions. After precipitation via centrifugation, LC-MS analysis of the collected supernatant quantified drug amount at each timepoint.

3.2.7 Animal care and subcutaneous implant surgeries

All procedures were approved by the University of Michigan's Institutional Animal Care and Use Committee (IACUC). Male C5BL6/Jc mice (total = 6/group) at age 4-6 weeks were used for in vivo experiments. Collagen sponges (GelFoam) were cut to size using a 5-mm biopsy punch. BMP2 (carrier-free recombinant human/mouse/rat BMP2, R&D Therapeutics) was reconstituted in sterile 0.4M HCl at a concentration of 100ng/μL. Implants were prepared by incubating trimmed collagen sponges with 15μL BMP2 (1.5μg/implant) or PBS an hour prior to surgery and maintained over ice until implantation.

For subcutaneous surgeries, all surgical procedures were performed in accordance with NIH guidelines for the care and use of animals. Animals were anesthetized with isoflurane and the surgical site was prepared by shaving and cleaning with iodine and sterile water. Animals were then transferred to the sterile surgical plane, atop a heating pad to maintain body temperature. A 1-cm incision was made perpendicular to the dorsal midline on the upper back

with scissors (World Precision Instruments). Blunt dissection with undermining forceps created subcutaneous pockets on either side of the midline. One implant was placed into each subcutaneous pocket (total 2 per animal for a total n of 6/group). Wound closure was performed with wound clips (BD Autoclip Wound Closure System).

Wounds were monitored for 7-10 days or until clips were removed at day 10 after surgery. Animals displaying any skin lesions were treated with silver sulfadiazine cream (1%; Ascend), applied daily until hair ingrowth was observed.

On each of the 14 days after surgery, pVTK (2mM, sterile filtered in PBS) or PBS (Gibco) was injected via 100µL-Hamilton syringe (26g needle) into each of the two bilateral subcutaneous pockets established during surgery. Animals were sacrificed 14 days post-implantation.

3.2.8 Micro-CT analysis

Implants (n = 6) were dissected from subcutaneous pockets, fixed in 4% paraformaldehyde (PFA) for 24 hours at 4℃, and transferred to 70% ethanol (EtOH) prior to submission to the MicroCT Core at the University of Michigan's School of Dentistry. Scanning was performed with a Scanco µCT 100 micro-computed tomography system at 70 kV, 114 Å, and with a 0.5 Al filter. Scans were acquired at 10µm voxel size and 12µm slice increments. For EM volumetric quantification, scans were loaded into Dragonfly (Comet Technologies). Segmentation of EM was performed utilizing the upper OTSU segmentation function and refining manually as needed. Total EM volume was measured based on the upper-OTSU-defined region of interest (ROI). EM volume fraction was measured as the ratio of the total EM volume to the filled ROI equivalent.

3.2.9 EM grading scheme

To assess severity of the EM, a grading scheme was developed based on guidelines developed in a study of traumatic heterotopic ossification (HO)[12]. The human traumatic HO study defined grades by the percent of the cross-sectional area of residual limbs occupied by EM, as observed in anteroposterior or lateral radiographs[12]. For translation to this animal study, EM grades were created based on EM volumes, as quantified via micro-CT. The distribution of HO grades in PBS-treated control samples was matched to the distribution of the human traumatic HO (Figure 3.6S). Then, the volume ranges for each grade were used to sort pVTK-treated samples.

3.2.9.1 Histology

Implants were incubated in 30% sucrose for at least 24 hours prior to embedding in optimal cutting temperature (OCT; Fisher Healthcare). 30μm sections were collected with the Leica CM1950 cryostat using CryoJane tape (Leica) and charged slides. Hematoxylin and eosin staining (H&E; Sigma) visualized the implant and cellular invasion. Von Kossa staining (1% silver nitrate, Sigma-Aldrich) visualized EM formation within the implants.

3.2.10 PLGA thin films

PLGA (poly-lactic-co-glycolic acid, 85:15; Evonik) was fully dissolved in chloroform (5% w/v). The solution was pipetted onto 15mm-diameter glass coverslips, covered, and allowed to sit overnight at room temperature while the chloroform evaporated, leaving the PLGA deposited on the surface of the coverslips (glass #2, Electron Microscopy Sciences).

3.2.11 Modified simulated body fluid (mSBF, 1x)

A supersaturated salt solution was made as described[13]. The components (141 mM NaCl, 4.0 mM KCl, 0.5 mM $MgSO_4$, 1.0 mM $MgCl_2$, 4.2 mM $NaHCO_3$, 5.0 mM $CaCl_2 \cdot 2H_2O$, 2.0 mM

KH_2PO_4) were added in order to deionized water, allowing each component to be completely dissolved before weighing out the next. Once all components were added, the solution was adjusted to pH 6.8 at 37°C, then vacuum filtered through a 30μm filter and stored at -4C.

3.2.12 Mineralizing thin films

The PLGA thin films were activated by incubating in a 0.5M NaOH solution for 7 minutes. Films were washed twice with distilled water. Then, the films were incubated with mSBF (2x) for 3-7 days with daily mSBF changes. Once the films were mineralized, the mSBF was removed and the films were allowed to air dry. If not being used immediately, the mineralized thin films were stored under vacuum in a desiccator.

3.2.13 Scanning electron microscopy (SEM)

Carbon-coated, mineralized PLGA thin films were scanned in the JEOL JSM-7800FLV Scanning Electron Microscope in the University of Michigan's Electron Microbeam Analysis Lab (10.0kV LED, WD 12.0μm) for visualization of mineral formation and microstructure.

3.2.14 Statistical analysis

All statistical analysis was carried out in GraphPad Prism 9. For in vitro data analysis, two-way ANOVAs were used to compare effects of pVTK and/or BMP2. For in vivo data analysis, Student's t-test was used to compare effects of PBS vs. pVTK. Significance was reported for $p < 0.05$ (*).

3.3 Results

3.3.1 pVTK inhibits BMP-stimulated mineralization in vitro

pVTK inhibited BMP-stimulated mineralization in vitro. At 50ng/mL BMP2, 400μM pVTK inhibited mineralization (von Kossa staining, Figure 3.1A) and >300μM pVTK inhibited calcification (Alizarin Red staining, Figure 3.1A). At 100ng/mL BMP2, 400μM pVTK reduced von Kossa and Alizarin Red staining, but did not achieve full inhibition (Figure 3.1A). At 50ng/mL BMP2, all levels of pVTK treatment significantly reduced ECM calcium (ANOVA $p < 0.0001$) compared to 0uM controls (Figure 3.1B). At 100ng/mL BMP2, pVTK treatment significantly reduced ECM calcium (ANOVA $p = 0.0074$) at 300μM ($p = 0.0144$) and 400μM ($p < 0.0001$) compared to 0μM controls (Figure 3.1C).

3.3.2 pVTK affects BMP-stimulated osteogenic signaling differently at different stages of differentiation

Phosphorylation of Smad 1/5/8 (represented by the ratio of phosphorylated Smad1/5/8 to unphosphorylated Smad1/5/8) is the immediate downstream result of BMP2 ligand-binding. As expected, BMP2 stimulated phosphorylation of Smad1/5/8 (Figure 3.2A). pVTK alone did not stimulate Smad phosphorylation, nor did pVTK alter the immediate cellular response to BMP2 stimulation (Figure 3.2A).

Runx2 is an early marker of osteogenic differentiation. pVTK slightly downregulated Runx2 by day 6 of osteogenic differentiation, but sustained and slightly upregulated Runx2 by day 12 (Figure 3.2B). BMP2 had the opposite effect of pVTK, upregulating Runx2 at 6 days and downregulating Runx2 by day 12. When administered together, BMP and pVTK downregulated Runx2 at both timepoints.

Intracellular tissue non-specific alkaline phosphatase (TNAP) is a mid-to-late marker of osteoblastic commitment, while extracellular alkaline phosphatase (ALP) activity is correlated with early stages of mineralization[14]. pVTK had no effect on TNAP levels at either timepoint

compared to controls (Figure 3.2B). BMP2 slightly upregulated TNAP at day 6 and downregulated TNAP by day 12 (Figure 3.2B). When administered separately, only BMP2 had an effect on TNAP levels compared to controls. When administered together, BMP and pVTK had no effect on TNAP at day 6 and a downward effect by day 12 (Figure 3.2B). ALP activity was slightly upregulated by pVTK at day 6 but not at day 12 (Figure 3.2C). BMP had no effect on ALP activity at either timepoint. When adminsitered separately, only pVTK had an effect on ALP activity levels. When administered together, BMP and pVTK significantly upregulated ALP activity at day 6 of osteogenic differentiation compared to control and BMP-only groups while co-delivery downregulated ALP activity at day 12 compared to pVTK treatment alone (Figure 3.2D).

3.3.3 pVTK inhibits ectopic mineral formation in vivo

For in vivo testing, a bilateral subcutaneous implant model was used (Figure 3.3A). EM formation is shown via animal radiographs in Figure 3B. Ex vivo peptide stability testing pVTK predicted at least 80% of pVTK remained intact after 2 hours in mouse plasma (Figure 3.3C). Ex vivo liver microsomal stability testing predicted at least 95% of pVTK remained intact after 1 hour (Figure 3.7S).

pVTK treatment significantly reduced EM volume compared to PBS controls ($p = 0.0101$, $n = 6$) (Figure 3.3D). Further, pVTK treatment achieved full inhibition in 50% of treated samples and limited mineralization to less than PBS controls in all pVTK-treated samples (Figure 3.3D). However, pVTK treatment had no effect on EM volume fraction (Figure 3.3E). Based on the grading scheme established for this study (Figure 3.3F), pVTK treatment downshifted the severity of EM to only the ‘Negligible’ or ‘Mild’ grades compared to PBS treatment (Figure 3.3G).

pVTK treatment reduced the intrusion of mineral into the collagen implant compared to PBS-treated controls (Figure 3.4, VKS). In both treatment groups, tissue reorganization at the periphery of the implants was observed through densely packed matrix (deep pink) and a surrounding shell (dark purple) (Figure 3.4, H&E 5X). However, the reorganized tissue in the PBS-treated groups corresponded with mineral, whereas the reorganized tissue in the pVTK-treated groups remained largely unmineralized. There was an effect of pVTK treatment on cell infiltration into the collagen implant, as seen in decreased numbers and penetration distance of cells into the implant (Figure 3.4, H&E 10X). However, low sample counts limit the conclusiveness of these observations.

3.3.4 pVTK disrupts spontaneous acellular mineralization

pVTK inhibited spontaneous formation and maturation of mineral clusters formed on polymer films subjected to a salt solution without cells, as seen via SEM (Figure 3.5). The morphology of mineral in this model is spherical clusters composed of plate-like outgrowths (Figure 3.5A and 3.5B, left columns). At 100μM, pVTK reduced the amount of mineral and the density of spherical clusters (Figure 3.5A, middle column). At 200μM pVTK (Figure 3.5A, right column), mineral was absent. Mineralization of thin films was unaffected by scrambled pVTK, indicating that the sequence of pVTK contributed to inhibition of the spontaneous mineralization process (Figure 3.5B).

3.4 Discussion

As a mineral-binding peptide, pVTK has many applications in bone tissue engineering, from guiding drug delivery to mineralized tissue to modulating mineralization. This was the first publication describing the use of pVTK to prevent non-physiological mineralization in-vivo,

expanding upon studies showing that pVTK inhibits physiological mineralization in osteoblasts in vitro[9,10]. To verify that pVTK would be an effective molecule for mitigating ectopic mineral formation, inhibition of BMP-stimulated mineralization with pVTK was assessed in vitro and in vivo. Further, experiments conducted in cellular and acellular environments provided evidence for how pVTK may act to inhibit mineralization. Altogether, these experiments showed that pVTK inhibits EM formation in vivo, likely by pVTK binding to early mineral clusters and preventing mineral growth.

In the case of BMP-stimulated mineralization, there needs to be a balance between inhibition of unwanted mineralization and preservation of desirable bone formation. The work presented here indicates that pVTK could be used to stem unwanted mineralization because its inhibitory function is not reliant on cellular machinery, specifically BMP2 osteogenic signaling. Control over where and when pVTK is delivered would be necessary to selectively inhibit unwanted mineral and achieve clinical efficacy of pVTK as a safeguard for ectopic mineralization due to BMP2 therapies.

3.4.1 pVTK inhibits BMP-stimulated mineralization in vitro

At the lower level of BMP stimulation (50ng/mL), pVTK inhibited mineralization at concentrations ≥300μM (Figure 3.1). However, at the higher level of BMP stimulation (100ng/mL), pVTK did not achieve full inhibition at any of the tested concentrations (Figure 3.1). Mineralization did not scale with BMP treatment since there was no difference in the amount of mineral deposited by MC3T3s stimulated at the two different levels of BMP (Figures 3.1B and 3.1C). A higher dose of BMP2 does not directly correlate with a higher level of mineralization, even though increasing BMP2 increases the osteogenic profile of MC3T3s (at gene and protein levels)[15]. Therefore, pVTK dosing strategies for mineral inhibition should

consider more than just the quantity of EM. Dosing strategies should also consider mineral formation rate, mineral composition, protein levels throughout osteogenic differentiation, and how MC3T3 sensitivity to BMP and/or pVTK administration changes throughout osteogenic differentiation.

3.4.2 pVTK affects BMP-stimulated osteogenic activity differently at different stages of differentiation

Agents for co-delivery with BMP2 would ideally not suppress osteogenic stimulation as a means to mitigate EM formation. Since BMP2 is delivered at supraphysiological levels, decreasing the concentration of the BMP2 would likely reduce efficacy. As the immediate downstream result of BMP2 ligand-binding, upregulation of phosphorylation of Smad1/5/8 due to BMP2 stimulation was unaffected by pVTK (Figure 3.2A). This means that MC3T3s can sense and respond to BMP2 ligand-binding without interference by pVTK.

pVTK administration was expected to upregulate osteogenic activity, suggesting a compensatory mechanism by the cells to make up for the lack of mineralization[10]. There was a slight compensatory reaction of the pVTK-only group, as evidenced by upregulated ALP activity at day 6 (Figure 3.2C) and upregulated Runx2 by day 12 (Figure 3.2B). Therefore, it is unlikely that pVTK inhibits mineralization by downregulating intracellular osteogenic protein levels.

Since mineralization in BMP-stimulated MC3T3s did not scale with BMP2 concentration, yet pVTK did not fully inhibit mineralization at the higher level of BMP stimulation, co-delivery of pVTK and BMP2 was assessed throughout the time course of osteogenic differentiation. Effects of co-delivery of pVTK and BMP2 on osteogenic differentiation were expected to be in line with that of pVTK-only treatments, as was evident at day 6 with the increased ALP activity in the co-delivery group compared to the BMP2-only

group (Figure 3.2C). However, by day 12, continuous BMP2 administration had an inhibitory effect on osteogenic differentiation (Figures 3.2B and 3.2D). This is consistent with studies showing that as cells undergo osteogenic differentiation, they become less sensitive to BMP2 stimulation[16] and that long-term dosing of BMP2 has an inhibitory effect on osteogenic activity[15,17]. Therefore, downregulation of osteogenic activity in the co-delivery group by day 12 were likely due to the effects of long-term BMP2 administration rather than pVTK interfering with osteogenic signaling. Given that pVTK is responsible for inhibiting mineralization in MC3T3 cultures (Figure 3.1A), future work may probe further into the relationship between pVTK and osteogenic signaling pathways.

3.4.3 pVTK inhibits ectopic mineralization in vivo

One of the limitations of peptides as therapeutics is their low in vivo stability when compared with small molecule drugs and biologics[18]. Ex vivo stability testing of pVTK predicted that pVTK was highly stable in mouse plasma (Figure 3.3C) and liver microsomes (Figure 3.7S). Upon injection into the subcutaneous space, pVTK would likely either bind to EM or be transported within the capillaries. For this study, the predicted stability in mouse plasma was the best predictor of stability upon subcutaneous injection. However, pVTK's predicted stability in liver microsomes is important for future drug delivery applications since the liver plays a prominent role in drug clearance.

pVTK inhibited mineralization of BMP2-loaded subcutaneous implants in vivo compared to PBS controls (Figure 3.3D), with an overall reduction in ectopic mineral volume of 92%. Grading of the EM deposits further emphasized the downregulation in ectopic mineral severity due to pVTK treatment with 50% of pVTK-treated samples in the 'Negligible' grade compared 0% of PBS controls (Figure 3.3G).

While micro-CT quantified differences in EM volume, histology showed how mineralization impacted the collagen implant itself. pVTK treatment reduced EM volume and depth of mineral infiltration into the implants when compared with PBS-treated samples (Figure 3.4, VKS). Zones of tissue reorganization at the implant peripheries in pVTK-treated groups corresponded to unmineralized tissue while those in PBS-treated groups corresponded with mineral formation (Figure 3.4, H&E 5X). Fewer cells penetrated into the center of the implant in pVTK-treated samples compared to PBS-treated samples (Figure 3.4, H&E 10X). These histological observations suggested that preventing mineralization via pVTK treatment may have directed cells toward implant encapsulation, though further characterization of the immune response is needed[19]. In the context of this paper, capsule formation could be interpreted positively, as it suggests that the local cells were not reprogrammed by administered BMP2 for ectopic mineralization. This provides preliminary evidence that pVTK may have a different role in non-osteoblast cells, such as immune cells, beyond inhibition of mineralization. More work is needed to understand the impact of reduced cell infiltration due to pVTK treatment, how pVTK interacts with non-osteoblast cell types, and the effect of pVTK on the host immune response to ectopic mineralization.

In the ultimate application of pVTK for prevention of ectopic mineralization with BMP2 therapies, capsule formation could impair the therapeutic effect of BMP2 by preventing integration of the BMP2-loaded sponge with the repairing bone[20]. It is not yet fully understood how pVTK inhibits mineralization and if pVTK's actions are different in ectopic mineralization versus physiological mineralization (e.g. binding differences due to compositional differences). Translational efforts using pVTK must be tailored to promote inhibition of ectopic mineralization without impairing BMP2-augmented bone repair and regeneration, potentially by

leveraging differences in how pVTK interacts with ectopic mineral or by controlling pVTK delivery (spatially and/or temporally).

3.4.4 pVTK inhibits spontaneous, acellular mineralization

Since pVTK was discovered for its mineral-binding capacity, it was hypothesized that pVTK inhibits mineralization by acting on mineral assembly and growth physically and/or chemically. For co-delivery with BMP2, it was important to demonstrate that pVTK does not prevent ectopic mineral formation by interfering with the BMP2 pathway (Figure 3.2). Spontaneous mineralization using mSBF on thin films establishes biomimetic heterogeneous carbonated apatite, resembling the inorganic phase of bone[21]. Additionally, pVTK has an even higher binding affinity for mineralized thin films than for pure hydroxyapatite or other carbonated apatites[7]. When pVTK was added to the mSBF during mineralization, pVTK disrupted spontaneous mineralization at increasing concentrations (Figure 3.5). pVTK not only reduced the amount of mineral formed, but it also altered the morphology of the mineral (Figure 3.5).

Since thin film mineralization is a spontaneous process, any addition to the mSBF solution could potentially disrupt the thermodynamic balance needed to achieve mineralization. In this study, when a scrambled version of pVTK was added to mSBF at the same concentrations as pVTK, the scrambled variant had no effect on spontaneous mineral deposition. Consistent with previous work[9-10], it can be concluded that the sequence of pVTK is critical to inhibit mineralization and that pVTK does not require cells to achieve inhibition. Therefore, pVTK is unlikely to reduce the potency of BMP2. For the larger context of ectopic mineral prevention, the fact that pVTK can inhibit EM formation outside of cellular mineralization mechanisms broadens its potential applications (e.g. spontaneous mineral deposition).

3.4.5 Limitations

While the subcutaneous BMP-loaded implant model has been widely used for ectopic mineralization studies[22], the clinical relevance of this model is limited. For this study, the model was sufficient to demonstrate that pVTK could inhibit ectopic mineral formation in-vivo without causing adverse reactions. However, this model simplifies the clinical scenario for BMP2-loaded implants by isolating the BMP2 drug from the ultimate target of osteoblasts and mesenchymal stem cells, isolating ectopic bone formation from physiological bone formation, and isolating surgical repair processes from bone regeneration processes. These simplifications allowed for the research question at hand to be answered, but future work should introduce more clinically relevant surgical applications (e.g. spinal fusion surgeries) and how pVTK would be targeted to the site of interest. Considering dosing, timing, vehicle, and spatial control for pVTK delivery would be vital to ensure that pVTK does not interfere with physiological mineralization. Further, investigating morphological or compositional differences between ectopic and physiological mineral and how pVTK interacts with different types of mineral formation could inform strategies for specifically targeting ectopic mineral formation.

Though effective in this study, daily subcutaneous injection of free peptide is unlikely to be an efficient strategy for administering pVTK to prevent EM formation. pVTK was predicted to have limited degradation when cultured in mouse plasma (Figure 3.3C) and with liver microsomes ex vivo (Figure 3.7S). However, further investigation is required to assess pVTK's bioactivity and bioavailability after being subjected to degradation, denaturation, or clearance in vivo. To preserve bioactivity and bioavailability, a controlled release system could be developed for long-term administration of pVTK. This would also reduce the clinical burden and increase patient compliance by incorporating pVTK delivery with BMP2 implant surgery rather than

requiring daily injections after surgery. Further, the inflammatory response due to surgery and to BMP2 therapies already causes adverse effects[3], so minimizing additional injections is crucial to limit further inflammation and other complications.

Finally, the sample size used for the in vivo experiment in this study was limited due to cost and the narrow experimental question. Additional studies would expand the sample size in each group and add additional controls (e.g. scram-pVTK or BMP2 antagonist) to further demonstrate the impact of pVTK in preventing ectopic mineral formation secondary to BMP therapies.

3.5 Conclusion

Ectopic mineral formation is a widely recognized side effect of BMP2 therapies, especially when used in off-label surgical scenarios, leading to additional surgeries[23,24] and rare, though life-threatening complications[4]. It was hypothesized that the mineral-binding peptide, pVTK, would decrease EM formation secondary to BMP2 therapy. In this work, pVTK administration significantly reduced EM formation in subcutaneous collagen implants loaded with BMP2. Further, pVTK inhibited BMP2-stimulated mineralization in a pre-osteoblast cell line undergoing osteogenic differentiation without affecting cellular response to BMP2 signaling. To demonstrate a cell-independent mechanism of EM inhibition, pVTK disrupted spontaneous mineral formation in an acellular environment. Therefore, it is believed that pVTK can be co-delivered with BMP2 to inhibit EM formation without competing with BMP2 to control osteogenic signaling.

3.6 Acknowledgements

Thank you to Henriette Remmer (Proteomics and Peptide Synthesis Core) for peptide synthesis. Thank you to Dalis Collins (ULAM Veterinarian) for help with animal surgeries and subsequent animal care. Thank you to Michelle Lynch (Micro-CT Core) for micro-CT scanning and to Rob Goulet (ORL) for assistance with quantification in Dragonfly. Thank you to Bo Wen (Pharmacokinetic and Mass Spectrometry Core) for peptide stability testing. Thank you to Amy Woo for SEM scanning and to Owen Niell (EMAL) for SEM training.

This publication was supported by NIH T32 DE007057 (SJM), NIH P30AR069620 (DHK), Department of Biologic & Materials Sciences BOOST Fund (DHK).

3.7 Figures

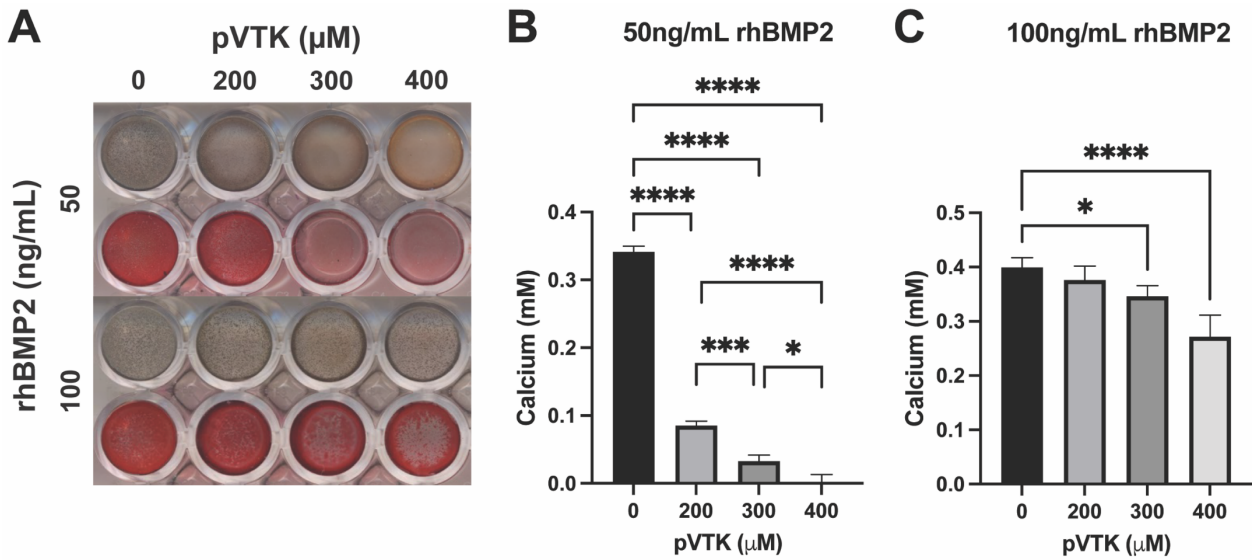


Figure 3.1 pVTK inhibits BMP-stimulated mineralization in vitro

Mineralization of MC3T3s with BMP2 (50 or 100ng/mL) and/or pVTK (0-400μM) was assessed after 12 days in osteogenic media. (A) von Kossa staining (black; first and third rows) identified mineral deposits and Alizarin Red staining (red; second and fourth rows) identified calcium deposits. (B, C) Extracellular matrix calcium was quantified for both BMP levels. Data is represented as means ± standard deviations (n = 3).

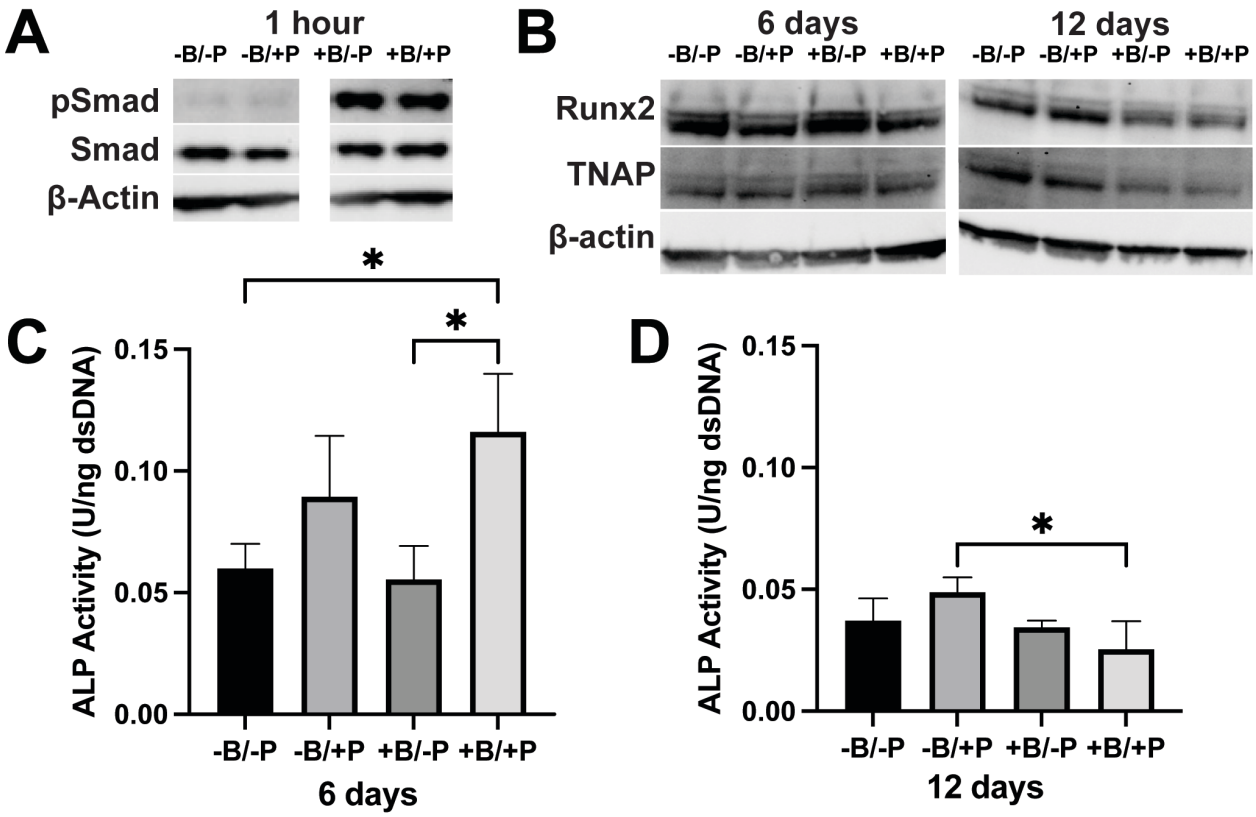


Figure 3.2 pVTK affects BMP-stimulated osteogenic activity differently throughout differentiation

Osteogenic activity in MC3T3s throughout osteogenic differentiation with pVTK (300μM, denoted by ±P) and/or BMP2 (50ng/mL, denoted by ±B). Western blotting evaluated (A) Smad phosphorylation (immediate downstream marker of BMP2 ligand-binding) and (B) intracellular protein levels of Runx2 (early osteogenic marker) and TNAP (mid-late osteogenic marker). Alkaline phosphatase (ALP) activity was quantified at (C) 6 days and (D) 12 days. For Western blot data, representative bands are shown. For ALP activity, data are represented as means ± standard deviations (n = 3).

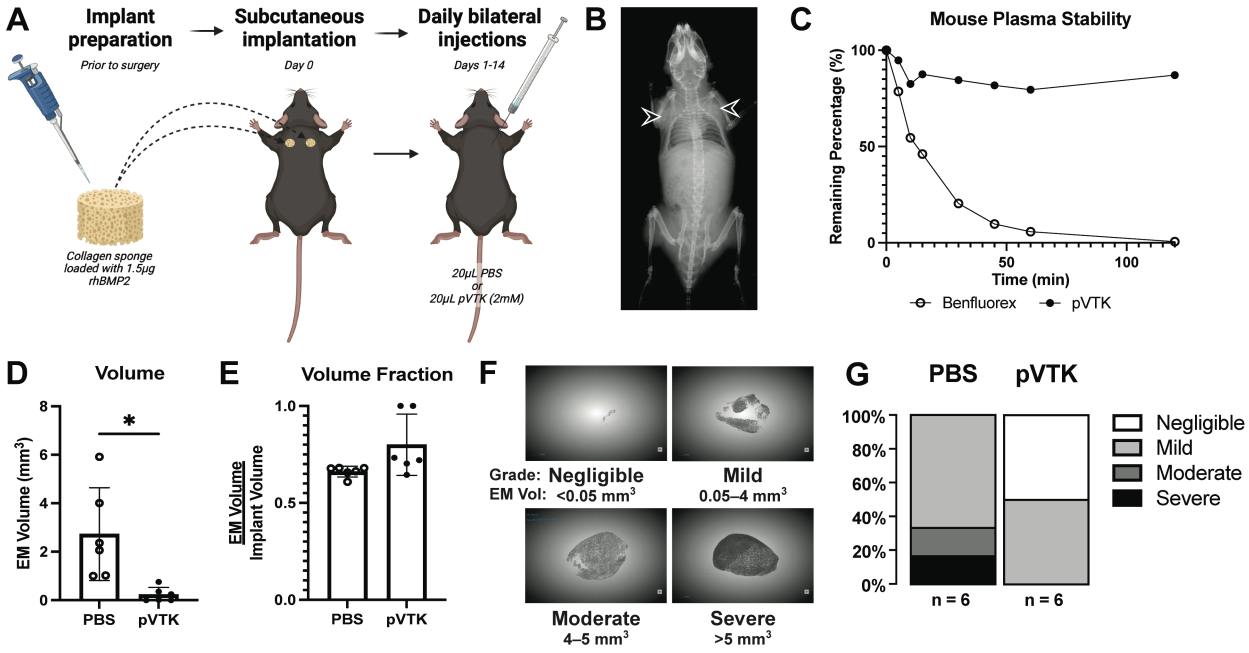


Figure 3.3 pVTK significantly reduces ectopic mineral formation in vivo

(A) Collagen sponges loaded with BMP2 were implanted subcutaneously (bilateral) and daily subcutaneous injections (2mM pVTK or PBS controls) commenced for 2 weeks. (B) Representative X-ray image showing resultant ectopic mineral formation (denoted by arrows). (C) Ex vivo stability testing of pVTK in mouse plasma. (D) Micro-CT quantification of EM volume. (E) Quantification of EM volume fraction (EM volume as a fraction of the total 3D space occupied by EM). (F) Representative images of the grading scheme established to stratify the intensity of EM formation based on EM volume. (G) Distribution of grades based on EM volume by treatment group. Data for volume and volume fraction are represented as means ± standard deviations with individual data points (n = 6).

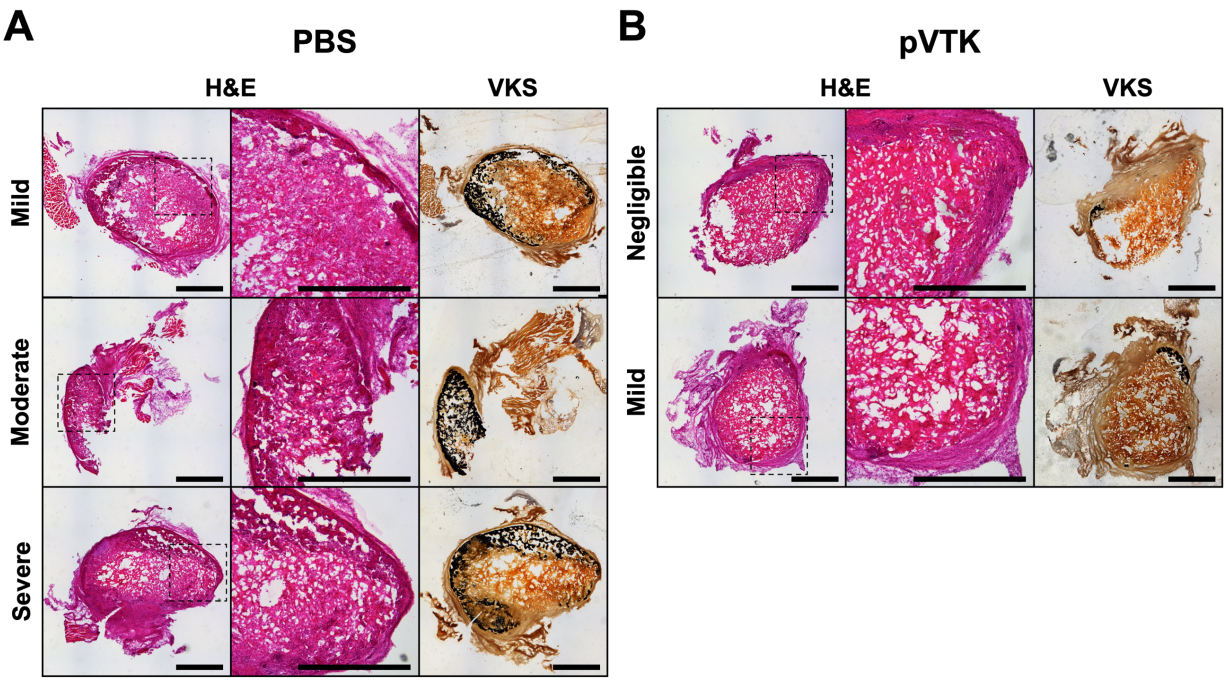


Figure 3.4 pVTK treatment reduces severity of EM formation in subcutaneous implant

Representative histological images of BMP2-loaded implants with (A) PBS or (B) pVTK treatment. H&E (left (5X) and middle (10X) middle columns) stains calcification (deep pink), cell nuclei (purple punctae), and extracellular matrix proteins such as collagen (pink). Von Kossa (right columns) stains calcium phosphate deposits (mineral = black). Images are from 50-µm cryo-sections of undecalcified implants (scale bar represents 1mm).

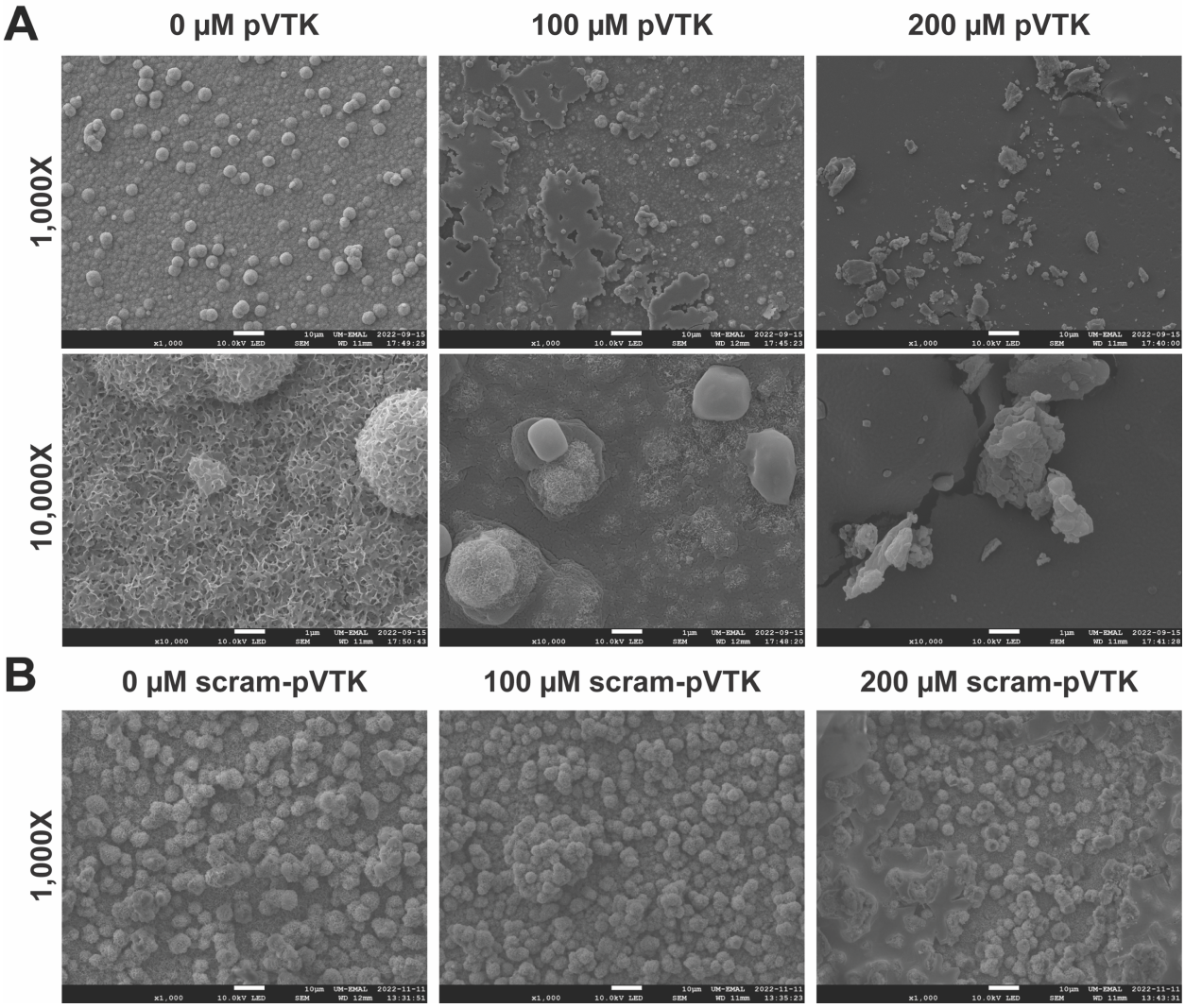


Figure 3.5 pVTK inhibits mineralization outside of cellular machinery

SEM images of thin polymer films mineralized in mSBF (2x) with pVTK (top row: 3,000X, 12µm WD; bottom row: 10,000X, 12µm WD) or scrambled pVTK (3500X, 11µm WD). Typical mineral morphology (as in the 0µM pVTK and 0µM scram-pVTK groups) appears as plate-like structures organized into spherical complexes.

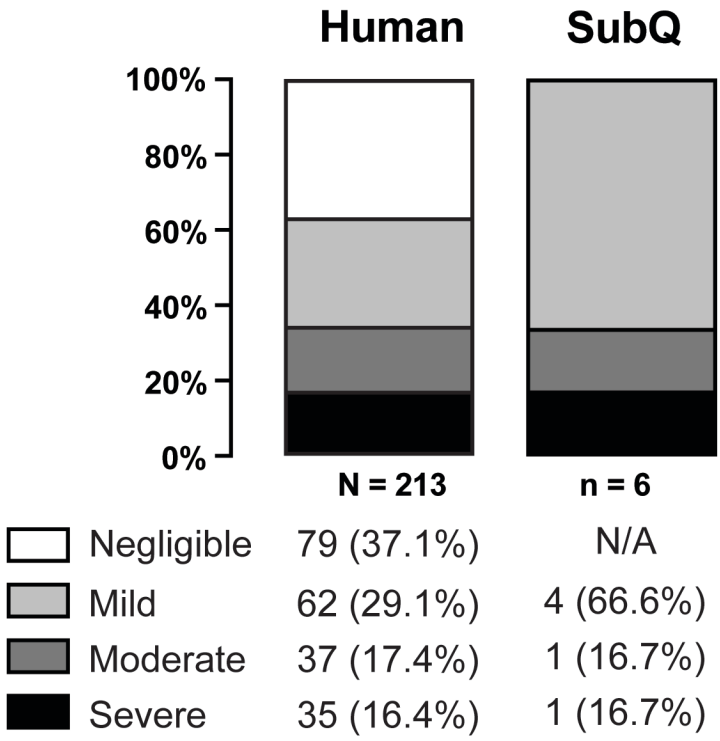


Figure 3.6S Development of EM grading scheme

Grades were established to sort samples by the severity of EM formation. A previous study graded heterotopic ossification (HO) in a large human study by the percent of cross-sectional area occupied by HO, visualized by X-ray[12]. In this study, PBS-treated controls were sorted to match the distribution of HO grades to establish ranges of EM volume for each grade. Distributions are represented visually as cumulative stacked percentages. The legend displays the numbers of samples (and corresponding percentages) for each grade.

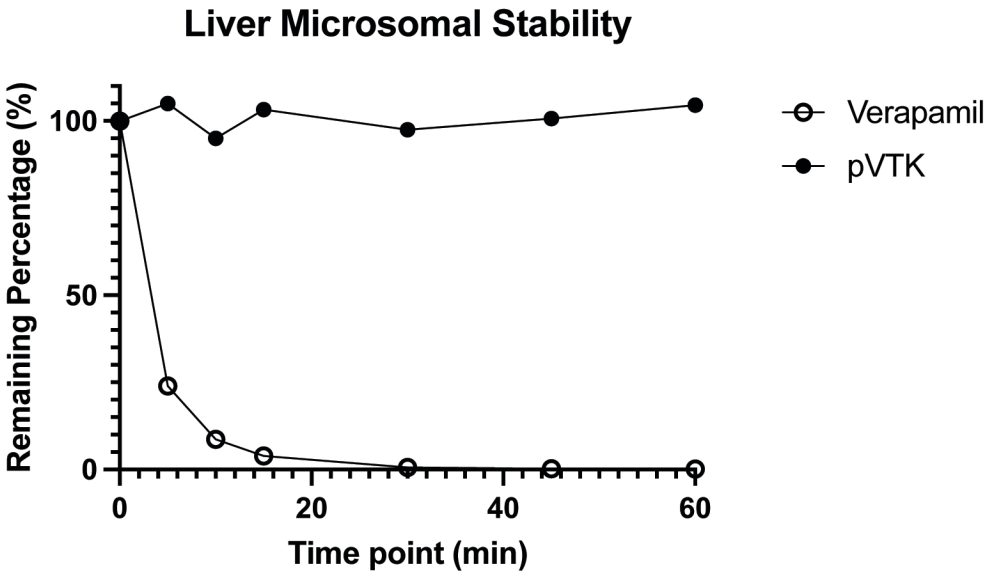


Figure 3.7S Metabolic stability of pVTK in liver microsomes

Metabolic stability of pVTK in liver microsomes isolated from mice was assessed and compared with the negative control Verapamil. pVTK and Verapamil were quantified at each timepoint via LC-MS (liquid chromatography-mass spectrometry). pVTK showed no degradation over the duration of this experiment (60 minutes) while Verapamil degraded fully by the mid-way point (30 minutes).

3.8 References

1. McKay, W. F.; Peckham, S. M.; Badura, J. M. A Comprehensive Clinical Review of Recombinant Human Bone Morphogenetic Protein-2 (INFUSE® Bone Graft). *Int. Orthop.* **2007**, *31* (6), 729–734. https://doi.org/10.1007/s00264-007-0418-6.

2. Lo, K. W.-H.; Ulery, B. D.; Ashe, K. M.; Laurencin, C. T. Studies of Bone Morphogenetic Protein Based Surgical Repair. *Adv Drug Deliv Rev.* **2012**, *64* (12), 1277–1291. https://doi.org/10.1016/j.addr.2012.03.014.Studies.

3. James, A. W.; LaChaud, G.; Shen, J.; Asatrian, G.; Nguyen, V.; Zhang, X.; Ting, K.; Soo, C. A Review of the Clinical Side Effects of Bone Morphogenetic Protein-2. *Tissue Eng. - Part B Rev.* **2016**, *22* (4), 284–297. https://doi.org/10.1089/ten.teb.2015.0357.

4. Wong, D. A.; Kumar, A.; Jatana, S.; Ghiselli, G.; Wong, K. Neurologic Impairment from Ectopic Bone in the Lumbar Canal: A Potential Complication of off-Label PLIF/TLIF Use of Bone Morphogenetic Protein-2 (BMP-2). *Spine J.* **2008**, *8* (6), 1011–1018. https://doi.org/10.1016/j.spinee.2007.06.014.

5. Kim, H. K. W.; Aruwajoye, O.; Du, J.; Kamiya, N. Local Administration of Bone Morphogenetic Protein-2 and Bisphosphonate during Non-Weight-Bearing Treatment of Ischemic Osteonecrosis of the Femoral Head: An Experimental Investigation in Immature Pigs. *J. Bone Jt. Surg. - Am. Vol.* **2014**, *96* (18), 1515–1524. https://doi.org/10.2106/JBJS.M.01361.

6. Kempen, D. H. R.; Lu, L.; Heijink, A.; Hefferan, T. E.; Creemers, L. B.; Maran, A.; Yaszemski, M. J.; Dhert, W. J. A. Effect of Local Sequential VEGF and BMP-2 Delivery on Ectopic and Orthotopic Bone Regeneration. *Biomaterials* **2009**, *30* (14), 2816–2825. https://doi.org/10.1016/j.biomaterials.2009.01.031.

7. Segvich, S. J.; Smith, H. C.; Kohn, D. H. The Adsorption of Preferential Binding Peptides to Apatite-Based Materials. *Biomaterials* **2009**, *30* (7), 1287–1298. https://doi.org/10.1016/j.biomaterials.2008.11.008.

8. Segvich, S.; Biswas, S.; Becker, U.; Kohn, D. H. Identification of Peptides with Targeted Adhesion to Bone-Like Mineral via Phage Display and Computational Modeling. *Cells. Tissues. Organs* **2008**, *189* (1–4), 245. https://doi.org/10.1159/000151380.

9. Addison, W. N.; Miller, S. J.; Ramaswamy, J.; Mansouri, A.; Kohn, D. H.; McKee, M. D. Phosphorylation-Dependent Mineral-Type Specificity for Apatite-Binding Peptide Sequences. *Biomaterials* **2010**, *31* (36), 9422–9430. https://doi.org/10.1016/j.biomaterials.2010.08.064.

10. Ramaswamy, J.; Nam, H. K.; Ramaraju, H.; Hatch, N. E.; Kohn, D. H. Inhibition of Osteoblast Mineralization by Phosphorylated Phage-Derived Apatite-Specific Peptide. *Biomaterials* **2015**, *73*, 120–130. https://doi.org/10.1016/j.biomaterials.2015.09.021.

11. Ling, C.; Zhao, W.; Wang, Z.; Chen, J.; Ustriyana, P.; Gao, M.; Sahai, N. Structure-Activity Relationships of Hydroxyapatite-Binding Peptides. *Langmuir* **2020**, *36* (10), 2729–2739. https://doi.org/10.1021/acs.langmuir.9b03779.

12. Potter, B. K.; Burns, T. C.; Lacap, A. P.; Granville, R. R.; Gajewski, D. A. Heterotopic Ossification Following Traumatic and Combat-Related Amputations. *J. Bone Jt. Surg.* **2007**, *89* (3), 476–486. https://doi.org/10.2106/JBJS.F.00412.

13. Luong, L. N.; Hong, S. I.; Patel, R. J.; Outslay, M. E.; Kohn, D. H. Spatial Control of Protein within Biomimetically Nucleated Mineral. *Biomaterials* **2006**, *27* (7), 1175–1186. https://doi.org/10.1016/j.biomaterials.2005.07.043.

14. Ansari, S.; Ito, K.; Hofmann, S. Alkaline Phosphatase Activity of Serum Affects Osteogenic Differentiation Cultures. *ACS Omega* **2022**, *7* (15), 12724–12733. https://doi.org/10.1021/acsomega.1c07225.

15. Luppen, C. A.; Smith, E.; Spevak, L.; Boskey, A. L.; Frenkel, B. Bone Morphogenetic Protein-2 Restores Mineralization in Glucocorticoid-Inhibited MC3T3-E1 Osteoblast Cultures. *J. Bone Miner. Res.* **2003**, *18* (7), 1186–1197. https://doi.org/10.1359/jbmr.2003.18.7.1186.

16. Luong, L. N.; Ramaswamy, J.; Kohn, D. H. Effects of Osteogenic Growth Factors on Bone Marrow Stromal Cell Differentiation in a Mineral-Based Delivery System. *Biomaterials* **2012**, *33* (1), 283–294. https://doi.org/10.1016/j.biomaterials.2011.09.052.

17. Heggebö, J.; Haasters, F.; Polzer, H.; Schwarz, C.; Saller, M. M.; Mutschler, W.; Schieker, M. Aged Human Mesenchymal Stem Cells: The Duration of Bone Morphogenetic Protein-2 Stimulation Determines Induction or Inhibition of Osteogenic Differentiation. *Orthop. Rev.* **2014**, *6* (2), 65–70. https://doi.org/10.4081/or.2014.5242.

18. Muttenthaler, M.; King, G. F.; Adams, D. J.; Alewood, P. F. Trends in Peptide Drug Discovery. *Nat. Rev. Drug Discov.* **2021**, *20* (4), 309–325. https://doi.org/10.1038/s41573-020-00135-8.

19. Bueno, C. R. E.; Sarmiento, J. L.; Vasques, A. M. V.; da Silva, A. C. R.; Cintra, L. T. A.; Santos, J. M. M.; Dezan-Júnior, E. Biocompatibility, Biomineralization and Induction of Collagen Maturation with the Use of Calcium Hydroxide and Iodoform Intracanal Dressing. *J. Funct. Biomater.* **2023**, *14* (10). https://doi.org/10.3390/jfb14100507.

20. Prochaska, J.; Benowitz, N. Domesticating the Foreign Body Response: Recent Advances and Applications. *Adv Drug Deliv Rev.* **2019**, *144*, 148–161. https://doi.org/10.1016/j.addr.2019.08.010.Domesticating.

21. Murphy, W. L.; Kohn, D. H.; Mooney, D. J. Growth of Continuous Bonelike Mineral within Porous Poly(Lactide-Co- Glycolide) Scaffolds in Vitro. *J. Biomed. Mater. Res.* **2000**, *50* (1), 50–58. https://doi.org/10.1002/(SICI)1097-4636(200004)50:1<50::AID-JBM8>3.0.CO;2-F.

22. Scott, M. A.; Levi, B.; Askarinam, A.; Nguyen, A.; Rackohn, T.; Kang, T.; Chia, S.; James, A. W. Brief Review of Models of Ectopic Bone Formation. *Stem Cells Dev.* **2012**, *21* (5), 655–667. https://doi.org/10.1089/scd.2011.0517.

23. Arzeno, A.; Wang, T.; Huddleston, J. I. Abundant Heterotopic Bone Formation Following Use of RhBMP-2 in the Treatment of Acetabular Bone Defects during Revision Hip Arthroplasty. *Arthroplast. Today* **2018**, *4* (2), 162–168. https://doi.org/10.1016/j.artd.2017.12.004.

24. Boraiah, S.; Paul, O.; Hawkes, D.; Wickham, M.; Lorich, D. G. Complications of Recombinant Human BMP-2 for Treating Complex Tibial Plateau Fractures: A Preliminary Report. *Clin. Orthop. Relat. Res.* **2009**, *467* (12), 3257–3262. https://doi.org/10.1007/s11999-009-1039-8.

Chapter 4 Mineral-Binding peptide Reduces Ectopic Mineralization in Conditional Alk2^{Q207D} Model of Heterotopic Ossification

4.1 Introduction

Ectopic mineralization describes the unwanted deposition of mineral that is non-physiological in terms of amount and/or location. Ectopic mineralization can impact a variety of soft tissues, e.g. vasculature, kidneys, muscle, tendons/ligaments, impairing function and often causing pain. One specific example of ectopic mineral (EM) formation occurs at the endpoint of heterotopic ossification (HO). HO describes the endochondral formation of lamellar bone in soft tissue. While not fully understood, HO is believed to be a dynamic process involving matrix stiffening and reorganization alongside osteochondral differentiation of local soft tissue cell populations (including, but not limited to, mesenchymal stem cells (MSCs), fibro-adipogenic progenitor cells (FAPs), endothelial cells, and immune cells) that ultimately leads to ectopic mineralization[1]. Due to a limited understanding of its etiology and associated risk factors, HO is often not diagnosed until EM is detectable via radiographs though earlier indications include reduced range-of-motion (ROM) and pain[1,2]. Additionally, treatment methods for HO decrease in efficacy as the severity of the disease state (i.e. amount of EM) increases[2].

The current clinical standard for treatment of HO is to use NSAIDs to reduce inflammation and physical therapy to maintain joint mobility to mitigate EM formation[3,4]. In more severe cases, surgical resection of HO is suitable, but only after a 6-month waiting period to ensure that the inflammatory response has subsided[1,5]. Bisphosphonates and radiation have

debatable efficacy and potential for rare, though serious side effects[6,7]. There is a gap in treatment/management options between the less severe cases of HO that can be managed with NSAIDs and physical therapy and the more severe cases of HO that require surgical resection 6 months after injury. Therapeutics currently in development are focused on managing a variety of signaling pathways implicated in HO, e.g. recombinant fetuin-A for immunosuppression[8], palovarotene (a small molecule RARγ antagonist) to suppress chondrogenesis[9,10], and small molecule Alk2 inhibitors (BLU-782, Blueprint Medicines; LDN-193189) to block bone morphogenetic protein signaling[11,12]. However, therapeutics that target specific signaling pathways are currently limited by our incomplete understanding of both HO itself and of any risk factors that could guide appropriate administration. The strategy proposed in this work is to directly limit EM formation, which could prevent disease progression during the wait period prior to surgical resection and/or supplement treatment strategies that target signaling pathways.

Though large biologics (e.g. recombinant fetuin-A) and small molecule drugs (e.g. palovarotene) make up much of drug development for HO, peptide therapeutics offer a promising alternative. Compared to small molecule drugs, peptides are more bioactive and have a higher specificity for their targets, resulting in broader therapeutic potential and fewer off-target effects respectively [13]. Compared to biologics, peptides are cheaper to manufacture and have a lower risk of instigating an immune response[13].

Phage display is a tool to discover peptide sequences with high affinity for a given substrate, providing more control over target specificity. A mineral-binding peptide, VTKHLNQISQSY (VTK), was discovered for its high affinity to hydroxyapatite[14]. Upon phosphorylation of the serine residues (pVTK), not only did pVTK demonstrate a 10-fold higher affinity to hydroxyapatite, but pVTK also inhibited mineralization of an osteoblast cell line[15].

Stability testing in vitro predicted pVTK to be stable in vivo (Chapter 3). Thus, the objective of this study was to test the hypothesis that pVTK could reduce ectopic mineralization in a model of HO both in vitro and in vivo. It is hypothesized that pVTK would interfere primarily with EM formation within the larger HO process to reduce the severity of the disease state. This HO model was the conditional $Alk2^{Q207D}$ model, which utilizes a derivative of the mutation implicated in fibrodysplasia ossificans progressiva (FOP), a disease characterized by spontaneous ossification of joints and soft tissues leading to near-full immobility[12].

4.2 Methods

4.2.1 *Animal model and care*

All procedures were approved by the University of Michigan's Institutional Animal Care and Use Committee (IACUC). All animals used were from the conditional $Alk2^{Q207D}$ (alternatively named ca-Acvr1) model of heterotopic ossification as previously developed[16,17]. The Q207D mutation makes ALK2 (aka ACVR1) constitutively active, i.e., this mutant receptor can transduce BMP-signaling in a ligand independent manner. The $Alk2^{Q207D}$ mutation is Cre-linked and therefore activatable, allowing for ligand-independent BMP signaling, which in combination with cardiotoxin-induced inflammation, induces HO in muscle tissue[12,17]. The $Alk2^{Q207D}$ mutation is maintained as homozygous in a mixture of 129S6 and C57BL6/J background. Animals (WT and mutant) were used at 4-5 days of age for primary cell isolation and animals (mutant only) at 3 weeks of age for in vivo HO induction.

4.2.2 HO induction

For in vivo experiments, HO was induced as described[17]. Briefly, a mixture of Ad5-CMV-cre (Adex-cre) ($0.71x10^9$ PFU/μL, Vector Development Laboratory, Baylor University)

and cardiotoxin (0.3mg/mL, 10μL total injection, Latoxan) was injected bilaterally into each gastrocnemius muscle using a 100μL Hamilton syringe with 26g needle. The Adex-cre mediated permanent Cre recombination to activate the conditional Alk2^{Q207D} mutation resulting in local ligand-independent BMP signaling[16]. Cardiotoxin was administered to increase local muscle inflammation, which is necessary for consistent EM formation[9,17]. EM formation was expected by 14 days post-induction but was apparent by 11 days as demonstrated by severe swelling, increased bleeding at injection site, and increased animal agitation.

4.2.3 Peptide synthesis

Peptide synthesis was performed by the University of Michigan's Proteomics and Peptide Synthesis Core. Peptides were synthesized using solid phase peptide synthesis at a purity of 90% or greater as confirmed by HPLC. Lyophilized peptides were stored at -20℃. For in vitro experiments, pVTK was dissolved in a carbonate-bicarbonate buffer (pH 9) (10mM, sterile-filtered) and stored at -20℃ for up to one month. For in vivo experiments, pVTK was dissolved in PBS (2mM, Gibco) at its maximum solubility, sterile filtered, aliquoted, and stored at -20℃.

4.2.4 Primary calvarial cell isolation

Primary calvarial cells from the conditional Alk2^{Q207D} model were isolated and cultured as described[18]. Animals were euthanized at postnatal days 4-5. Cells isolated from wildtype (WT) animals would not carry the activatable Alk2^{Q207D} mutation, thus are referred to as caAlk2- cells; cells isolated from mutant animals are termed caAlk2+ cells. Calvaria were dissected and cleaned of connective tissue. Then calvaria were cut into 5mm squares and washed in PBS. The first set of digestions was performed in collagenase A (1mg/mL; Roche Diagnostics) and dispase II (1.5mg/mL; Roche Diagnostics) for 10 minutes at 37℃ with rocking (200-300 rpm) and

repeated twice. The second set of digestions was performed in collagenase A (2mg/mL) and dispase II (2mg/mL) for 15 minutes each at 37℃ with rocking (200-300 rpm) repeated twice. Digestion media was collected during each round of the second set of digestions and kept over ice until completion of the final digestion. Digestion media was filtered through a cell strainer and centrifuged at 1500 rpm for 5 minutes. The resultant cell pellet was resuspended, and cells were plated in a 6-well plate at a density of 50,000 cells/cm^2. Cells isolated from the calvaria are a heterogeneous population, so for the purpose of this study, any cells that adhered to the plate were considered capable of osteogenic differentiation. While proliferating to confluence, all cells were treated every other day for 3 total treatments of tamoxifen (100ng/mL, Sigma-Aldrich) which would induce the Alk2^{Q207D} mutation when present. Because the transgenic construct has IRES-EGFP cassette[16,18], Cre-dependent activation of the Alk2^{Q207D} allele in vitro was verified by observing GFP fluorescence (Figure 4.8S)[18].

4.2.5 Cell culture

Primary calvarial cells were maintained in growth media (alphaMEM, Gibco 12561-056; 10% lot-matched fetal bovine serum, Gibco 10082147, Reserve 77813196; 1% penicillin-streptomycin, Gibco 15140-122). For all experiments, cells were plated at a density of 50,000 cells/cm^2. Once plated and allowed to attach overnight, cells were transitioned to osteogenic media made of growth media supplemented with β-glycerophosphate (10mM, Sigma-Aldrich) and ascorbic acid (50μg/mL, Sigma-Aldrich) with or without pVTK (600μM). Osteogenic media was made fresh and changed every 2 to 3 days. Cells were differentiated in osteogenic media for 7 to 21 days.

4.2.6 Staining

Primary calvarial cell mineralization was visualized with von Kossa staining (Figure 4.9S). Cell monolayers were fixed in 10% neutral-buffered formalin for 10 minutes, then washed three times with distilled water. To detect mineral deposits, von Kossa staining was performed via incubation with 5% (w/v) silver nitrate (Sigma-Aldrich) solution for one hour under UV light. Following staining method, cell monolayers were washed at least three times with deionized water or until the wash solution ran clean.

4.2.7 Calcium quantification

Fixed cell monolayers were incubated with 0.5M hydrochloric acid overnight at 4℃. The supernatant was collected, centrifuged at 13,000 rpm for 5 minutes, and assayed for calcium content using the o-cresolphthalein complexone assay method (Stanbio Calcium Liquicolor Kit). Three biological replicates for each experimental group were assayed in triplicate at each timepoint.

4.2.8 Alkaline phosphatase activity

Cell culture lysates were assayed via p-nitrophenyl phosphate assay method (Colorimetric Alkaline Phosphatase Activity Assay, Abcam) and normalized to DNA content (Quant-iT PicoGreen dsDNA Assay, Invitrogen). Briefly, cell culture lysates were harvested in assay buffer after one freeze/thaw cycle at -20℃, sonicated for 5 minutes on ice, and centrifuged at 13,000 rpm for 5 minutes at 4℃. Then, supernatant was collected and used for ALP activity quantification and DNA quantification. Three biological replicates for each experimental group were assayed in duplicate at each timepoint.

4.2.9 Peptide administration in vivo

Starting the day after HO induction, daily peptide injections commenced. Each day, bilateral injections of pVTK (10μL, 2mM) or PBS controls (10μL) were administered into the gastrocnemius muscle using a 100μL Hamilton syringe with 26g needle for 11 days total.

4.2.10 Micro-CT analysis

Following sacrifice at day 11, hindlimbs were dissected, isolating the EM deposit by cutting proximal to the ankle and distal to the femur. Samples were fixed in 4% paraformaldehyde (PFA) overnight at 4°C, transferred to 70% ethanol (EtOH), and submitted to the MicroCT Core at the University of Michigan's School of Dentistry. Samples were scanned with a Scanco μCT 100 micro-computed tomography system at 70 kV, 114 Å, and with a 0.5 Al filter. Scans were acquired at 10μm voxel size, 12μm slice increments, and 1000 projections.

Scans were visualized and analyzed using Dragonfly. First, scans were imported into the software, cropped, and filtered (Median filter). To roughly segment the tibia/fibula from the EM deposit, thresholding was utilized. Then, the ROIs (Regions of Interest) were further refined using the local OTSU segmentation algorithm and manually segmentation as necessary. EM Volume was taken directly from the ROI defined for the EM deposit. To determine volume fraction, the ROI for the EM deposit was expanded using the dilate and close functions until the entire 3D space was filled, then corrected to have the same surface as the original EM ROI using the erode function. Then EM Volume Fraction was defined as the ratio of the EM Volume to the volume of the corresponding filled ROI.

To analyze connectivity of the EM volume, two different approaches were utilized (Figure 4.1)[19]. First, a multi-ROI was created to break the total EM volume into discrete regions (minimum 9 points of connectivity required between voxels to consider them in the same ROI). The resultant parameters were total number of regions, average size of regions, and unity of

discrete regions (defined as the ratio of the largest region volume to total EM volume). Second, the OpenPNM plug-in was used to model the solid EM volume as a (pore) network made of mineral nodules (pores) and connections between nodules (throats)[20]. Since the HO deposit is a solid volume rather than a porous network, OpenPNM models where the mass is concentrated; either in larger, spherical volumes (nodules) or thinner, elongated areas connecting two nodules (connections)[20]. The main requirement placed on the network model was that a throat connected only two pores while pores had an unrestricted number of connecting throats[20]. The resultant parameters were total number of nodules, total number of connections, ratio of connections to nodules, average volume of nodules, average length of connections, and total length of connections.

4.2.11 EM grading scheme

To qualify EM mineral formation, a grading scheme was developed based on EM formation in trauma induced HO[21]. The grading scheme for human trauma-induced HO was based on the percent mineralized area of affected limbs as observed in anteroposterior or lateral radiographs (None, 0%; Mild, <25%; Moderate, >25 - <50%; Severe, >50%)[21]. In this study, EM volume ranges were established to sort the PBS-treated control samples into four grades to match the distribution of grades in the human study: Negligible, 0 - 5 mm^3; Mild, 5 - 30 mm^3; Moderate, 30 - 35 mm^3; Severe, >35 mm^3 (Figure 4.7S). Then, pVTK-treated samples were sorted according to the grades defined by PBS-treated controls.

4.2.12 Histology

Fixed hindlimbs were incubated in 30% sucrose solution overnight at 4°C. Then, samples were embedded in optimal cutting temperature compound (Fisher Healthcare) over dry ice and

stored at -80℃. Embedded tissues were sectioned with the Leica CM1950 cryostat using the CryoJane tape transfer system (Leica) at 50-μm thickness and stored at -20℃. Prior to staining, frozen tissue sections were submerged in 70% EtOH and post-fixed in 4% PFA to ensure thick, undecalcified sections remained attached to glass slides. Hematoxylin and eosin staining (H&E, Sigma) (black; purple; pink) was used to identify general inflammation levels and von Kossa staining (5% silver nitrate) was used to identify mineralized deposits.

4.2.13 Statistical analysis

All statistical analysis was carried out in GraphPad Prism 9. For in vitro data analysis, two-way ANOVAs were used to compare effects of PBS vs. pVTK and caAlk2- vs. caAlk2+. For in vivo data analysis, data was tested for normality using the Shapiro-Wilks test. For normal data (volume, volume fraction, and OpenPNM analysis), t-tests were used to compare effects of PBS vs. pVTK. For non-normal data (MultiROI analysis), Mann-Whitney test was used to compare effects of PBS vs. pVTK. Significance was reported for $p < 0.05$ (*).

4.3 Results

4.3.1 pVTK reduced osteogenic activity and mineralization in vitro

pVTK treatment significantly decreased ALP activity in caAlk2+ cells at 14 days (Figure 4.2B, $p = 0.0340$) but had no effect on either cell type at 7 days (Figure 4.2A). pVTK treatment significantly decreased calcium content in both caAlk2- ($p = 0.0300$) and caAlk2+ cells ($p = 0.0479$). However, there was no difference in calcium content between untreated caAlk2- cells and untreated caAlk2+ cells at 21 days.

4.3.2 pVTK reduced amount and severity of ectopic mineralization in vivo

Visualization of HO 11 days after induction of the conditional Alk2^{Q207D} mutation was accomplished via X-ray imaging (Figure 4.3A). Micro-CT quantification showed that pVTK treatment resulted in a significant decrease of EM volume (Figure 4.3B, $p = 0.0117$) and no difference in EM fraction (Figure 4.3C). For in vivo analysis, the term 'HO' will be used when discussing the overall process resulting EM formation, and the term 'EM' will be used in reference to the output of the HO model. Any effect of pVTK will be discussed relative to 'EM' only since pVTK's role within the overall HO process is not examined in this work.

Representative images for the EM grading system are shown in Figure 4.3D and the distributions of samples for each treatment group are shown in Figure 4.3E. pVTK treatment downshifted the severity of EM formation, resulting in only Negligible or Mild EM formation. No EM formation occurred in 3 of 20 hindlimbs (15%). Since all instances of no EM formation occurred in PBS-treated animals, the hindlimbs with no EM were removed from micro-CT quantification (Figure 4.3B and 4.3C) but not from the analysis of EM grade distribution (Figure 4.3E).

Representative histological images of HO after PBS and pVTK treatment are shown in Figure 4.4. H&E staining (Figure 4.4, left columns) showed tissue reorganization related to HO and EM formation in all groups, with no grade dependence, demonstrated by sections high cellular density (light purple punctae) and dense collagen regions (continuous deep pink regions). Comparing the H&E staining with the von Kossa staining (Figure 4.4) verified that tissue reorganization expanded beyond the boundaries of formed EM.

4.3.3 pVTK fragmented ectopic mineral formation without altering density

Multi-ROI analysis showed that pVTK treatment significantly decreased both the number of discrete regions (Figure 4.5B, $p = 0.0250$) and the average volume of the discrete regions

(Figure 4.5C, p = 0.0133). Additionally, a measure of region unity was established as the ratio between the volume of the largest region in the multi-ROI over the volume of the EM. pVTK treatment significantly decreased this region unity measure (Figure 4.5D, p = 0.0431). pVTK treatment significantly reduced the number of nodules (p = 0.0108; Figure 4.6B) and the average volume of nodules (p = 0.0097; Figure 4.6E) of the EM networks. pVTK treatment also reduced the number of connections (p = 0.0236; Figure 4.6C) and the total length of connections (p = 0.0177; Figure 4.6G). However, pVTK treatment had no effect on the ratio of connections to nodules or the average length of connections (Figures 4.6C and 4.6F, respectively).

4.4 Discussion

The goal of this work was to investigate the therapeutic potential of pVTK for EM prevention in severe cases of HO where current treatment and management options are limited. Since pVTK successfully inhibited mineralization in a pre-osteoblast cell line, it was hypothesized that pVTK would have the capacity to inhibit or disrupt non-physiological mineralization as well. In the caAlk2 model, pVTK reduced mineralization and osteogenic activity in vitro (Figure 4.2) and reduced EM formation and EM severity in vivo (Figure 4.3). pVTK increased fragmentation of the EM deposits in-vivo without affecting the density or packing of mineral (Figures 4.5 and 4.6). Altogether, pVTK has potential as a peptide therapeutic with the ability to prevent severe cases of EM formation, to prevent coalescence of smaller EM deposits, and prevent EM formation in HO at higher dosing.

4.4.1 pVTK reduced osteogenic activity in vitro

During the 21-day differentiation scheme, osteogenesis of primary calvarial cells was demonstrated through increases in ALP activity (days 7 and 14) and calcium secretion (day 21)

(Figure 4.2). At day 14, pVTK treatment limited ALP activity in caAlk2+ cells to the level of caAlk2- cells with or without pVTK treatment, negating the effect of the Alk2 mutation on increasing ALP activity (Figure 4.2B). Additionally, pVTK treatment resulted in significant reductions of the extractable calcium content in the extracellular matrices in both caAlk2+ and caAlk2- cells (Figure 4.2C). Taken together, these results demonstrated that pVTK reduced mineralization and osteogenic activity in primary calvarial cells from a genetic model of HO. By demonstrating a capacity to limit both osteogenic activity and mineralization in vitro, pVTK shows potential to disrupt the mineralization pathway earlier than just limiting mineralization itself, broadening its therapeutic impact.

However, this result is not consistent with data showing that pVTK has no effect on the BMP osteogenic signaling pathway (Figure 3.2) and a stimulating effect on the Enpp1-TNAP-Ank mineralization pathway[22]. pVTK operates primarily by physically inhibiting mineral deposition and growth (Figure 3.5)[23]. In this paper, pVTK treatment resulted in decreased ALP activity by day 14 in caAlk2+ cells, indicating that pVTK may affect cell activity. caAlk2+ cells were an uncharacterized heterogeneous population of cells isolated from mouse calvaria, potentially including but not limited to osteoblasts, osteoclasts, fibroblasts, and mesenchymal stem cells. Since this cell population is not purely comprised of osteoblasts, ALP activity may be attributed to other cell activities beyond osteogenic differentiation. Therefore, more work is needed to understand how pVTK inhibits mineralization and affects non-osteoblast cell types.

4.4.2 pVTK reduced amount and severity of ectopic mineralization in vivo

pVTK treatment significantly reduced EM formation in vivo compared to PBS treatment (Figure 4.3B). There was no difference in volume fraction between treatment groups, indicating no difference in EM density (Figure 4.3C). A grading scheme was developed to classify samples

based on EM volume, modified from an area-based grading scheme to classify human HO. pVTK-treated hindlimbs occupied only the two least severe grades compared to the wider range of severity in the PBS-treated controls (Figure 4.3E). These results answered the main question of this study, demonstrating that pVTK was successful in alleviating EM formation.

High levels of inflammation, attributed to daily intramuscular injections, were expected due to observed animal discomfort and increased bleeding. Further, range-of-motion evaluations did not correlate with increased ectopic mineral formation, indicating that range of motion may be influenced more by soft tissue swelling and inflammation (observational data not shown). At the microscopic level, not all samples showed histological evidence of an inflammatory reaction; high cellular density associated with tissue reorganization was noticed in samples in the 'Moderate' PBS-treated and 'Mild' pVTK-treated groups (Figure 4.4, H&E). Further work is needed to characterize the inflammatory response to daily intramuscular injections (e.g. identification and quantification of infiltrating cell types) and/or develop a different delivery mechanism that reduces or eliminates the need for daily injections.

Histological imaging was also done to visualize relative levels and corresponding areas of tissue reorganization and mineralization (Figure 4.4). All samples with EM formation showed tissue reorganization largely surrounding any EM (Figure 4.4, H&E and VKS). However, some samples showed more tissue reorganization than others, not necessarily corresponding with increasing grade (i.e. increasing EM volume). Since tissue reorganization was not correlated with ultimate EM formation, two potential explanations for the tissue reorganization are inflammation (due to injections and/or HO development) and cartilage formation (since HO is known to form via endochondral ossification). More characterization of these tissue reorganization area, in terms of cell types and cell activities, may add insight into how pVTK treatment impacts non-

osteoblast cells and stages of HO development prior to EM formation. Additionally, when looking at the 'Moderate' PBS-treated sample, EM ingrowth into the tibia altered the physiological appearance of the tibia itself, a side effect noticed in other samples with no preference to treatment. Since these histological observations did not correlate with EM grades, this may indicate that a grading scheme based solely on EM volume may not be appropriate for such a dynamic disease state. Future work may work to incorporate these qualitative measures (e.g. inflammation, cartilage formation, and interference of EM with native bone) into an optimized grading scheme for EM severity.

Current prophylactic strategies are more effective at preventing EM formation in milder cases of HO[2]. Additionally, improvements of peptide delivery (e.g. controlled release, increased concentration, co-delivery with other agents to reverse EM formation) could position pVTK as a preventative therapeutic as well. In MC3T3s, pVTK has a threshold for complete mineral inhibition with incomplete inhibition at concentrations below the threshold[15]. Therefore, it is expected that at a yet-to-be-determined in-vivo threshold concentration, pVTK would fully prevent ectopic mineralization.

4.4.3 pVTK fragmented ectopic mineral formation without altering density

During the initial X-ray imaging, qualitative observations were made that HO intensity was increased in PBS-treated limbs compared to pVTK-treated limbs. While volume fraction was shown to be the same between the two treatment groups (Figure 4.3C), volume fraction is an averaged measure of density. Therefore, additional quantitative micro-CT analyses were developed to further explore differences in EM packing due to treatment method.

Multi-ROI analysis was performed to assess EM packing under the assumption that the EM volume not continuous. Using multi-ROI analysis, EM volume was broken into discrete

regions based on voxel connectivity. It was shown that pVTK treatment significantly reduced the number (Figure 4.5B) and the average volume of discrete regions (Figure 4.5C). Additionally, pVTK treatment decreased the region unity of the EM volume (defined as the ratio of the largest discrete ROI from the multi-ROI analysis to the total EM volume) (Figure 4.5D). This resulted in more pVTK-treated samples with multiple large ROIs making up 30-60% of the full EM volume rather than one large ROI making up greater than 90% of the full EM volume, as in the PBS-treated samples (Figure 4.5D). The decreases in number, size, and unity of the multi-ROIs indicates that pVTK treatment resulted in smaller individual deposits of EM. It is hypothesized that pVTK inhibits mineralization by binding to early mineral nucleates and preventing crystal growth and organization. Therefore, it could be possible that pVTK reduced EM region number, size, and unity by binding to early, smaller EM deposits and interfering with mineral growth and fusion into larger EM deposits.

Network analysis was then performed to assess EM packing under the assumption that EM volume was one connected body. Network analysis represented the EM volume as a web of nodules and connections. pVTK treatment significantly reduced nodule number and size compared to PBS controls (Figure 4.6B). pVTK treatment also reduced connection number (Figure 4.6C) and total length (Figure 4.6G), but not average connection length or the ratio of connections to nodules. The changes in the EM network due to pVTK treatment were all in extrinsic values that should not be considered separately from decrease in total EM volume due to pVTK treatment. Rather than causing the EM to compact and become denser to fit into a smaller volume, pVTK treatment shrunk the web as a whole. This aligns with the proposed hypothesis that pVTK interferes with crystal growth and the resultant amalgamation of EM deposits as growth progresses.

The two different morphological analyses placed emphasis on different aspects of spatial distribution. Multi-ROI analysis assumed that the EM volume was not entirely connected, leading to analysis of the individual pieces that make up the EM volume. Multi-ROI analysis resulted in a skewed distribution of many smaller, non-connected mineral deposits and one large main mineral deposit. This highlighted a key difference between treatments: peptide therapy resulted in more instances of the largest deposit making up a smaller percentage of the total EM volume. On the other hand, OpenPNM analysis assumed that the EM volume was connected, which led to analysis of how the mineral mass was distributed throughout the EM volume and placing less emphasis on the smaller, non-connected mineral nodules. OpenPNM analysis verified that the density of the EM mineral was unchanged by pVTK treatment, as shown in the volume fraction quantification (Figure 4.3C).

While standard micro-CT analysis showed that pVTK decreased EM formation (Figure 4.3), additional analyses added context to this decrease by showing that the EM volume formed in the presence of pVTK was broken into smaller pieces that retained a similar density to control EM (Figures 4.5 and 4.6). It is likely that pVTK slowed or constrained EM formation and coalescence. Importantly, fewer, smaller EM deposits would be easier to sustain or even reduce via range of motion therapies and non-steroidal anti-inflammatory drugs (NSAIDs) which are the current standards of care effective for mild cases of HO[4]. Additionally, slowed EM formation would prevent EM progression during the waiting period prior to surgical resection. Further, reducing the size of individual nodules without packing the nodules tighter together results in a larger surface area upon which resorption agents or pro-osteoclastic agents can act to break down already formed EM. The additional morphological assessment of EM formation provided

evidence that pVTK could aid in treatment of EM, even at sub-inhibitory levels, since pVTK treatment interfered with mineral growth and coalescence.

4.4.4 Limitations and Future Directions

pVTK reduced ALP activity in caAlk2+ cells and significantly reduced calcium deposition in caAlk2- and caAlk2+ cells, but there was no difference in the baseline mineralization between WT and mutant cells (Figures 4.2C and 4.7S). Validation of the methods for in vitro activation of the genetic mutation confirmed that caAlk2+ cells were positive for the $Alk2^{Q207D}$ mutation throughout the duration of culture (Figure 4.8S). However, the isolated calvarial cell populations were heterogeneous, so the percentage of cells capable of mineralization may not have been high enough to demonstrate differences in mineral output due to the $Alk2^{Q207D}$ mutation. Future studies may aim to characterize this cell population further and optimize methods for osteoblast isolation and osteogenic differentiation in vitro.

Delivering pVTK via daily intramuscular injection was deemed sufficient to answer the question of whether pVTK affected EM formation in vivo. pVTK was predicted to have a high stability in vivo and intramuscular injections allowed for administration at or near the site of EM formation. However, the maximal peptide dose was limited to the solubility of the pVTK in PBS. Future work could focus on increasing the available dosing, e.g. through changing the delivery solvent or developing a controlled release system, to achieve full inhibition of EM formation.

Another drawback to daily intramuscular injections is that they appeared to exacerbate HO in the caAlk2 model. Previous work with this model reliably showed HO 14 days after induction, with little to no mineral formation noticed within the first 7 days after induction[24]. However, in this study, HO was noticeable at day 7 (data not shown) and the study was ended prematurely at day 11 due to noticeable distress and bleeding in both treatment groups. Human

patients with FOP are recommended to avoid intramuscular injections since even that small wound can be enough to cause flare-ups[25]. A similar response was unanticipated in this mouse model due to the localization of the genetic mutation, but this was the first instance of using daily intramuscular injections. Future studies would focus on developing a controlled release system for pVTK to eliminate daily injections while maximizing bioavailability of pVTK at the site of HO.

While the primary goal of this study was to demonstrate that pVTK could be a peptide therapeutic for ectopic mineralization, pVTK's inhibitory ability is not unique to EM formation in HO. Having demonstrated that pVTK can limit physiological mineralization in a pre-osteoblast cell line and non-physiological mineralization in a mutant primary calvarial cell population, it is predicted that pVTK would be effective against many different pathological biomineralization phenotypes. Though more work is needed to characterize any role of pVTK within osteogenic or other mineral-forming mechanisms, pVTK could likely be employed as an interventional or preventative therapeutic in a variety of disease states involving ectopic mineralization, such as vascular calcification, kidney stones, and breast cancer.

4.5 Conclusion

Results from this study showed that pVTK can reduce ectopic mineralization in a model of HO at both the in vitro and in vivo levels. In primary calvarial cells, pVTK offset the upregulation in ALP activity due to the presence of the Alk2 mutation by 14 days and significantly reduced calcification of the extracellular matrix by 21 days. In vivo, pVTK reduced total EM formation by 61% and reduced the severity of resultant EM formation. Morphological analysis of the EM volumes showed that pVTK reduced the unity of formed EM deposits and scaled down the EM volume without increasing EM density. Altogether, this study demonstrates

that limiting ectopic mineralization via mineral-binding peptides could be added to the current treatment and management strategies for HO.

4.6 Acknowledgements

Thank you to Yuji Mishina for providing the animals used in this study and performing the in vivo experiments. Thank you to Haichun Pan for providing the protocol, training, and genotyped animals for primary cell isolation. Thank you to Henriette Remmer (Proteomics and Peptide Synthesis Core) for peptide synthesis. Thank you to Michelle Lynch (Micro-CT Core) for micro-CT scanning and to Rob Goulet (ORL) for assistance with micro-CT analysis in Dragonfly.

This publication was supported by NIH T32 DE007057 (SJM), NIH P30AR069620 (DHK), Department of Biologic & Materials Sciences BOOST Fund (DHK), International Fibrodysplasia Ossificans Progressiva Association (YM), RIKEN Institute (YM), National Institutes of Health NIDCR R01DE020843 (YM).

4.7 Figures

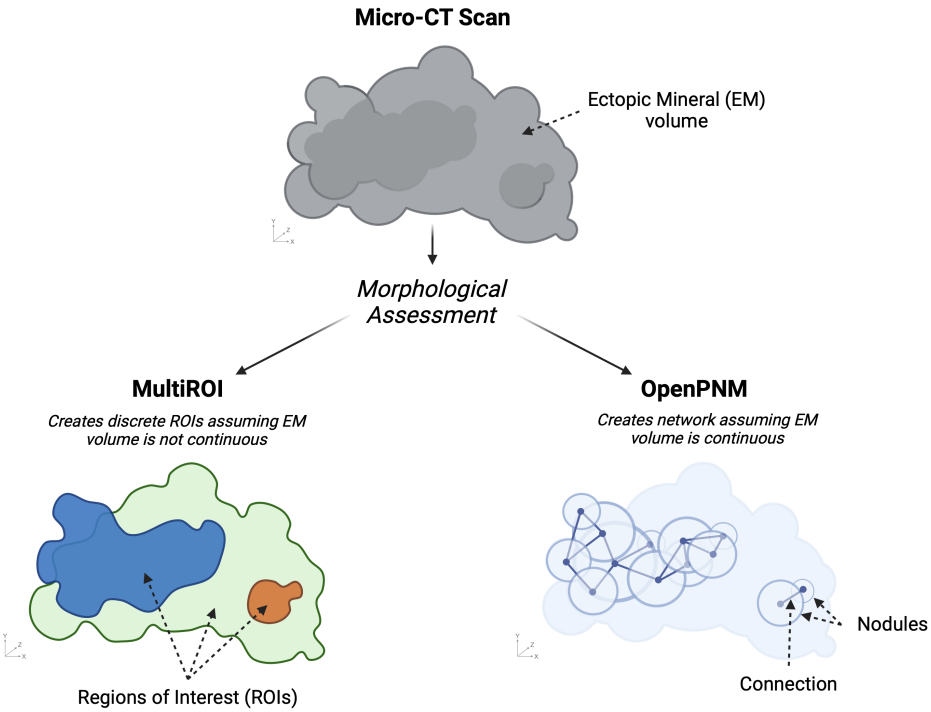


Figure 4.1 Schematic for morphological analysis of ectopic mineral

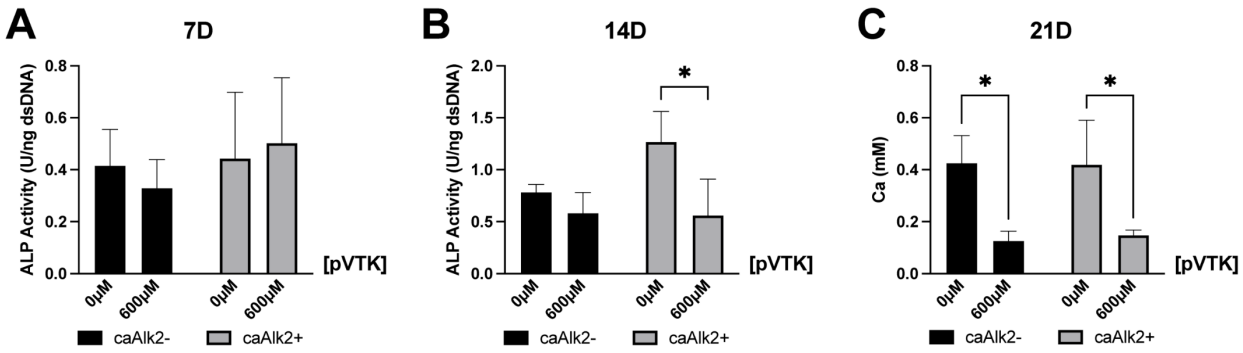


Figure 4.2 pVTK reduces osteogenic activity and mineralization in primary calvarial cells in vitro

caAlk2- and caAlk2+ cells were subjected to a 21-day osteogenic differentiation scheme with or without pVTK. Osteogenic activity was assessed via ALP activity at 7 days (A) and 14 days (B), and mineralization was assessed via extracellular matrix calcium quantification at 21 days (C). Data is presented as means ± standard deviations (n = 3).

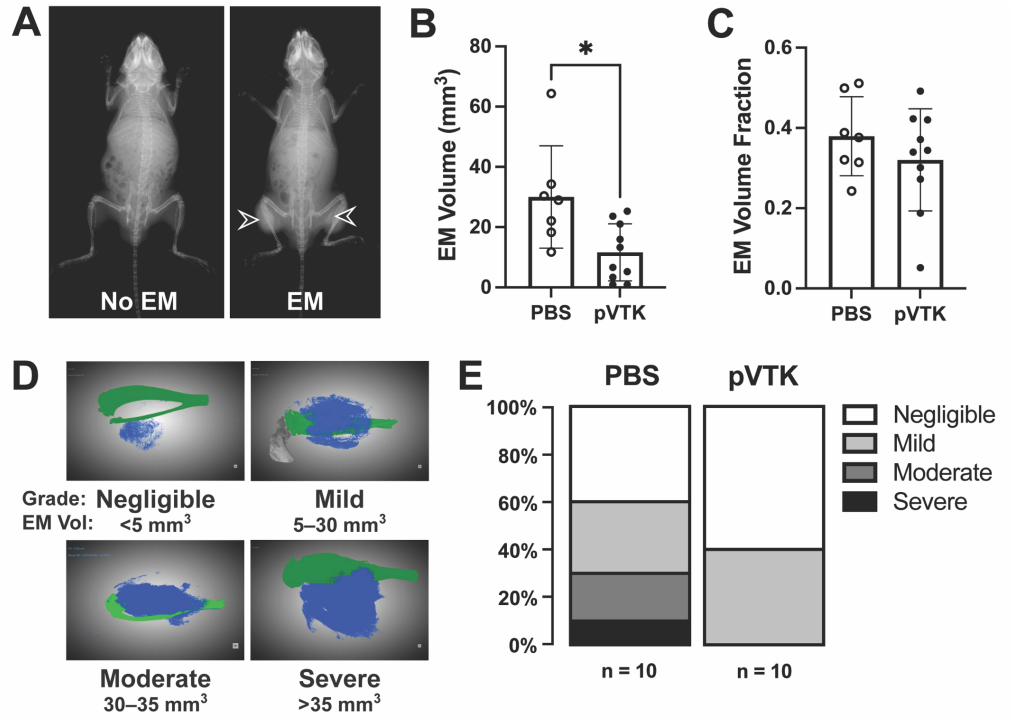


Figure 4.3 pVTK reduces in vivo EM formation in conditional Alk2^{Q207D} model

(A) X-ray images of caAlk2+ animals that exhibited no HO (left panel) and intense HO (right panel, indicated by arrows). (B) Quantification of EM volume via micro-CT. (C) Quantification of EM fraction as the ratio of EM volume to the 3D space occupied by the EM. (D) Representative images to demonstrate the EM grading scheme along with the corresponding EM volume ranges. The green ROI encompasses the tibia and fibula; the blue ROI includes the EM. (E) Distribution of EM grades within each treatment group according to the grading system in (D). Data for volume and volume fraction is presented as means ± standard deviations with individual data points (n_{PBS} = 7; n_{pVTK} = 10).

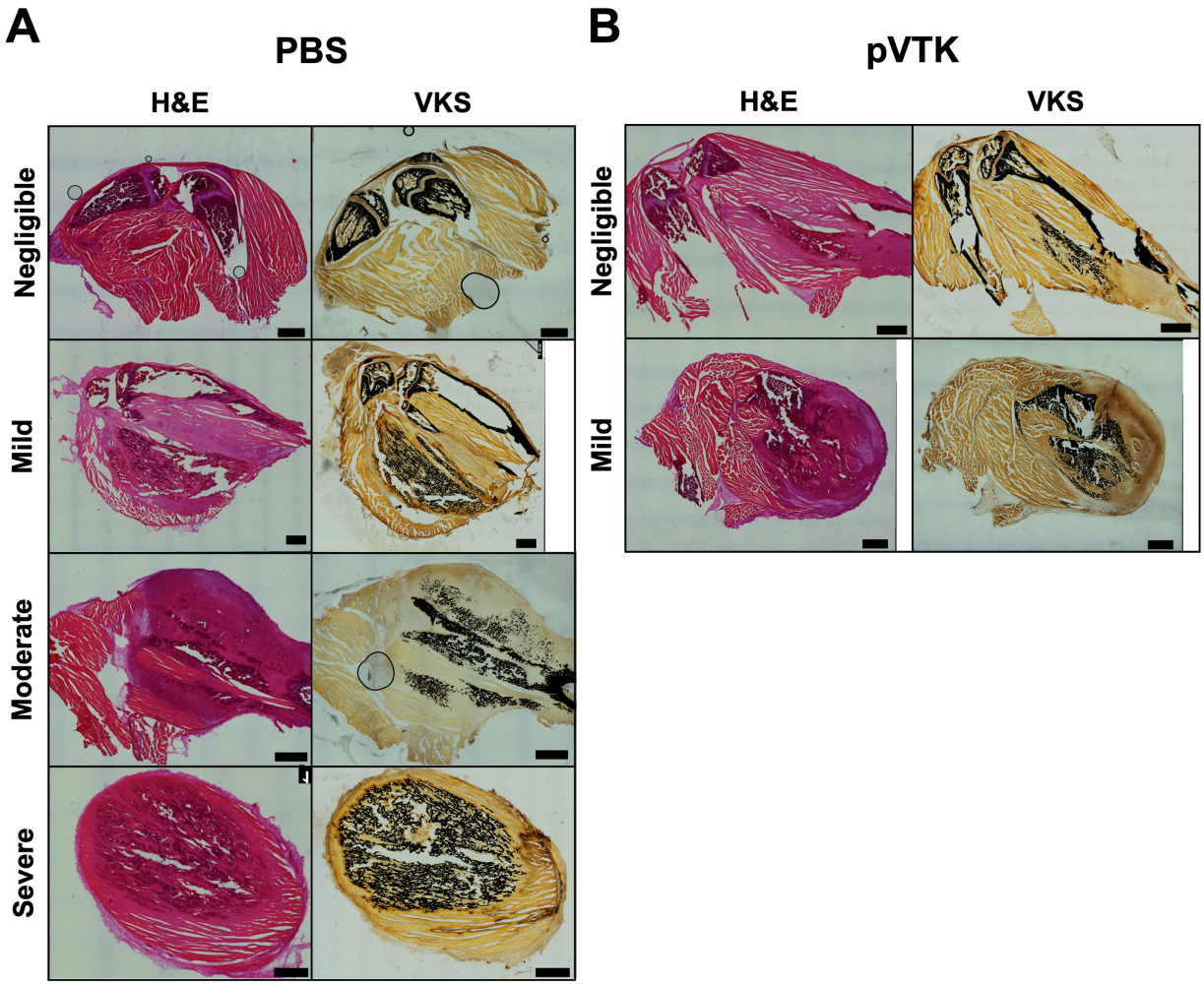


Figure 4.4 pVTK treatment reduces ectopic mineral severity but not tissue reorganization

Representative histological images of HO with (A) PBS or (B) pVTK treatment. H&E (left columns) stains calcification (deep pink), cell nuclei (purple punctae), and extracellular matrix proteins such as collagen (pink). Von Kossa (right columns) stains calcium phosphate deposits (mineral = black). Images are from 50-µm cryo-sections of undecalcified hindlimbs (scale bar represents 1mm).

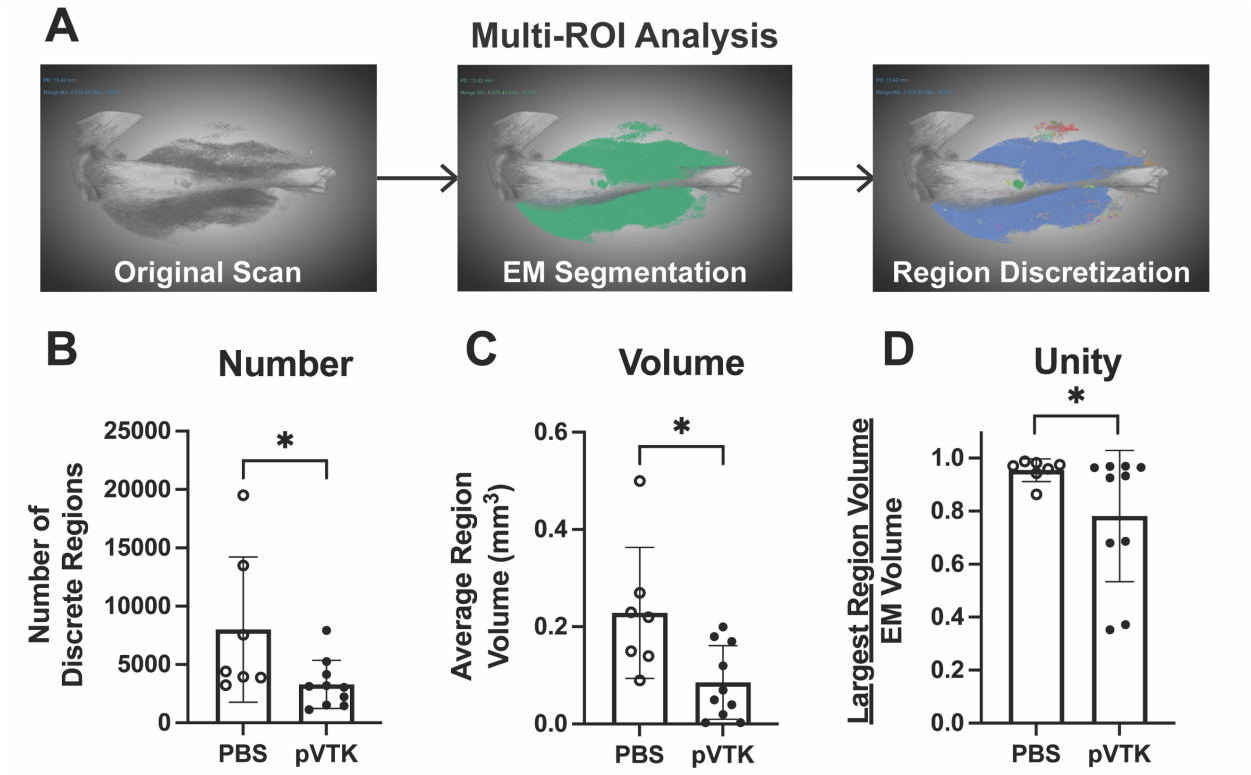


Figure 4.5 pVTK treatment resulted in fragmentation of EM

(A) Sample images to demonstrate Dragonfly's Multi-ROI analysis. Parameters quantified with the Multi-ROI analysis include: (B) Number of discrete regions; (C) Average volume of discrete regions; and (D) Unity of discrete regions for each sample (as a ratio of the volume of the largest region of the multi-ROI over the total EM volume). Data presented as means ± standard deviations with individual data points ($n_{PBS} = 7$; $n_{pVTK} = 10$).

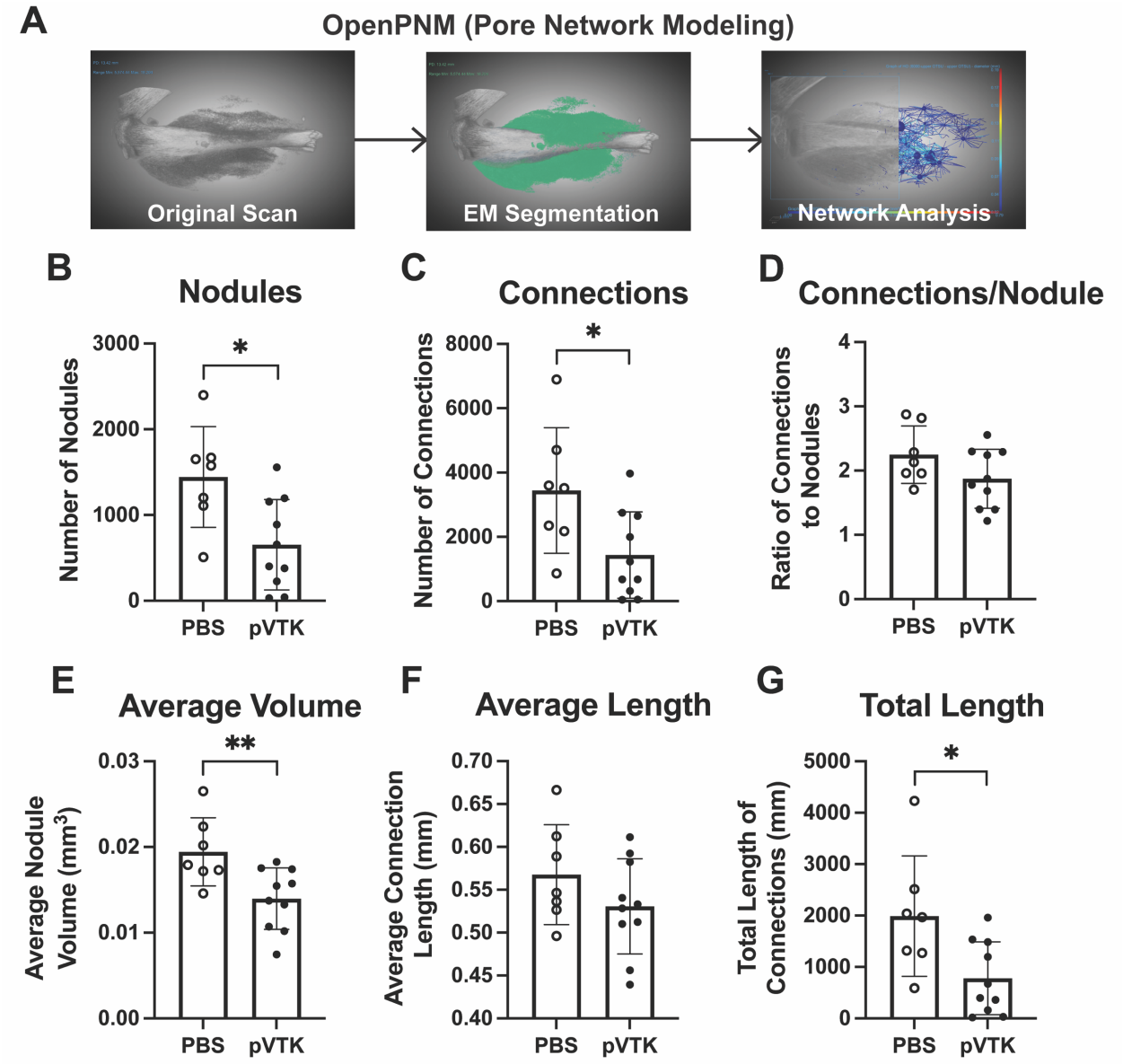


Figure 4.6 pVTK treatment reduced size of EM network without altering overall connectivity

(A) Sample images to demonstrate Dragonfly's OpenPNM analysis. Parameters quantified with the OpenPNM analysis include: (B) Number of nodules; (C) Number of connections; (D) Ratio of connections to nodules; (E) Average volume of nodules; (F) Average length of connections; and (G) Total length of connections. Data presented as means ± standard deviations with individual data points ($n_{PBS} = 7$; $n_{pVTK} = 10$).

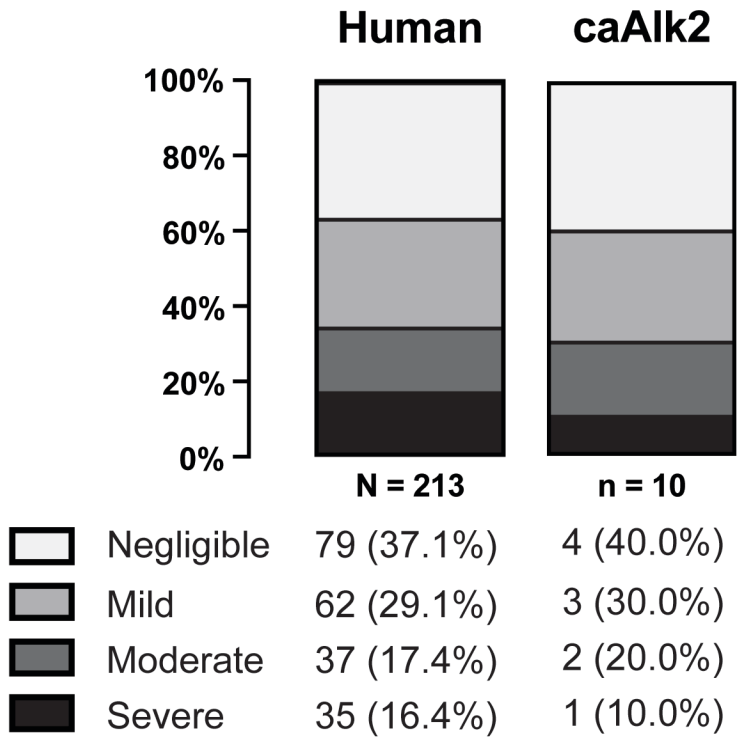


Figure 4.7S Compared distributions of human and caAlk2 mouse samples within EM grading schemes

To qualify the severity of EM formation, an EM grading scheme was developed for this study based on results from a large human study of EM in trauma-induced HO (N =213)[21]. In the human study, grades were defined by the percent of the cross-sectional area taken up by EM in affected limbs (visualized via 2D radiographs). Sorting of the human radiographs into respective grades established an expected distribution of EM that was used to define ranges for EM in the PBS-treated controls. Ranges of EM volume (quantified and visualized via micro-CT) were established to achieve the same distribution of PBS-treated control mice (n = 10) as previously published in the human study (N = 213). Distributions are represented visually as cumulative stacked percentages. The legend displays the numbers of samples (and corresponding percentages) for each grade.

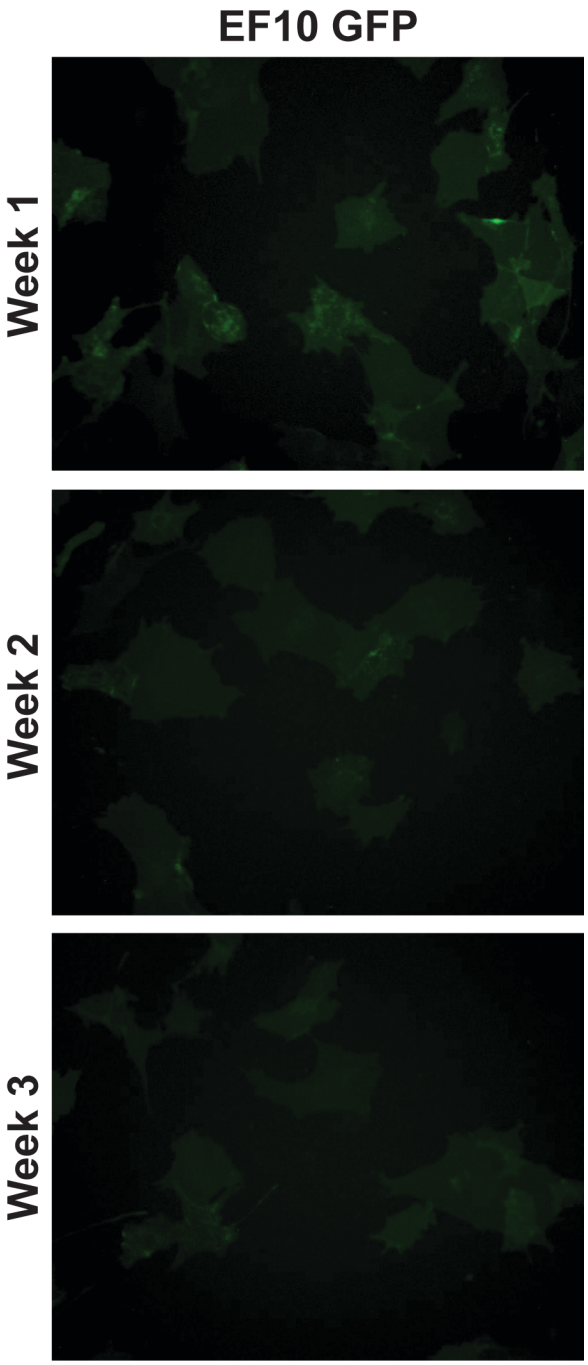


Figure 4.8S Verification of in vitro induction of $Alk2^{Q207D}$ gene expression and maintenance through culture period

Fluorescent images of calvarial cells after mutation induction and up to 3 weeks of culture in osteogenic differentiation medium. Cells were previously isolated by HP from caA2(+)(+)mT/mTTAK1+/+Ubc(+) mice, which contained a GFP protein linked to the mutated Alk2 insert, to verify in vitro activation of the Cre-inducible mutation[16]. Brightness/contrast of these images has been adjusted to normalize background fluorescence.

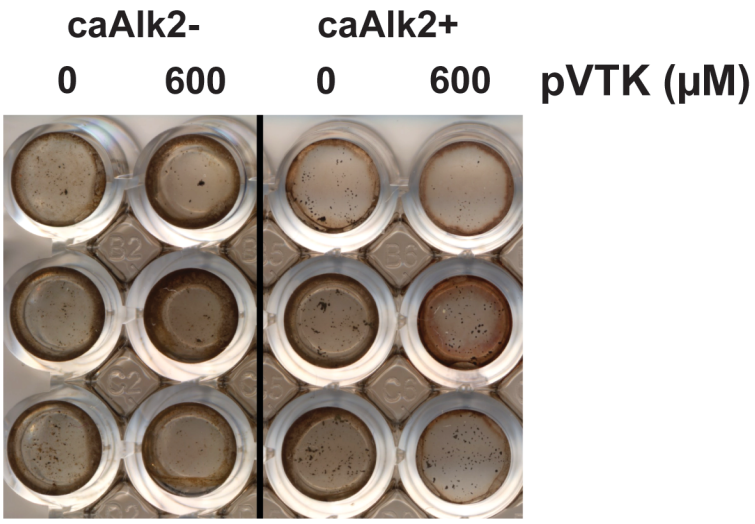


Figure 4.9S Visualization of mineralization patterns in caAlk2- and caAlk2+ cells

Primary calvarial cells were cultured in osteogenic media for 3 weeks and then subjected to von Kossa staining to identify calcium deposits. Minimal differences were observed between caAlk2- and caAlk2+ cells, counter to expectations that caAlk2+ cells would have more robust mineralization due to unrestricted BMP signaling.

4.8 References

1. Hwang, C. D.; Pagani, C. A.; Nunez, J. H.; Cherief, M.; Qin, Q.; Gomez-Salazar, M.; Kadaikal, B.; Kang, H.; Chowdary, A. R.; Patel, N.; James, A. W.; Levi, B. Contemporary Perspectives on Heterotopic Ossification. *JCI Insight* **2022**, *7* (14), 1–20. https://doi.org/10.1172/jci.insight.158996.

2. Edwards, D. S.; Kuhn, K. M.; Potter, B. K.; Forsberg, J. A. Heterotopic Ossification: A Review of Current Understanding, Treatment, and Future. *J. Orthop. Trauma* **2016**, *30* (10), S27–S30. https://doi.org/10.1097/BOT.0000000000000666.

3. Joice, M.; Vasileiadis, G. I.; Amanatullah, D. F. Non-Steroidal Anti-Inflammatory Drugs for Heterotopic Ossification Prophylaxis after Total Hip Arthroplasty. *Bone Jt. J.* **2018**, *100B* (7), 915–922. https://doi.org/10.1302/0301-620X.100B7.BJJ-2017-1467.R1.

4. Coons, D.; Godleski, M. Range of Motion Exercises in the Setting of Burn-Associated Heterotopic Ossification at the Elbow: Case Series and Discussion. *Burns* **2013**, *39* (4), e34–e38. https://doi.org/10.1016/j.burns.2012.10.014.

5. Cole, P. A.; Dugarte, A. J.; Talbot, M.; Routt, M. L. (Chip. Early Resection of Ectopic Bone in Patients with Heterotopic Ossification about the Hip after Trauma. *Injury* **2020**, *51* (3), 705–710. https://doi.org/10.1016/j.injury.2020.01.021.

6. Ranganathan, K.; Loder, S.; Agarwal, S.; Wong, V. W.; Forsberg, J.; Davis, T. A.; Wang, S.; James, A. W.; Levi, B.; Levi, B. Heterotopic Ossification. *J. Bone Jt. Surg.* **2015**, *97* (13), 1101–1111. https://doi.org/10.2106/JBJS.N.01056.

7. Kennel, K. A.; Drake, M. T. Adverse Effects of Bisphosphonates: Implications for Osteoporosis Management. *Mayo Clin. Proc.* **2009**, *84* (7), 632–638. https://doi.org/10.4065/84.7.632.

8. Kan, C.; Yang, J.; Fan, H.; Dai, Y.; Wang, X.; Chen, R.; Liu, J.; Meng, X.; Wang, W.; Li, G.; Zhou, J.; Zhang, Y.; Zhu, W.; Fang, S.; Wei, H.; Zheng, H.; Wang, S.; Ni, F. Fetuin-A Is an Immunomodulator and a Potential Therapeutic Option in BMP4-Dependent Heterotopic Ossification and Associated Bone Mass Loss. *Bone Res.* **2022**, *10* (1). https://doi.org/10.1038/s41413-022-00232-x.

9. Shimono, K.; Tung, W. E.; MacOlino, C.; Chi, A. H. T.; Didizian, J. H.; Mundy, C.; Chandraratna, R. A.; Mishina, Y.; Enomoto-Iwamoto, M.; Pacifici, M.; Iwamoto, M. Potent Inhibition of Heterotopic Ossification by Nuclear Retinoic Acid Receptor-γ Agonists. *Nat. Med.* **2011**, *17* (4), 454–460. https://doi.org/10.1038/nm.2334.

10. Pignolo, R. J.; Baujat, G.; Hsiao, E. C.; Keen, R.; Wilson, A.; Packman, J.; Strahs, A. L.; Grogan, D. R.; Kaplan, F. S. Palovarotene for Fibrodysplasia Ossificans Progressiva (FOP): Results of a Randomized, Placebo-Controlled, Double-Blind Phase 2 Trial. *J. Bone Miner. Res.* **2022**, *37* (10), 1891–1902. https://doi.org/10.1002/jbmr.4655.

11. Davis, A.; Albayya, F.; Lobbardi, R.; Palmer, M.; Sherwin, C. A.; Green, S.; Stevison, F.; Kim, S.; Wilkie, G.; Kadambi, V. A Clinical Update on BLU-782, an Investigational Selective ALK2 Inhibitor in Development for Fibrodysplasia Ossificans Progressiva (FOP). *J. Bone Miner. Res.* **2019**, *34* (2006), 290.

12. Yu, P. B.; Deng, D. Y.; Lai, C. S.; Hong, C. C.; Cuny, G. D.; Bouxsein, M. L.; Hong, D. W.; McManus, P. M.; Katagiri, T.; Sachidanandan, C.; Kamiya, N.; Fukuda, T.; Mishina, Y.; Peterson, R. T.; Bloch, K. D. BMP Type I Receptor Inhibition Reduces Heterotopic Ossification. *Nat. Med.* **2008**, *14* (12), 1363–1369. https://doi.org/10.1038/nm.1888.

13. Muttenthaler, M.; King, G. F.; Adams, D. J.; Alewood, P. F. Trends in Peptide Drug Discovery. *Nat. Rev. Drug Discov.* **2021**, *20* (4), 309–325. https://doi.org/10.1038/s41573-020-00135-8.

14. Segvich, S.; Biswas, S.; Becker, U.; Kohn, D. H. Identification of Peptides with Targeted Adhesion to Bone-Like Mineral via Phage Display and Computational Modeling. *Cells. Tissues. Organs* **2008**, *189* (1–4), 245. https://doi.org/10.1159/000151380.

15. Addison, W. N.; Miller, S. J.; Ramaswamy, J.; Mansouri, A.; Kohn, D. H.; McKee, M. D. Phosphorylation-Dependent Mineral-Type Specificity for Apatite-Binding Peptide Sequences. *Biomaterials* **2010**, *31* (36), 9422–9430. https://doi.org/10.1016/j.biomaterials.2010.08.064.

16. Fukuda, T.; Scott, G.; Komatsu, Y.; Araya, R.; Kawano, M.; Ray, M. K.; Yamada, M.; Mishina, Y. Generation of a Mouse with Conditionally Activated Signaling through the BMP Receptor, ALK2. *genesis* **2006**, *44* (4), 159–167. https://doi.org/10.1002/dvg.20201.

17. Pan, H.; Fleming, N.; Hong, C. C.; Mishina, Y.; Perrien, D. S. Methods for the Reliable Induction of Heterotopic Ossification in the Conditional Alk2Q207D Mouse. *J. Musculoskelet. Neuronal Interact.* **2019**, 1–11.

18. Yang, J.; Toda Nakamura, M.; Hallett, S. A.; Ueharu, H.; Zhang, H.; Kelley, K.; Fukuda, T.; Komatsu, Y.; Mishina, Y. Generation of a New Mouse Line with Conditionally Activated Signaling through the BMP Receptor, ACVR1: A Tool to Characterize Pleiotropic Roles of BMP Functions. *Genesis* **2021**, *59* (5–6), 1–11. https://doi.org/10.1002/dvg.23419.

19. Reedy, C. L.; Reedy, C. L. Micro-Computed Tomography with 3D Image Analysis to Reveal Firing Temperature Effects on Pore Systems in Archaeological and Ethnographic Ceramics. *Appl. Sci.* **2022**, *12* (22). https://doi.org/10.3390/app122211448.

20. Gostick, J.; Aghighi, M.; Hinebaugh, J.; Tranter, T.; Hoeh, M. A.; Day, H.; Spellacy, B.; Sharqawy, M. H.; Bazylak, A.; Burns, A.; Lehnert, W.; Putz, A. OpenPNM: A Pore Network Modeling Package. *Comput. Sci. Eng.* **2016**, *18* (4), 60–74. https://doi.org/10.1109/MCSE.2016.49.

21. Potter, B. K.; Burns, T. C.; Lacap, A. P.; Granville, R. R.; Gajewski, D. A. Heterotopic Ossification Following Traumatic and Combat-Related Amputations. *J. Bone Jt. Surg.*

2007, *89* (3), 476–486. https://doi.org/10.2106/JBJS.F.00412.

22. Ramaswamy, J.; Nam, H. K.; Ramaraju, H.; Hatch, N. E.; Kohn, D. H. Inhibition of Osteoblast Mineralization by Phosphorylated Phage-Derived Apatite-Specific Peptide. *Biomaterials* **2015**, *73*, 120–130. https://doi.org/10.1016/j.biomaterials.2015.09.021.

23. Ling, C.; Zhao, W.; Wang, Z.; Chen, J.; Ustriyana, P.; Gao, M.; Sahai, N. Structure-Activity Relationships of Hydroxyapatite-Binding Peptides. *Langmuir* **2020**, *36* (10), 2729–2739. https://doi.org/10.1021/acs.langmuir.9b03779.

24. Agarwal, S.; Loder, S. J.; Brownley, C.; Eboda, O.; Peterson, J.; Hayano, S.; Wu, B.; Zhao, B.; Kaartinen, V.; Wong, V. C.; Mishina, Y.; Levi, B. BMP Signaling Mediated by Constitutively Active Activin Type 1 Receptor (ACVR1) Results in Ectopic Bone Formation Localized to Distal Extremity Joints. *Dev. Biol.* **2015**, *400* (2), 202. https://doi.org/10.1016/J.YDBIO.2015.02.011.

25. Kaplan, F. S.; Le Merrer, M.; Glaser, D. L.; Pignolo, R. J.; Goldsby, R. E.; Kitterman, J. A.; Groppe, J.; Shore, E. M. Fibrodysplasia Ossificans Progressiva. *Best Pract. Res. Clin. Rheumatol.* **2008**, *22* (1), 191–205. https://doi.org/10.1016/j.berh.2007.11.007.

Chapter 5 Development of Drug Delivery Systems for Controlled Release of pVTK

5.1 Introduction

The studies in Chapters 3 and 4 demonstrated that pVTK inhibited EM formation in two different animal models. Nonetheless, more work is necessary to improve peptide delivery for clinical translation. Daily injections to manage EM formation in humans would present a burden to clinicians and to patients, in terms of time, money, comfort and compliance. Additionally, since many diseases/disorders involving EM formation have a major inflammatory component, repeated injections are likely to exacerbate local inflammation and potentially increase EM formation[1]. While pVTK may be employed for inhibiting EM formation in different disease states, it is important to tailor pVTK administration for each disease state, as EM formation varies in terms of amount and accessibility via typical drug administration routes.

Drug delivery projects were undertaken to develop controlled release methods for pVTK to achieve inhibition of mineralization. Controlled release systems gradually release a drug from a reservoir, as compared to burst release mechanisms which administer the entire dose at one timepoint (e.g. intramuscular or subcutaneous injections). For treatment of EM formation due to BMP therapies, an injectable natural hydrogel was developed. For treatment of EM formation due to HO/FOP, degradable nanoparticles for drug encapsulation and controlled release were developed. Proof-of-concept studies were conducted to fabricate the respective controlled release systems for in vitro pVTK delivery.

5.1.1 Drug delivery considerations for BMP therapies

In Chapter 3, pVTK delivered via daily subcutaneous injections reduced EM formation from BMP2-loaded implants. Ideally, pVTK would be delivered via controlled release that exerts spatial and temporal control over its release without interfering with the therapeutic effect of BMP2.

Design considerations for the controlled release delivery system for pVTK in conjunction with BMP2 therapies are presented in Table 5.1. Based on the needs and design considerations, a gelling hydrogel composed of collagen and alginate was deemed suitable for pVTK delivery (Table 5.1). There is precedent for collagen and alginate gels in biomedical applications. FDA-approved BMP2 therapies utilize collagen sponges for delivery[2], and injectable collagen hydrogels are FDA-approved for use as facial fillers[3]. Further, injectable alginate hydrogels are European Medicines Agency (EMA)-approved and undergoing FDA clinical trials for treatment of heart failure[4]. The combination of collagen and alginate in an injectable, gelling hydrogel is tailorable for controlled release of drugs[5].

5.1.2 Drug delivery considerations for HO/FOP

When considering EM management in patients with HO or with FOP, activating any excess inflammatory response is likely to cause adverse reactions, potentially resulting in increased EM formation[1]. Patients with FOP are recommended to avoid all soft tissue injury, including intramuscular injections (e.g. vaccinations)[1].

Data presented in Chapter 4 showed that pVTK reduced EM formation in a model of HO/FOP via daily intramuscular injections in vivo. However, EM typically forms approximately 14 days after induction of the genetic mutation in this model[6]. Daily injections may have exacerbated inflammation and animal discomfort, ultimately leading to early experimental termination by 11 days post-induction. Reducing the number of injections for drug did not seem

to exacerbate inflammation (unpublished observations based on injections every 3 days). Additionally, other reports demonstrated successful drug administration via intraperitoneal injection[6,7] or oral gavage[8].

Design considerations for a controlled release delivery system for pVTK to prevent EM formation in HO/FOP are presented in Table 5.2. Based on the needs and design considerations, PLGA particles were deemed suitable for pVTK delivery. PLGA is FDA-approved for biomedical applications, including but not limited to controlled release of drugs in vivo[9].

5.2 Methods

5.2.1 Peptide synthesis and fluorescent tagging

Solid phase peptide (pVTK: VTKHNLQI(pS)Q(pS)Y, pS = phosphoserine and scram-pVTK: IYQ(pS)KHTL(pS)NQV) synthesis was performed (purity ≥ 90% by HPLC) by the University of Michigan's Proteomics and Peptide Synthesis Core. pVTK was reconstituted in carbonate-bicarbonate buffer (pH 9). Peptide tagging with fluorescein isothiocyanate (FITC) was performed via conjugation reaction. Briefly, 0.5mL of pVTK (10mg/mL in carbonate-bicarbonate buffer, pH 9) was mixed with 50uL of FITC (1mg/mL in dimethyl sulfoxide). The reaction proceeded for 1 hour at room temperature with stirring and protection from light. Then, unreacted FITC was removed from the reaction solution via column purification (PD MidiTrap G-10).).

5.2.2 Hydrogel fabrication and model protein encapsulation

Hydrogel fabrication was derived from published protocols[5]. Hydrogel composition was divided into two precursor solutions: collagen and alginate. The collagen precursor solution was formulated with rat tail Type I collagen (3 mg/mL; Gibco) mixed with calcium sulfate (10% in

deionized water). The alginate precursor solution was formulated with alginate (1w/v% in calcium-free DMEM (Gibco); Millipore-Sigma) mixed with sodium hydroxide (0.1M in deionized water). Then, the two precursor solutions were mixed well via pipetting at 4°C before being transferred into a 96-well plate for gelation overnight at 37°C. For protein encapsulation, FITC-Dextran (10 μL 25mg/mL in deionized water; MW 3,000-5,000, Millipore-Sigma) or FITC-pVTK (30 μL) was incorporated in the mixing step of the two precursor solutions.

Gelling and protein release were used to assess permutations of hydrogel composition (see Table 5.3). Parameter variations tested (a) the level of alginate crosslinking (as controlled by calcium sulfate concentration) (1 vs. 2 and 5 vs. 6; 1-4 vs. 5-8) and (b) the level of collagen crosslinking (as controlled by NaOH concentration) (2 vs. 3 vs. 4 and 6 vs. 7 vs. 8). For all permutations, the multiplication factors listed apply to the corresponding volumes for the alginate and collagen sulfate solutions added to the total hydrogel mixture.

5.2.3 Particle synthesis

Particle preparation was adapted from published protocols of the double emulsion technique[10]. Briefly, the double emulsion technique uses aqueous and organic phases to establish an aqueous, drug-loaded core with a polymer particle shell.

For the emulsifier solution, PVA (poly-vinyl alcohol; Millipore-Sigma) solution was prepared by dissolving PVA in double distilled water (1 or 2 w/v%) for a total volume of 50mL. For the polymer solution, PLGA (poly-lactic-co-glycolic acid, 50:50; Resomer RG 503) was dissolved in ethyl acetate (2.5, 5, or 10 w/v%) for a total volume of 1 mL. For the first emulsion, 50uL drug (40mg/mL bovine serum albumin (Fisher) or 2mM FITC-Dextran (MW 3,000-5,000; Millipore-Sigma), FITC-pVTK) in solution was added to the polymer solution and ultrasonicated three times (10 seconds, 40% amplitude, 700W sonicator). For the second emulsion, the

polymer/drug solution was added dropwise to 2mL of the emulsifier solution during vortexing. The polymer/drug/emulsifier solution was then ultrasonicated three times (30 seconds, 40% amplitude, 700W sonicator) on ice. The sonicated polymer/drug/emulsifier solution was then poured into the remaining emulsifier solution (stirring). Particles were allowed to harden while stirring for 3 hours at room temperature.

To collect the particles, the full polymer/drug/emulsifier was centrifuged (30 minutes, maximum speed 4686g) and washed with double distilled water three times. The final particle pellet was resuspended in 5mL of double distilled water, frozen overnight at -80°C, and lyophilized for 72 hours. Long-term particle storage occurred at -80°C.

5.2.4 Scanning electron microscopy (SEM)

Prior to freezing and lyophilization, 20uL samples were taken and allowed to dry on glass coverslips overnight in preparation for SEM. Carbon coating and scanning were performed in the University of Michigan's Electron Microbeam Analysis Lab. SEM images were acquired using the JEOL JSM-7800FLV Scanning Electron Microscope (10.0kV LED, WD 12.0μm). Particle diameters were measured in ImageJ using SEM images (2000X, n = 3).

5.2.5 Encapsulation efficiency

To measure hydrogel encapsulation efficiency, gelled hydrogels (n = 2) were rinsed well with PBS. The wash liquid was evaluated for protein content via measurement of fluorescence (λ_{ex} = 480nm; λ_{em} = 520 nm) and comparison to a standard curve. Then, encapsulation efficiency was calculated as $\frac{Total\ added\ protein - protein\ content\ in\ wash\ liquid}{Total\ added\ protein} * 100\%$.

Particle encapsulation efficiency was not measurable due to the large volume of emulsifier solution compared to volume of added protein.

5.2.6 Protein release quantification

For hydrogel release, gelled hydrogels containing FITC-Dextran (n = 2) were incubated with PBS at 37°C with protection from light for up to 5 days. PBS supernatant samples were taken for protein quantification via measurement of fluorescence and normalization to a standard curve.

For particle release, protein and peptide release in solution were quantified using a BCA and micro-BCA assay kit (Pierce), respectively (n = 3). Briefly, particles were re-suspended in PBS and incubated at 37°C for up to 72 hours. Daily supernatant samples were taken and quantified using the BCA assays for protein/peptide content.

5.2.7 Cell culture

MC3T3s (murine calvarial pre-osteoblasts) were maintained in growth media: alpha-MEM (Gibco 12561-056) with 10% FBS (Gibco 10082147, Reserve 77813196) and 1% penicillin-streptomycin (Gibco, 15140-122). For osteogenic differentiation, growth media was supplemented with β-glycerophosphate (10mM, Sigma-Aldrich) and ascorbic acid (50μg/mL, Sigma-Aldrich). Cells were plated at a density of 30,000 cells/cm^2 and allowed to reach full confluence throughout the 12-day differentiation scheme.

For hydrogel administration, hydrogel precursor solutions with FITC-Dextran or FITC-pVTK were fabricated under sterile conditions, allowed to gel overnight at 37°C, and placed directly onto cell monolayers for a total of two biological replicates per group. For particle

administration, particles were resuspended in growth media for administration to MC3T3s in solution for a total of two biological replicates per group.

5.2.8 Staining of deposited calcium/calcium phosphate and cell nuclei

Alizarin Red and von Kossa staining were performed on fixed cells (n = 2) to identify calcification and mineralization, respectively. MC3T3s were fixed in 10% neutral-buffered formalin for 10 minutes, then washed three times with double distilled water. For Alizarin Red staining, fixed cells were incubated with a 2% Alizarin Red S (Sigma-Aldrich) staining solution (pH 4.2) for 45 minutes protected from light. For von Kossa staining, fixed cells were incubated with a 5% silver nitrate (Sigma-Aldrich) solution for 60 minutes under UV light. Following each incubation, stained monolayers were washed with double distilled water until the washing liquid ran clear.

5.2.9 Alizarin Red staining quantification

Bound Alizarin Red was extracted from cell matrices via incubation with an extraction solution (20% methanol, 10% acetic acid in double distilled water) for 45 minutes with protection from light. Samples were collected from the extraction solution and run on a plate reader (450 nm) against a serial dilution of the original Alizarin Red staining solution in the extraction solution.

5.2.10 Staining of cell nuclei

Hoechst staining to identify cell nuclei was performed on live cells. Sterile Hoechst 33342 (Thermo Scientific) was reconstituted to a concentration of 0.02 mg/mL in sterile PBS. Live cell monolayers (n = 2) were incubated with Hoechst staining solution at a concentration of 0.5ug/mL in media for 15 minutes at 37°C. Then, cells were washed with sterile PBS and

incubated with fresh media prior to imaging. Images (with or without Hoechst staining) were obtained on the Leica Thunder Imager (Leica DMi8 microscope).

5.2.11 Fluorescent imaging

Hydrogels incorporated with FITC-tagged pVTK (n = 2) were imaged using a Leica Thunder Imager (Leica DMi8 microscope) to view release of FITC-Dextran or FITC-pVTK from respective hydrogels.

5.2.12 Statistical analysis

No statistical analysis was performed on this preliminary data due to insufficient technical replicates.

5.3 Results

5.3.1 Injectable hydrogel for pVTK delivery to inhibit EM formation as an off-target effect of BMP therapies

5.3.1.1 Hydrogel composition analysis

Hydrogel composition parameters (Table 5.2) were evaluated in terms of their effect on gelling and protein release over time (Figure 5.1). Increasing the ratio of the alginate precursor solution to the collagen precursor solution resulted in increases in structural integrity after the gelation period, as assessed by ease of removal of gelled hydrogel from the fabrication well and by the maintenance of the well shape after removal (1:1 ratio not presented in Figure 5.1). Increasing the ratio of calcium sulfate to alginate increased structural integrity but had no impact on the release profiles (1-4 vs. 5-8, observation based on user handling). Increasing the added volume of NaOH from 4μL to 5μL increased gelation (2 vs. 3 and 6 vs. 7), beyond which

increasing NaOH appeared to negatively impact gelation (3 vs. 4 and 7 vs. 8, observations based on user handling). Therefore, since cumulative protein release was largely unchanged by the tested parameters, gelling and resultant handleability led to the choice of hydrogel compositions 3 and 4 for further studies.

5.3.1.2 Peptide incorporation into hydrogels and in vitro testing

Incorporation of FITC-pVTK into hydrogels was visualized (Figure 5.2A), demonstrating more incorporation into hydrogel composition 3. MC3T3s differentiated in the presence of pVTK or scram-pVTK (delivered freely vs. via hydrogel encapsulation) showed decreases in Alizarin Red staining when peptides were encapsulated hydrogel 3, but not hydrogel 4. However, free pVTK (positive control) did not reduce calcification compared to ODM controls while scram-pVTK (negative control) did reduce calcification compared to ODM controls.

5.3.2 Polymer particles for pVTK delivery to mitigate EM formation in HO/FOP

5.3.2.1 Particle fabrication parameter assessment

Different fabrication parameters for PLGA particles (polymer concentration and emulsifier concentration) were assessed in terms of their effects on morphology, particle size, and protein release profiles. Increasing PLGA concentration resulted in more particles with more consistent morphology (Figure 5.3A). Increasing PVA concentration resulted in more consistent particle size (Figures 5.3A and 5.3B). Increasing PLGA concentration resulted in slower, albeit lower protein release, while increasing PVA concentration resulted in faster and higher protein release (Figure 5.3C). Since the main parameter of interest was the protein release profile, the parameters with the most consistency and control were chosen for future experiments: 10% PLGA and 2% PVA. Ideally, release would extend over 14 days to allow for a single injection of

pVTK-loaded PLGA particles. However, the 3-day release profile was sufficient for these early studies since prior work showed that the caAlk2 model can withstand extra injections on every third day.

5.3.2.2 In vitro pVTK release from PLGA particles

Release of encapsulated peptide and peptide mimics are demonstrated in Figure 5.4. Release of FITC-Dextran increased with increasing concentration, as expected (Figure 5.4A, top row). While FITC-pVTK release increased with increasing concentration, release of FITC-pVTK was lower than FITC-Dextran at the same concentrations (Figure 5.4A). Quantification of pVTK release from particles showed a steady decrease in the concentration of pVTK in supernatant over 72 hours (Figure 5.4B), though FITC-pVTK remained present in culture through 96 hours (Figure 5.4C).

Controlled release of pVTK from particles was assessed during osteogenic differentiation of MC3T3s. After the course of osteogenic differentiation, cell groups treated with particles (encapsulating both FITC-pVTK and FITC-Dextran) and with free pVTK showed inhibition of mineralization (Figure 5.5). Cell monolayers were lost during osteogenic differentiation due to infection since the particles were not sterilized prior to administration to cells.

5.4 Discussion

To improve the potential clinical impact of pVTK for prevention of EM formation, controlled drug release systems would be more suitable than subcutaneous or intramuscular injections of free peptide. Due to high levels of inflammation and improper repair processes associated with EM formation, encapsulation for local delivery of pVTK would be ideal. In this chapter, two controlled release systems were developed for each of the models of EM formation investigated in previous chapters.

5.4.1 Injectable hydrogel for pVTK delivery to inhibit EM formation as an off-target effect of BMP therapies

An injectable collagen-alginate hydrogel was created to deliver pVTK in a controlled manner for prevention of EM due to BMP2 therapy off-target effects. There is precedent for using collagen and alginate hydrogels in the clinic (e.g. collagen sponges for BMP2 implants), and these natural polymers are well tolerated by the body and customizable for a variety of applications. The studies reported here present efforts to adapt collagen-alginate hydrogels for delivery of pVTK for EM prevention.

The effect of hydrogel composition on gelation and protein release were explored to determine the best composition for this application. Hydrogel compositions 3 and 4 (standard calcium sulfate with medium (3) or high (4) NaOH) had the ideal balance of structural integrity after gelation, consistency in fabrication, and controlled release profiles. The hydrogel formulation is designed to be injectable at room temperature and solid at body temperature. Therefore, it is important that the hydrogel retains its structure after the gelling period to potentially allow for spatially controlled drug release. The hydrogel compositions ruled out based on poor gelation were compositions 1 and 2 (low calcium sulfate with medium NaOH (1) and standard calcium sulfate with low NaOH (2)). Increasing the concentration of calcium sulfate resulted in difficulties maintaining homogeneity during mixing and inconsistent gelation. Therefore, hydrogel compositions 5-8 (with higher calcium sulfate to alginate ratio) were ruled out.

Hydrogel compositions 3 and 4 were further evaluated via incorporation of peptide and inhibition of osteogenic differentiation when incubated with cells. FITC-tagged pVTK was incorporated within each of the two hydrogel compositions (Figure 5.2A). Differences in amount

of incorporated peptide are likely due to differences in gelation and handling. When administered to MC3T3s undergoing osteogenic differentiation, hydrogel composition 3 had an inhibitory effect on ECM calcification, regardless of incorporated peptide variant (Figure 5.2B). Hydrogel composition 4 with incorporated pVTK reduced calcification more than with incorporated scram-pVTK (Figure 5.2B). However, the overall calcification levels in all groups were low, and the free peptide negative controls had opposite results than anticipated. This indicates that osteogenic activity in these cells was limited by factors outside of hydrogel or peptide administration (e.g. errors with osteogenic media or older cell lines). Despite this, hydrogel 4 was deemed a candidate for delivery of pVTK to inhibit calcification in differentiating osteoblasts because inhibitory effects could be attributed to pVTK rather than to the hydrogel itself. Future optimization of hydrogel formulation (in terms of gelation and peptide release kinetics) and in vitro administration are needed to validate hydrogel composition.

In all, efforts to adapt hydrogel formulation for pVTK administration yielded promising results. However, more work is needed to tailor the peptide release profile, understand degradation effects, and improve administration in vitro and in vivo.

5.4.2 Polymer particles for pVTK delivery to mitigate EM formation in HO/FOP

PLGA particles were synthesized to deliver pVTK over time with minimal intramuscular injections for prevention of EM in HO/FOP. There is precedent for using PLGA for controlled drug delivery since PLGA degrades into products that are easily metabolized by cells. The work presented demonstrates pVTK incorporation into PLGA particles for controlled release, though further testing is necessary to ensure that this delivery system reduces mineralization without exacerbating inflammation in vivo.

Particle development focused on fabrication parameters (polymer concentration, emulsifier concentration) and functional outputs (particle size and morphology, release profile). To guide this development project, consistency in particle size and controlled release profiles were considered the most important outputs. While more work is necessary to ensure consistent particle fabrication and to lengthen the duration of protein release, based on the data generated, the parameters selected were 10% PLGA and 2% PVA.

Particles were initially developed for encapsulation of a mock protein (BSA), and peptide encapsulation and release were characterized using the same particle fabrication parameters. Release of FITC-Dextran or FITC-pVTK had no negative affect on cell survival or cell density (over 48 hours of incubation) (Figure 5.4A). The presence of FITC signal after encapsulation, regardless of amount, was a positive sign that encapsulation did not negatively impact bioactivity of the peptides. Quantification of pVTK release indicates that there is a burst release on day 1 with lower, controlled release over 72 hours (Figure 5.4B), with FITC-pVTK still active at 96 hours (Figure 5.4C). Further adjustments would be necessary to extend this release profile and ensure that pVTK delivery remains in the therapeutic window. The ideal therapeutic window still needs to be defined, but it is sufficient for pVTK (≥200μM) to be administered every 2-3 days alongside media changes. Additionally, pVTK was predicted to be highly stable in mouse plasma (Chapter 2), though the effects of cell-mediated degradation and systemic clearance on pVTK are yet to be characterized.

While FITC-Dextran release matched expectations, the concentration of FITC-pVTK released was lower than anticipated (Figure 5.4A). FITC-conjugation of pVTK was performed manually, so efficiency was likely lower than the FITC-Dextran purchased from the supplier.

Optimization or outsourcing of the post-conjugation filtration steps would ensure higher efficiency of the FITC-pVTK conjugation reaction.

When administered in vitro, mineralization was inhibited in all treatment groups (Figure 5.5). Since the data is incomplete due to infection and resultant cell loss, it cannot be determined that inhibition of mineralization was due to pVTK released from PLGA particles. Future studies would repeat this in vitro work with sterilized particles. Ideally, after modifying particle fabrication to extend peptide release, particles would be delivered in such a way to separate media changes from particle administration (e.g. using cell culture insert).

5.4.3 Limitations

Development of each of these delivery systems was limited by time and personnel constraints. However, full customization for each of these controlled release systems was limited due to incomplete understanding of (a) how pVTK inhibits mineralization and (b) the appropriate dosing scheme for full inhibition (duration of release profile and therapeutic window). Knowing how pVTK inhibits mineralization would inform targeting strategies in terms of location and timing. Characterizing the appropriate dosing scheme would guide system optimization toward the desired release kinetics. Future studies would build on the work presented in this chapter to further develop controlled release delivery systems for pVTK.

5.5 Conclusion

This chapter describes efforts to develop two controlled release systems, each tailored for the delivery of pVTK for EM prevention in two different disease states: BMP2 therapies and HO/FOP. The most important design considerations were inspired by current treatment/management strategies within the clinic for each disease state. An injectable collagen-

alginate hydrogel for pVTK encapsulation was proposed to be delivered alongside or after BMP2 implant insertion. The hydrogel system was shown to have high encapsulation efficiency, controllable properties for modulating gelation, and capacity for controlled peptide release. PLGA particles were proposed for intramuscular injection to control EM formation in cases of HO/FOP. Particles had high encapsulation efficiency, tunable protein release rates, and potential inhibitory effects of in vitro mineralization. Though more system optimization is necessary to demonstrate full in vitro efficacy for both release systems, this work successfully demonstrates pVTK encapsulation and release with no observed effects on bioactivity.

5.6 Acknowledgements

Thank you to Amy Woo (particles) and Victoria Maglaras (hydrogels) for performing all the hands-on work described in these drug delivery projects. Thank you to Henriette Remmer (Proteomics and Peptide Synthesis Core) for peptide synthesis and Owen Niell (EMAL) for assistance with SEM.

This publication was supported by NIH T32 DE007057 (SJM), NIH P30AR069620 (DHK), Department of Biologic & Materials Sciences BOOST Fund (DHK), Summer Undergraduate Research in Engineering (SURE) (AW).

5.7 Figures and Tables

Table 5.1 Engineering considerations for delivery of pVTK for prevention of EM due to BMP therapies

Need	Design Consideration	Design Solution
Bioavailability at site of EM formation	EM formation generally occurs due to leakage of BMP2 into extracellular space, so delivery system would require spatial control over pVTK administration	Gelling hydrogel allows for injection and solidification for long-term drug release at site of interest
Administration that does not impede BMP2 delivery/efficacy	BMP2 therapies are effective when restricted to the intended site; any controlled delivery system should not interfere with or restrict BMP2 administration	Gelling hydrogel could be used to either (a) create a pVTK-buffered zone immediately surrounding BMP2 implant to prevent off-target effects or (b) spatially restrict pVTK to area where EM formation has begun
Biocompatibility	Inflammatory response to BMP2 leakage has resulted in severe swelling and EM formation; controlled release system of pVTK should not exacerbate the immune response to the implants	Collagen and alginate are both natural polymers and incorporated within federally approved medical implants
Sterilizability	Systems must be sterilized before implantation or injection into the body	Creation of the hydrogel mixture can be performed under sterile conditions
Clinical translatability	Preservation and reconstitution of drug delivery system must incorporate easily into BMP implant surgery workflow	Hydrogel mixture components can be lyophilized and reconstituted
		Mixture of two precursor solutions can be performed immediately prior to injection

Table 5.2 Engineering considerations for delivery of pVTK for EM prevention in HO/FOP

Need	Design Consideration	Design Solution
Bioavailability at site of EM formation	Inflammation in tHO/FOP may lead to increased drug degradation, so drug must be protected from the inflammatory environment	PLGA particles encapsulate drugs, preserving bioactivity until drugs are released
	Transport within muscle tissue is limited due to the high cellular density and low extracellular transport space	PLGA particles can be embedded in implantable materials or injected into intramuscular space
Minimal intramuscular injections	Minor injury from intramuscular injections can cause flare-ups in FOP patients	PLGA particles can be tailored for drug release over the course of weeks or months, lowering the # of required injections
		Peptide stability via encapsulation is higher than proteins; smaller molecule size allows for higher levels of encapsulated drug
Biocompatible	Exacerbating inflammation in HO/FOP may lead to increased EM formation so system must not elicit any additional immune response	PLGA's degradation products are processed by cells and do not exacerbate immune response
Sterilizability	Systems must be sterilized before ultimate implantation or injection into the body	PLGA particles can be sterilized after synthesis
System handling	Preservation and reconstitution of drug delivery system must work within confines of current system	PLGA particles can be lyophilized with cryoprotectants for storage and reconstituted in sterile liquid immediately prior to injection

Table 5.3 Hydrogel composition descriptions

	DMEM (µL)	Collagen (µL)	Calcium Sulfate (µL)	FITC-Dextran (µL)	Alginate (µL)	NaOH (µL)	Encapsulation Efficiency
			2x		**2x**		
1	50	50	20	10	250	5	98.88%
2	50	50	30	10	250	4	98.87%
3	50	50	30	10	250	5	98.47%
4	50	50	30	10	250	16	98.46%
			4x		**2x**		
5	50	50	20	10	250	5	99.28%
6	50	50	30	10	250	4	97.85%
7	50	50	30	10	250	5	98.05%
8	50	50	30	10	250	16	98.52%

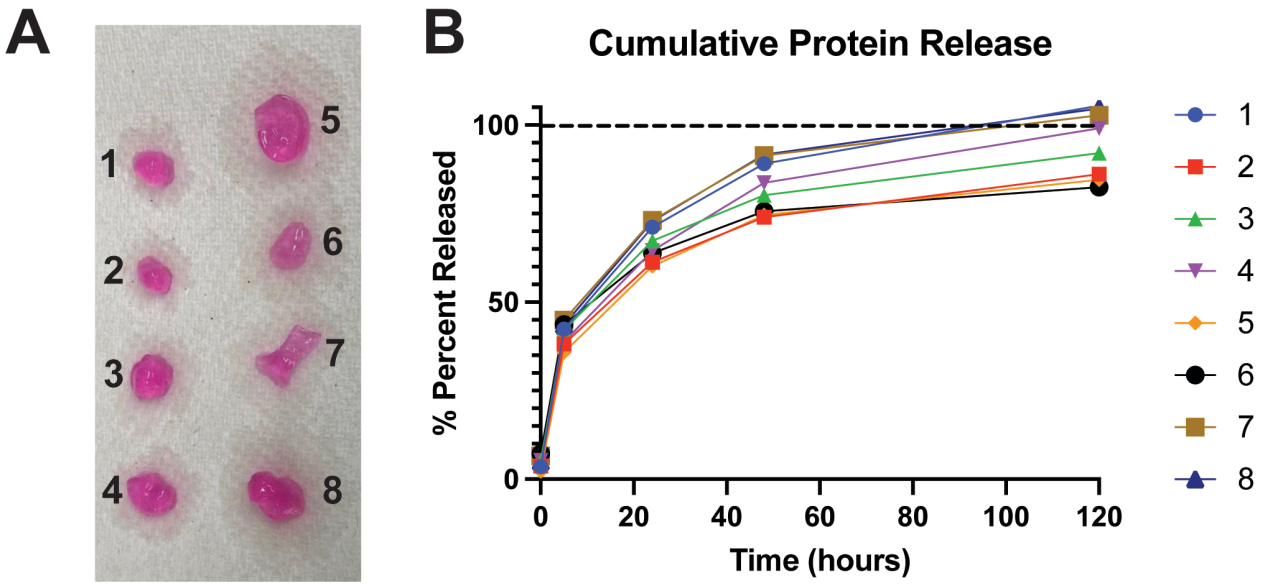


Figure 5.1 Effect of composition on hydrogel structure and protein release

(A) Representative images of set hydrogels and (B) cumulative mock protein release from hydrogels over time. Hydrogel composition numbers correspond to formulations described in Table 1. Data are represented as means with the dashed horizontal line representing maximum possible value.

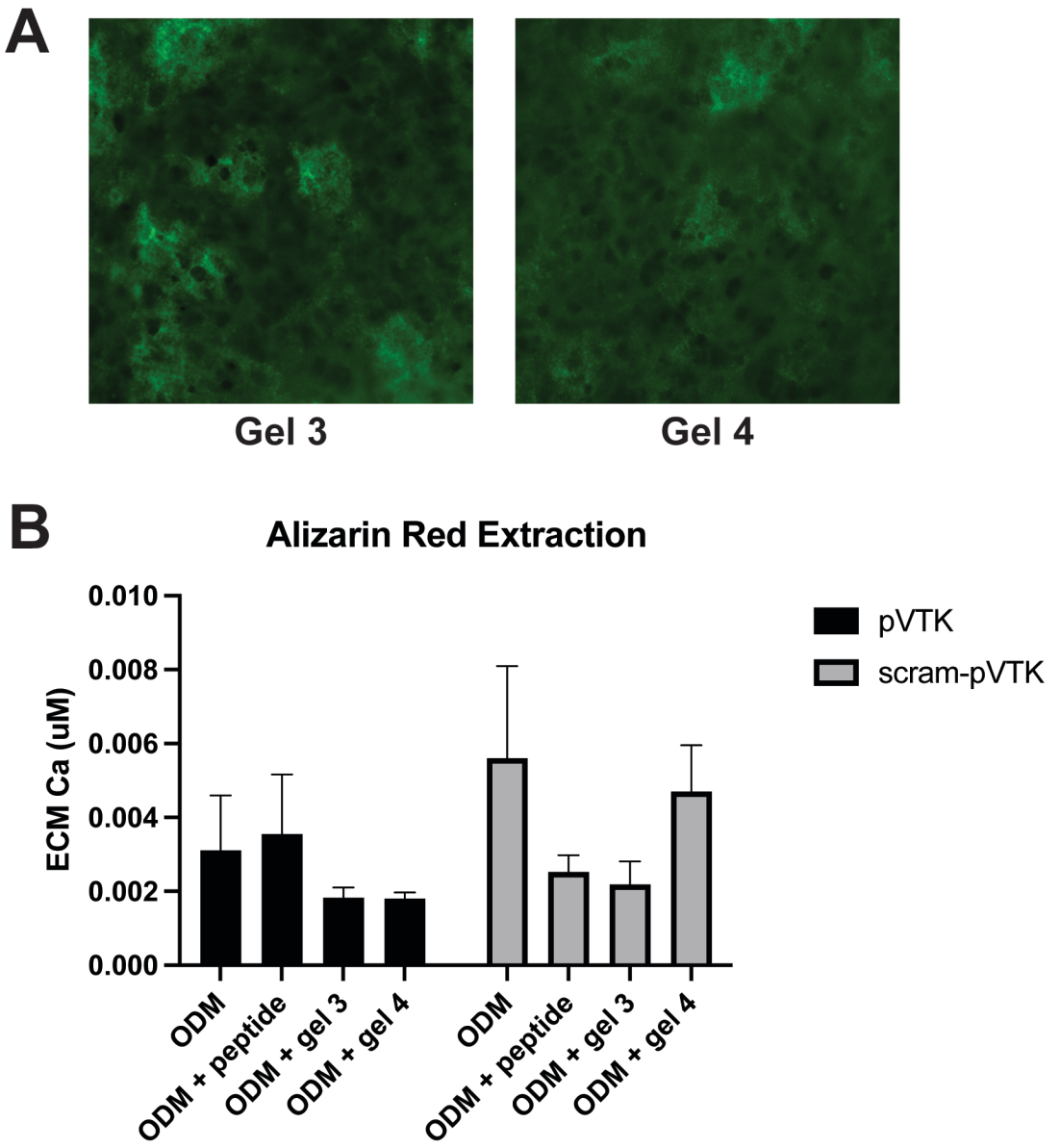


Figure 5.2 Incorporation of FITC-pVTK into hydrogel compositions 3 and 4 for in vitro assessment

(A) Fluorescent images of FITC-pVTK incorporation into hydrogels and (B) quantification of Alizarin red staining of MC3T3s at the end of a 12-day differentiation scheme in osteogenic differentiation media (ODM) plus free peptide (pVTK or scrambled pVTK, scram-pVTK) or pre-gelled hydrogels with incorporated peptide. Hydrogel composition 3 was high calcium sulfate and medium sodium hydroxide; hydrogel composition 4 was high calcium sulfate and high sodium hydroxide. Data are presented as means ± standard deviations.

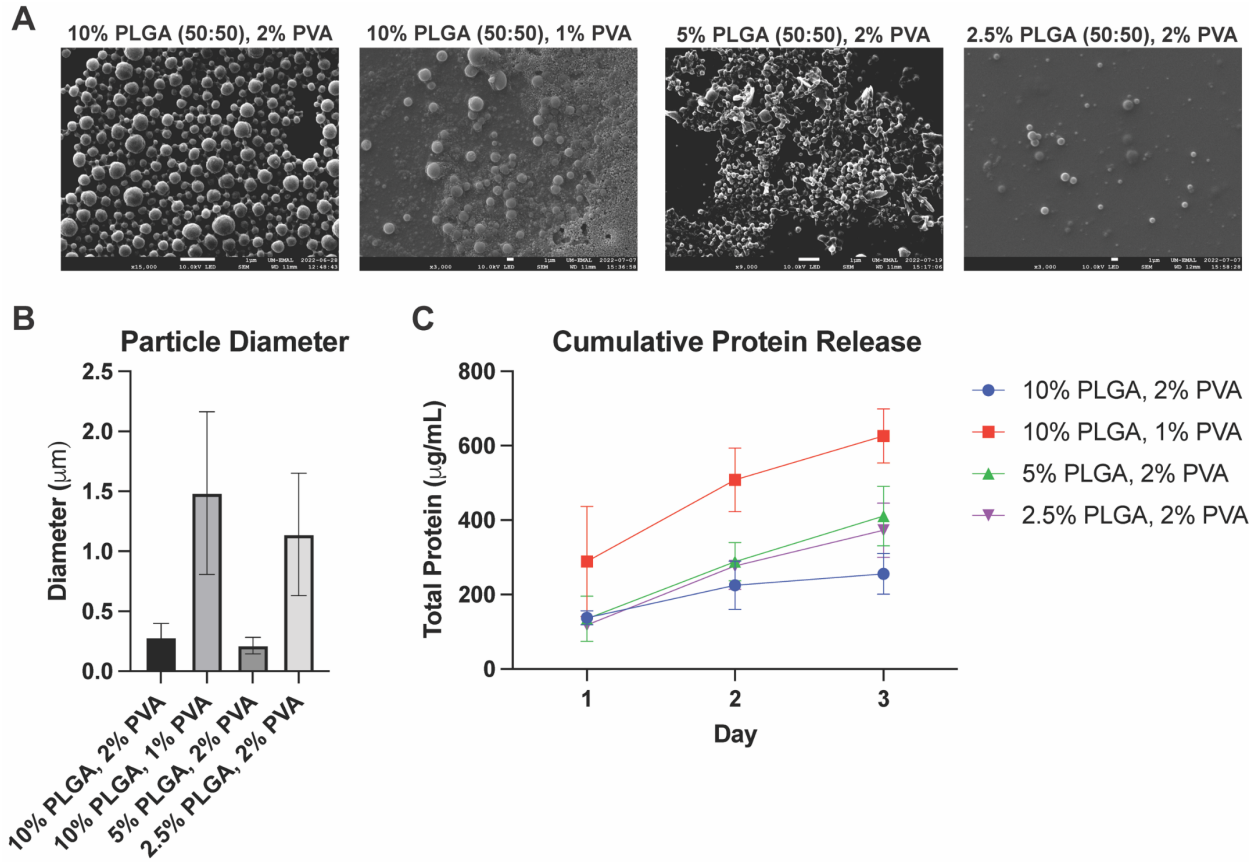


Figure 5.3 Effect of fabrication parameters on particle size and model protein release

(A) Representative SEM images, (B) quantification of particle size distribution, and (C) cumulative BSA release. Data is presented as means ± standard deviations.

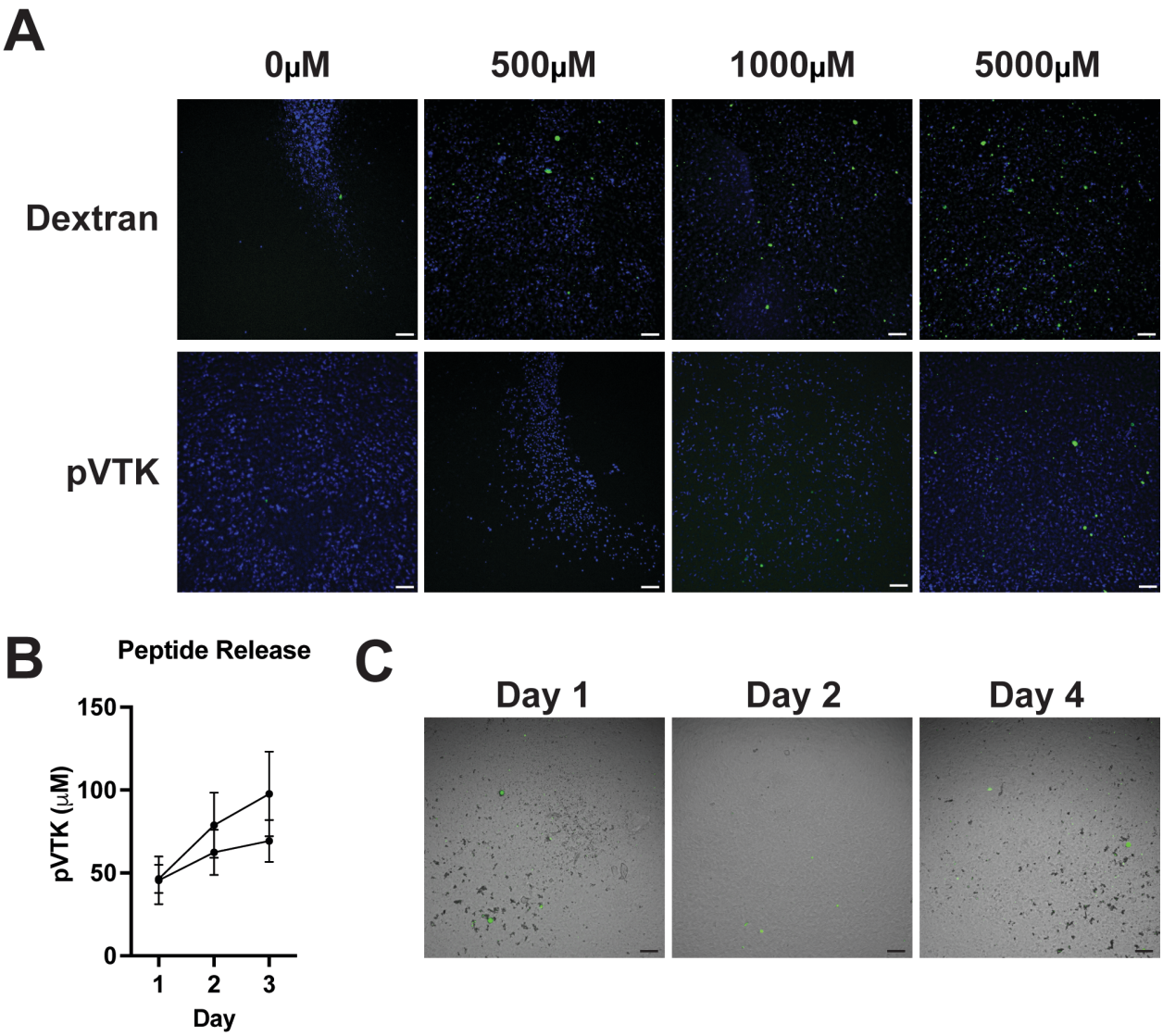


Figure 5.4 Peptide release from PLGA particles

(A) Fluorescent images of MC3T3s incubated with PLGA particles (reconstituted at different concentrations) for 48 hours (blue = cell nuclei; green = FITC tag on pVTK or dextran); (B) pVTK release over time (two batches of particles with same fabrication parameters); (C) Combined brightfield and fluorescent images of FITC-pVTK released from particles (1000μM) over 4 days. Data is presented as means ± standard deviations. Scale bar in each image represents 100μm.

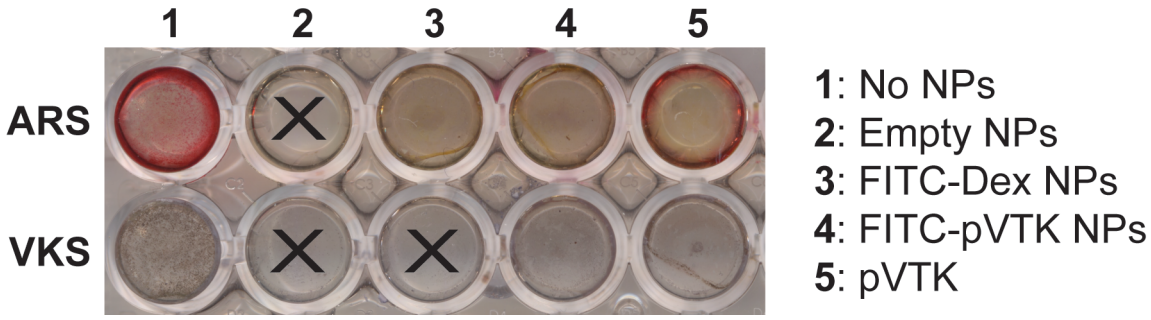


Figure 5.5 Effect of PLGA particles containing pVTK on MC3T3s undergoing osteogenic differentiation

(Top row) Alizarin red staining for calcium deposits and (Bottom row) von Kossa staining for calcium phosphate deposits. 'X' symbol indicates that cell monolayer was removed due to infection.

5.8 References

1. Glaser, D. L. & Kaplan, F. S. Treatment considerations for the management of fibrodysplasia ossificans progressiva. *Clin. Rev. Bone Miner. Metab.* **3**, 243–250 (2005).

2. McKay, W. F., Peckham, S. M. & Badura, J. M. A comprehensive clinical review of recombinant human bone morphogenetic protein-2 (INFUSE® Bone Graft). *Int. Orthop.* **31**, 729–734 (2007).

3. Salvatore, L., Natali, M. L., Brunetti, C., Sannino, A. & Gallo, N. An Update on the Clinical Efficacy and Safety of Collagen Injectables for Aesthetic and Regenerative Medicine Applications. *Polymers (Basel).* **15**, 1–39 (2023).

4. Choy, J. S. *et al.* Efficacy of intramyocardial injection of Algisyl-LVR for the treatment of ischemic heart failure in swine. *Int. J. Cardiol.* **255**, 129–135 (2018).

5. Moeinzadeh, S., Park, Y., Lin, S. & Yang, Y. P. In-situ stable injectable collagen-based hydrogels for cell and growth factor delivery. *Mater.* **Mar**, 100954 (2021).

6. Pan, H., Fleming, N., Hong, C. C., Mishina, Y. & Perrien, D. S. Methods for the reliable induction of heterotopic ossification in the conditional Alk2Q207D mouse. *J. Musculoskelet. Neuronal Interact.* 1–11 (2019).

7. Yu, P. B. *et al.* BMP type I receptor inhibition reduces heterotopic ossification. *Nat. Med.* **14**, 1363–1369 (2008).

8. Shimono, K. *et al.* Potent inhibition of heterotopic ossification by nuclear retinoic acid receptor-γ agonists. *Nat. Med.* **17**, 454–460 (2011).

9. Makadia, H. K. & Siegel, S. J. Poly Lactic-co-Glycolic Acid (PLGA) as Biodegradable Controlled Drug Delivery Carrier. *Polymers (Basel).* **3**, 1377–1397 (2011).

10. McCall, R. L. & Sirianni, R. W. PLGA nanoparticles formed by single- or double-emulsion with vitamin E-TPGS. *J. Vis. Exp.* 51015 (2013). doi:10.3791/51015

Chapter 6 Summary and Future Work

6.1 Summary of Dissertation

6.1.1 pVTK for inhibition of ectopic mineral (EM) formation

Prior work in the Kohn Lab utilized phage display technology to identify unique peptide sequences for bone tissue engineering strategies[1]. In particular, pVTK was identified for its high affinity to mineralized substrates, e.g. bone-like mineral (BLM)[2]. pVTK also demonstrated the unique ability to inhibit mineralization in MC3T3s (a pre-osteoblast cell line) undergoing osteogenic differentiation[2,3]. The main goal of this thesis was to investigate if and how pVTK could inhibit non-physiological mineralization in a therapeutic capacity.

Ectopic mineral (EM) formation is a common complication in a variety of disease states, resulting in pathological mineral formation and leading to tissue dysfunction and pain. The two cases of EM formation that were examined in this thesis are largely understood and therefore replicable in animal models: EM formation as a side effect of BMP2 therapies[4] and EM formation in heterotopic ossification/fibrodysplasia ossificans progressiva (HO/FOP)[5]. These two models operate on the same osteogenic signaling pathway by stimulating aberrant BMP2 osteogenic signaling, but differ in ultimate EM volume, effect of EM formation on soft tissue function, and the influence of inflammation.

In the BMP2-stimulated model, exogenous rhBMP2 was delivered via subcutaneous implant to induce ectopic mineralization. Daily administration of pVTK significantly inhibited EM formation, with an overall EM volume reduction of 92% (Figure 3.3). Further, EM volume

of all pVTK-treated samples fell below the range of PBS-treated controls (Figure 3.3). Histological evaluation provided evidence that pVTK inhibited the infiltration of cells into the subcutaneous implant (Figure 3.4), suggesting a potential role for pVTK in non-osteoblast cells. This study demonstrated that pVTK can inhibit EM formation in the subcutaneous BMP2-loaded implant model.

In the caAlk2 model, a conditionally activated genetic mutation in Alk2 (a BMP2 receptor protein) results in dysregulated activation of the BMP2 pathway to induce ectopic mineralization[6]. Daily administration of pVTK reduced EM formation, with an overall volume reduction of 61% (Figure 4.2). pVTK downshifted the severity of EM formation, as quantified by a grading system based on distribution of traumatic HO in a large human study[7] (Figure 4.2). Primarily, this study demonstrated that pVTK has the capacity to prevent severe EM formation. In addition, the caAlk2 study demonstrated that pVTK treatment resulted in more fragmented EM deposits. The volume fraction of EM formation was no different between treatment groups. pVTK treatment altered the geometry of the EM by reducing the unity of the EM deposits (defined as the percent of total EM volume made up of the largest discrete region), without reducing the connectivity within EM deposits (Figures 4.4 and 4.5). These morphological changes would potentially translate to EM with less impact on the surrounding muscle tissue (primarily in terms of movement restriction and pain) and increased surface area for pro-resorptive therapeutic strategies.

Since daily injections are difficult to implement in the clinic in each of these two disease states, drug delivery methods for sustained release and peptide encapsulation were explored. To prevent EM formation due to BMP2 therapies, an injectable controlled release collagen-alginate gelling hydrogel was adapted for pVTK delivery[8]. This system gels at body temperature,

allowing for easy injection and spatial control over pVTK administration to either surround the BMP2 sponge upon implantation or directly target EM. Proof-of-concept studies were conducted to demonstrate peptide encapsulation into and release from the collagen-alginate hydrogels alongside preliminary in vitro studies to demonstrate biocompatibility of the hydrogel system (Chapter 5). To limit EM formation in HO/FOP within muscle tissue, delivery of pVTK from PLGA particles would minimize the number of required injections for local administration and preserve peptide bioactivity for sustained release over long periods of time[9]. Proof-of-concept studies were performed to demonstrate the controlled release of pVTK from PLGA particles. Taken together, these engineering projects sought to ideate simple designs for controlled peptide release that could be readily implemented in the clinic.

6.1.2 Mechanism of pVTK action

pVTK was identified for its high affinity to mineralized substrates, such as hydroxyapatite and bone-like mineral[2]. However, it is not fully understood how pVTK inhibits mineralization. Based on previous work, it was hypothesized that pVTK primarily disrupts mineralization by binding to the early mineral nucleates and preventing crystal growth[3].

Osteoblasts upregulate mineralization promoters and downregulate mineralization inhibitors in response to mineralization inhibition by pVTK treatment[3]. To investigate pVTK's role in cell-mediated mineralization mechanisms, osteoblast behavior was assessed after stimulation with BMP2 and/or pVTK (Chapter 3). With increasing levels of BMP2, there was no increase in mineral deposition, yet pVTK only managed full inhibition of mineral deposition at the lower dose of BMP2 (Figure 3.1). pVTK did not impact the immediate cellular response to BMP2 stimulation, demonstrating that pVTK does not compete with the BMP2 ligand (Figure 3.2). On its own, pVTK upregulated osteogenic protein levels by the end of osteogenic

differentiation compared to untreated controls (Figure 3.2). Long-term administration of BMP2 may have an inhibitory effect on the osteoblastic cell behavior without impacting mineralization output. This is the opposite effect of pVTK, which appears to upregulate osteoblastic cell behavior while inhibiting mineralization. These results are in line with previous studies of pVTK's impact on osteogenic differentiation, which suggested a compensatory pro-osteogenic mechanism by osteoblasts to make up for pVTK's inhibition of mineralization[3].

pVTK reduces calcium deposition in mineralizing osteoblasts without chelating calcium ions[3]. In solution, pVTK interrupts calcium phosphate nucleation and slows the amorphous-to-crystalline transition[10]. This provides evidence that pVTK may inhibit mineralization by preventing nucleation and crystallization. In Chapter 3, pVTK was shown to disrupt mineral deposition and organization in solution, while scram-pVTK failed to do so at the same concentrations (Figure 3.5). This suggests that pVTK is not achieving inhibition by disrupting the critical balance of mineralization components needed for spontaneous mineralization. Rather, pVTK has the unique ability to disrupt mineral deposition and organization.

6.2 Future Directions

Since pVTK has a therapeutic effect against EM formation in vivo, the immediate next steps for this project may focus on drug development for pVTK: designing drug delivery systems, determining how pVTK inhibits mineralization, and predicting pharmacodynamics/ pharmacokinetics (PK/PD). pVTK also has many potential applications in targeted drug delivery and tissue engineering due to its high affinity to mineralized substrates. Beyond pVTK and mineralization, the unanswered questions about how pVTK interacts with osteoblasts and cell-mediated mineralization inspire broader applications in therapeutic design and molecular biology research.

6.2.1 Drug delivery for prevention of EM formation

Daily injections were sufficient to inhibit EM but are unlikely to be adopted clinically due to increased stress on patient compliance, high cost, and injury to soft tissue leading to sustained inflammation. As discussed in Chapter 5, two sustained release mechanisms were proposed for the models of EM formation used in this thesis: gelling hydrogels to be administered alongside BMP2 implants and degradable particles for intramuscular injection in HO/FOP. Additionally, co-delivery of pVTK with other molecules could establish multi-faceted approaches to treating disease states involving EM formation. For example, combining pVTK and non-steroidal anti-inflammatory drugs (NSAIDs), to regulate mineralization and inflammation respectively, into one therapeutic approach could enhance the effects of either drug alone to mitigate severe HO formation.

Drug delivery strategies for other diseases involving EM formation may involve more sophisticated biomaterial design. It is important to design the drug delivery system to match the needs of the disease state. In vascular calcification, localizing pVTK to the area of interest is complicated by blood flow and vessel accessibility. One option would be to create a drug-eluting stent or coated valve replacement for localized EM prevention with pVTK. Strategies for using deformable nanoparticles that localize to vessel walls are in development, providing another option for delivering pVTK to prevent vascular calcification[11]. In connective tissue mineralization, EM formation is generally preceded by tissue reorganization and stiffening. Stimuli-responsive gels could be utilized to time the administration of pVTK with matrix stiffening to prevent EM formation. Since EM formation affects a wide variety of systems throughout the body, creative drug delivery solutions are vital to demonstrating the utility of pVTK in different EM disease states.

One of the limitations for demonstrating pVTK's utility in a variety of diseases was the availability and reliability of animal models for ectopic mineralization. Many cases of ectopic mineralization are still not fully understood, in terms of etiology, risk factors, mechanisms, and role within the larger disease state. More work is needed to understand the human diseases involving ectopic mineralization and to translate them into reliable mouse models for study. Further, elucidating the impact of inflammation on ectopic mineralization (and vice versa) would guide both research and treatment strategies. In each of the two models examined in this thesis, the transition from in vitro to in vivo was complicated by an active immune response. In the BMP2-laden subcutaneous implant model, pVTK altered local cell interaction with the collagen implant itself by preventing cell infiltration (Figure 3.4). In the caAlk2 model, high levels of inflammation were observed at the macroscopic level but did not correlate with ultimate EM formation. Future steps for this thesis would aim to characterize any differences in immune response with respect to treatment (e.g. immunohistochemical staining to identify cells and proteins within and around the implant or HO deposit). More broadly, the relationship between inflammation and ectopic mineralization still needs to be characterized in BMP therapies, HO/FOP, and other disease states involving ectopic mineralization.

6.2.2 Mechanisms of pVTK function

There are additional questions that need to be answered in terms of how cells interact with pVTK and how pVTK inhibits mineralization. MC3T3s internalize pVTK into vesicular structures in the absence of mineral in the extracellular matrix[3]. These vesicle-like structures containing pVTK were lacking in Rab5, the characteristic membrane protein for early endosomes, and were larger than Rab5-labelled endosomes (Figure 6.1). Pharmacological inhibition of different internalization mechanisms may elucidate how and why pVTK is

internalized[12]. Alternatively, live cell imaging and/or lysosomal tracking may show where pVTK localizes within the cell after internalization. Two possible explanations for why cells internalize pVTK include (a) internalization for degradation of the foreign substance or (b) internalization into matrix vesicles, which are thought to play an active role in cell-mediated mineralization. Further characterization of the vesicular proteins and contents is recommended to determine why cells are internalizing pVTK and if there is a way to capitalize on this internalization mechanism (e.g. using drug-peptide conjugates).

In this work, pVTK was shown to not interfere with canonical BMP2 osteogenic signaling. Previous work showed that pVTK did not interfere with the Ank-TNAP-Enpp1 axis, which regulates mineralization through extracellular balance of pyrophosphate and inorganic phosphate[3]. However, there are other signaling pathways that contribute to both physiological and ectopic mineralization (e.g. TGF-β signaling is crucial for osteogenesis[13] but pathogenic TGF-β signaling has been linked to EM formation in chronic kidney disease[14] and osteoarthritis[15]). Utilizing knockout models or exogenous upregulation would allow for investigation into how pVTK may interact within other signaling pathways to achieve inhibition of mineralization.

Disease states involving ectopic mineral formation may recruit non-osteoblast cells that participate in aberrant signaling outside of osteogenesis (e.g. inflammatory cells for tissue repair or endothelial cells for angiogenesis). It is known that pVTK disrupts mineral formation by osteoblasts without interfering with certain osteogenic signaling pathways: BMP2 osteogenic signaling (Chapter 3) and the Ank-TNAP-Enpp1 axis[3]. However, pVTK may have alternative roles in non-osteoblast cells. In Chapter 3, pVTK limited cell infiltration into the BMP2-loaded subcutaneous collagen implants (Figure 3.4). In Chapter 4, pVTK reduced ALP activity in a

primary calvarial cell population (Figure 4.2C), whereas pVTK had no effect on ALP activity in BMP stimulated MC3T3s (Figure 3.2) and upregulated ALP activity in MC3T3s[3]. Importantly, both experiments in this thesis involved heterogeneous cell populations, potentially containing immune cells, endothelial cells, fibro-adipogenic progenitor cells, etc. Therefore, characterization of the cell population, baseline cell activities, and how those cell activities are affected by pVTK administration may help to explain why pVTK upregulates or has no effect on osteoblast behavior but downregulates osteogenic behavior in non-osteoblast cells. If pVTK were to prevent non-osteoblastic cells from participating in ectopic mineralization, the potential clinical application for using pVTK for ectopic mineralization expands to include preventative treatment alongside management and symptomatic treatment.

There is ample evidence that pVTK may have an additional role outside of cell-mediated mineralization. In both cellular and acellular mineralization studies, pVTK's unique ability to inhibit mineralization has been attributed to the unique combination of residue order (pVTK vs. scrambled pVTK) and post-translational modification (pVTK vs. VTK)[2,16]. The number and location of post-translational phosphorylations had no impact on pVTK's adsorption to mineralized substrates (pVTK(pSpS) vs. pVTK(pY) vs. pVTK(pSpSpY))[17] or pVTK's ability to inhibit mineralization (pVTK(pSpS) vs. pVTK(pY)) (Appendix B). But scrambled pVTK(pSpS) cannot inhibit mineralization despite having similar adsorption and adhesion strength to mineralized substrates as compared to pVTK(pSpS)[2,17]. Modeling of pVTK's binding to mineralized structures[2,16] demonstrates that phosphorylation is key to explaining the differences in binding energies of different VTK variants (including scrambled and phosphorylated variants) but not the differences in mineralization inhibition. Future work could elucidate if changes in mineral binding strength have effects on how VTK variants interact with the mineralization

process. Further, since pVTK uniquely inhibits mineralization, studies aimed at characterizing the mineralization processes more broadly (spontaneous or cell-mediated and biological or non-biological) could utilize pVTK as an antagonist to mineralization. For instance, investigation may aim to define mineralization stages more clearly, the role pVTK plays at each stage of mineralization, and how those stages (and the corresponding roles of pVTK) may change between acellular and cellular mineralization contexts.

6.2.3 Pharmacokinetics

pVTK is predicted to be stable in vivo, based on ex vivo incubation with mouse plasma and liver microsomes (Chapter 3). pVTK is non-toxic to MC3T3s in vitro[2]. However, there are other pharmacokinetic factors to consider when conducting lead optimization and validation work. The University of Michigan's Pharmacokinetic and Mass Spectrometry Core specializes in lead optimization and pre-clinical study development. Further collaborative efforts would aim to understand pVTK's long-term in vivo stability, to understand distribution and clearance upon systemic and targeted administration, and to define appropriate and safe pVTK dosing levels.

6.2.4 Targeted drug delivery

Bone metastases associated with prostate cancer result in poorer quality of life, increased pain and disability, and higher mortality rates[18]. Guiding therapies to a specific location, especially one within a mineralized tissue, is difficult. Instead, using peptide modalities to target specific cell populations has been explored for guided drug delivery. To demonstrate targeted delivery of chemotherapeutic agents to sites of bone metastases, pVTK-conjugated micelles were preferentially uptaken by osteoblasts (MC3T3s) and prostate cancer cells (C4-SB) in vitro compared to bisphosphonate-conjugated micelles which were preferentially uptaken by

macrophages (RAW 264.7) and prostate cancer cells (PC-3)[19]. To improve cell-cell communication in bone fracture repair, an implant coating was developed to combine the MSC-binding peptide DPI (DPIYALSWSGMA) with a Connexin 43 lentivirus to preferentially recruit MSCs for communication upregulation and resultant bone repair[20]. These examples demonstrate that using peptides to target specific cell populations may allow for tailored delivery of drugs in dynamic and complex disease states like bone metastases and fracture repair.

Due to its high affinity for mineralized substrates, pVTK can guide drugs to bone or to sites of EM formation. Bone remodeling occurs with bone metastases, resulting in more immature hydroxyapatite (as defined by smaller and less perfect nanocrystals) with primary tumor formation and prior to secondary tumor formation[21]. It is not known if pVTK targets or binds immature mineral differently than mature mineral (with maturity defined by crystallinity or crystal size), though there is evidence that pVTK can disrupt early stages of mineralization likely through physical means. Mineral-binding peptides, such as pVTK, could be modified to preferentially bind to abnormal mineralization patterns unique to specific disease states, allowing for targeted delivery drugs and imaging agents.

6.2.5 Tissue engineering strategies

For tissue engineering applications, pVTK could be a valuable tool for modulating mineralization and pioneering next-generation implants. Within the musculoskeletal system, connective tissue meets bone at joints and entheses, requiring careful control over mineralization during development and throughout repair. However, with aging and improper repair, mineralization of the connective tissue impairs function and causes pain[22]. This presents a problem, particularly in tendon/ligament engineering, since these tissues are largely acellular and avascular, so have poor repair that results in calcification and scar tissue[23]. Since pVTK is not

believed to rely on cellular machinery to inhibit mineralization, one strategy for tendon/ligament tissue engineering could utilize gradient patterning of pVTK onto biomaterials to spatially limit mineralization. For example, this could be applied in next-generation implants in periodontal tissue engineering where regenerative efforts are focused on maintaining the balance and appropriate spatial distribution of ligament tissue, alveolar bone, and cementum[24]. Other applications for pVTK in musculoskeletal tissue engineering could involve preventing mineralization in osteoarthritis and guiding osteochondral defect repair.

Further investigation of the activity of free vs. bound peptide may yield additional applications for pVTK. There is evidence that coating mineralized substrates with pVTK can induce further mineralization on the substrate surface and even increase cell viability[25]. This demonstrates that pVTK could potentially be used to coat implants to promote bone-implant integration and bone regeneration.

6.2.6 Broader Impacts

Though pVTK's ability to inhibit mineralization is not yet characterized, there are many interesting aspects to the research into how this mineral-binding peptide works that have broad application beyond ectopic mineral and bone.

One of the theories for how pVTK inhibits mineralization is that pVTK inhibits unwanted mineral growth. In this scenario, unwanted mineral formation may be initiated, but pVTK stops this process in its early stages and prevents rapid growth and stabilization into the final crystal structure. This could be used as inspiration for strategies in other disease states involving unwanted growth and/or structure maturation. Especially in cases where a cure is not yet available, maintaining a disease state within the currently manageable (or even treatable) realm would improve patient prognoses.

Inhibition of mineralization by pVTK forces the osteoblast cells to undergo a compensatory reaction, upregulating pro-mineralization gene expression and down-regulating anti-mineralization gene expression[3]. In this scenario, the osteoblasts are programmed to mineralize their matrix, but when that output is blocked by pVTK, they increase their efforts to no avail. Blocking a desired output and forcing a compensatory reaction could be used to prime cells for a specific behavior. When the block is released, cells would be ready to engage in the desired behavior. This strategy could be expanded for a variety of applications from programming cell therapies to studying cell processes in a controlled setting.

On the other hand, pVTK inhibits mineralization without being an antagonist. pVTK does not inhibit osteogenic behavior of osteoblasts or interrupt pro-mineralization signaling cascades to prevent mineralization. In the context of ectopic mineralization, pVTK prevents the progression of the disease state without directly interfering with the signaling cascade. Fencing in the output of the disease state without aiming to re-program cell signaling could be an alternative therapeutic strategy as well. In cases where a given signaling cascade has different roles and different outputs in different cell types, using a fencing molecule could prevent unwanted outputs without decommissioning the entire signaling pathway. In cases where the traditional therapeutic may have unwanted side effects due to cellular re-programming, using a fencing strategy could be a safer alternative. In cases where the signaling pathway is not yet understood fully, using a fencing strategy could be a creative alternative therapeutic strategy and a means to further characterize the signaling pathway itself.

Altogether, the unknown questions about pVTK's inhibition of mineralization can inspire further creative therapeutic strategies to previously untreatable disease states and research strategies to understand biological processes.

6.3 Concluding Remarks

This thesis presents evidence that the mineral-binding peptide, pVTK, can be used to prevent or mitigate EM formation in various disease states. pVTK acts to inhibit mineralization by physically impairing nucleation, crystallization, and mineral growth. Therefore, pVTK is presented as a broadly applied therapeutic for EM inhibition, regardless of cause. EM inhibition using mineral-binding peptides adds a vital management tool for challenging-to-treat diseases since EM progression is often associated with worse patient outcomes. Beyond inhibition of EM, pVTK has potential applications in musculoskeletal tissue engineering and targeting drug delivery to mineralized tissues. Further, this supports the use of phage display and subsequent posttranslational modifications to identify and optimize bioactive peptide therapeutics.

6.4 References

1. Segvich, S.; Biswas, S.; Becker, U.; Kohn, D. H. Identification of Peptides with Targeted Adhesion to Bone-Like Mineral via Phage Display and Computational Modeling. *Cells. Tissues. Organs* **2008**, *189* (1–4), 245. https://doi.org/10.1159/000151380.

2. Addison, W. N.; Miller, S. J.; Ramaswamy, J.; Mansouri, A.; Kohn, D. H.; McKee, M. D. Phosphorylation-Dependent Mineral-Type Specificity for Apatite-Binding Peptide Sequences. *Biomaterials* **2010**, *31* (36), 9422–9430. https://doi.org/10.1016/j.biomaterials.2010.08.064.

3. Ramaswamy, J.; Nam, H. K.; Ramaraju, H.; Hatch, N. E.; Kohn, D. H. Inhibition of Osteoblast Mineralization by Phosphorylated Phage-Derived Apatite-Specific Peptide. *Biomaterials* **2015**, *73*, 120–130. https://doi.org/10.1016/j.biomaterials.2015.09.021.

4. James, A. W.; LaChaud, G.; Shen, J.; Asatrian, G.; Nguyen, V.; Zhang, X.; Ting, K.; Soo, C. A Review of the Clinical Side Effects of Bone Morphogenetic Protein-2. *Tissue Eng. - Part B Rev.* **2016**, *22* (4), 284–297. https://doi.org/10.1089/ten.teb.2015.0357.

5. Shore, E. M.; Xu, M.; Feldman, G. J.; Fenstermacher, D. A.; Brown, M. A.; Kaplan, F. S. A Recurrent Mutation in the BMP Type I Receptor ACVR1 Causes Inherited and Sporadic Fibrodysplasia Ossificans Progressiva. *Nat. Genet.* **2006**, *38* (5), 525–527. https://doi.org/10.1038/ng1783.

6. Pan, H.; Fleming, N.; Hong, C. C.; Mishina, Y.; Perrien, D. S. Methods for the Reliable Induction of Heterotopic Ossification in the Conditional Alk2Q207D Mouse. *J. Musculoskelet. Neuronal Interact.* **2019**, 1–11.

7. Potter, B. K.; Burns, T. C.; Lacap, A. P.; Granville, R. R.; Gajewski, D. A. Heterotopic Ossification Following Traumatic and Combat-Related Amputations. *J. Bone Jt. Surg.* **2007**, *89* (3), 476–486. https://doi.org/10.2106/JBJS.F.00412.

8. Moeinzadeh, S.; Park, Y.; Lin, S.; Yang, Y. P. In-Situ Stable Injectable Collagen-Based Hydrogels for Cell and Growth Factor Delivery. *Mater.* **2021**, *Mar* (15), 100954. https://doi.org/10.1016/j.mtla.2020.100954.In-situ.

9. Makadia, H. K.; Siegel, S. J. Poly Lactic-Co-Glycolic Acid (PLGA) as Biodegradable Controlled Drug Delivery Carrier. *Polymers (Basel).* **2011**, *3* (3), 1377–1397. https://doi.org/10.3390/polym3031377.

10. Ling, C.; Zhao, W.; Wang, Z.; Chen, J.; Ustriyana, P.; Gao, M.; Sahai, N. Structure-Activity Relationships of Hydroxyapatite-Binding Peptides. *Langmuir* **2020**, *36* (10), 2729–2739. https://doi.org/10.1021/acs.langmuir.9b03779.

11. Fish, M. B.; Banka, A. L.; Braunreuther, M.; Fromen, C. A.; Kelley, W. J.; Lee, J.; Adili, R.; Holinstat, M.; Eniola-Adefeso, O. Deformable Microparticles for Shuttling Nanoparticles to the Vascular Wall. *Sci. Adv.* **2021**, *7* (17).

https://doi.org/10.1126/sciadv.abe0143.

12. Zakrewsky, M.; Muraski, J. A.; Mitragotri, S. Mechanistic Analysis of Cellular Internalization of a Cell- and Skin-Penetrating Peptide. *Regen. Eng. Transl. Med.* **2016**, *2* (1), 23–36. https://doi.org/10.1007/s40883-016-0011-x.

13. Wu, M.; Chen, G.; Li, Y. P. TGF-β and BMP Signaling in Osteoblast, Skeletal Development, and Bone Formation, Homeostasis and Disease. *Bone Res.* **2016**, *4* (March). https://doi.org/10.1038/boneres.2016.9.

14. Iwasaki, Y.; Yamato, H.; Fukagawa, M. TGF-Beta Signaling in Bone with Chronic Kidney Disease. *Int. J. Mol. Sci.* **2018**, *19* (8). https://doi.org/10.3390/ijms19082352.

15. Liu, W.; Feng, M.; Jayasuriya, C. T.; Peng, H.; Zhang, L.; Guan, Y.; Froehlich, J. A.; Terek, R. M.; Chen, Q. Human Osteoarthritis Cartilage-Derived Stromal Cells Activate Joint Degeneration through TGF-Beta Lateral Signaling. *FASEB J.* **2020**, *34* (12), 16552–16566. https://doi.org/10.1096/fj.202001448R.

16. Zhao, W.; Xu, Z.; Cui, Q.; Sahai, N. Predicting the Structure-Activity Relationship of Hydroxyapatite-Binding Peptides by Enhanced-Sampling Molecular Simulation. *Langmuir* **2016**, *32* (27), 7009–7022. https://doi.org/10.1021/acs.langmuir.6b01582.

17. Davidson, T. A. Interface Engineering through Adhesion and Remineralization for Dental Composites using Mineral Binding Peptides. Ph.D. Dissertation, University of Michigan, Ann Arbor, MI, **2022**.

18. Body, J. J.; Casimiro, S.; Costa, L. Targeting Bone Metastases in Prostate Cancer: Improving Clinical Outcome. *Nat. Rev. Urol.* **2015**, *12* (6), 340–356. https://doi.org/10.1038/nrurol.2015.90.

19. Aydin, O.; Tiruchinapally, G.; Youssef, I.; Ramaraju, H.; Durmaz, Y. Y.; Kozloff, K. M.; Kohn, D. H.; Elsayed, M. E. H. Selective Binding of PVTK Peptide-and Bisphosphonate-Functionalized Micelles to Prostate Cancer Cells, Osteoblasts, and Osteoclasts. *Precis. Nanomedicine* **2022**, *5* (1), 851–869. https://doi.org/10.33218/001c.33142.

20. Mededovic, M. Enhanced cell-cell communication using gene delivery coating for accelerated bone fracture healing. Unpublished Ph.D. Dissertation, University of Michigan, Ann Arbor, MI, **2024** (forthcoming).

21. He, F.; Chiou, A. E.; Loh, H. C.; Lynch, M.; Seo, B. R.; Song, Y. H.; Lee, M. J.; Hoerth, R.; Bortel, E. L.; Willie, B. M.; Duda, G. N.; Estroff, L. A.; Masic, A.; Wagermaier, W.; Fratzl, P.; Fischbach, C. Multiscale Characterization of the Mineral Phase at Skeletal Sites of Breast Cancer Metastasis. *Proc. Natl. Acad. Sci.* **2017**, *114* (40), 10542–10547. https://doi.org/10.1073/pnas.1708161114.

22. Kraus, R.; Stahl, J. P.; Meyer, C.; Pavlidis, T.; Alt, V.; Horas, U.; Schnettler, R. Frequency and Effects of Intratendinous and Peritendinous Calcifications after Open Achilles Tendon Repair. *Foot Ankle Int.* **2004**, *25* (11), 827–832.

https://doi.org/10.1177/107110070402501113.

23. Walden, G.; Liao, X.; Donell, S.; Raxworthy, M. J.; Riley, G. P.; Saeed, A. A Clinical, Biological, and Biomaterials Perspective into Tendon Injuries and Regeneration. *Tissue Eng. Part B. Rev.* **2017**, *23* (1), 44–58. https://doi.org/10.1089/ten.TEB.2016.0181.

24. Liu, J.; Ruan, J.; Weir, M. D.; Ren, K.; Schneider, A.; Wang, P.; Oates, T. W.; Chang, X.; Xu, H. H. K. Periodontal Bone-Ligament-Cementum Regeneration via Scaffolds and Stem Cells. *Cells* **2019**, *8* (6). https://doi.org/10.3390/cells8060537.

25. do Nascimento, M.; dos Santos Almeida, A. R.; Hirata, M. C.; Elzubair, A.; Navarro da Rocha, D.; Prado da Silva, M. H. Biomineralization of Calcium Phosphates Functionalized with Hydroxyapatite-Binding Peptide. *J. Mech. Behav. Biomed. Mater.* **2023**, *146* (August), 106082. https://doi.org/10.1016/j.jmbbm.2023.106082.

6.5 Appendix A: Peptide Internalization Imaging

6.5.1 Methods

MC3T3s (murine calvarial pre-osteoblast cell line) were plated in 8-well chamber slides in growth medium (αMEM with 10% fetal bovine serum and 1% penicillin-streptomycin). After 1 day to allow for cell adherence, MC3T3s were exposed to FITC-E7 or FITC-pVTK for 1 hour. E7 (EEEEEEEPRGDT) is a peptide derived from bone sialoprotein with hydroxyapatite-binding domain (E7) and an integrin-binding domain (RGD)[1,2]. As such, E7 served a negative control for endocytosis by mediating the attachment between matrix and cells. Then, cells were washed in phosphate-buffered saline (PBS, Gibco), fixed in 10% neutral-buffered formalin (NBF) for 10 minutes at room temperature, and washed twice with PBS. Fixed cell monolayers were permeabilized in 0.25% TritonX-100 (Sigma-Aldrich) for 5 minutes at room temperature followed by one wash step in PBS. Next, monolayers were incubated with blocking solution (5% goat serum, 0.3% Triton X-100) for 1 hour at room temperature with protection from light. The primary antibody (Rab5 (C8B1) rabbit mAb, Cell Signaling Technology) solution (1:200 dilution in 1% bovine-serum albumin (BSA, Fisher) was then applied to cells overnight at 4°C with protection from light. After 3 wash steps with PBS, cells were incubated with the secondary antibody (Anti-rabbit IgG (H+L), F(ab')2 Fragment (AlexaFluor 647), Cell Signaling Technology) solution (1:500 dilution in 1% BSA) for 1 hour at room temperature with protection from light. After 3 wash steps with PBS, cells were counter-stained with Hoechst dye (1 μg/mL in PBS; Hoechst 33342 (Thermo Scientific)). After one final wash in PBS, the chamber insert was removed, and cells were protected with Vectashield (Vector Laboratories) and coverslipped.

Fluorescent imaging was performed with the Leica Thunder Imager (Leica DMi8 microscope). Z-stacks were taken of the full thickness of the cell monolayers with Thunder

clearance of each slice. Then, maximum intensity projections were acquired to represent the full thickness of the samples.

6.5.2 Figure

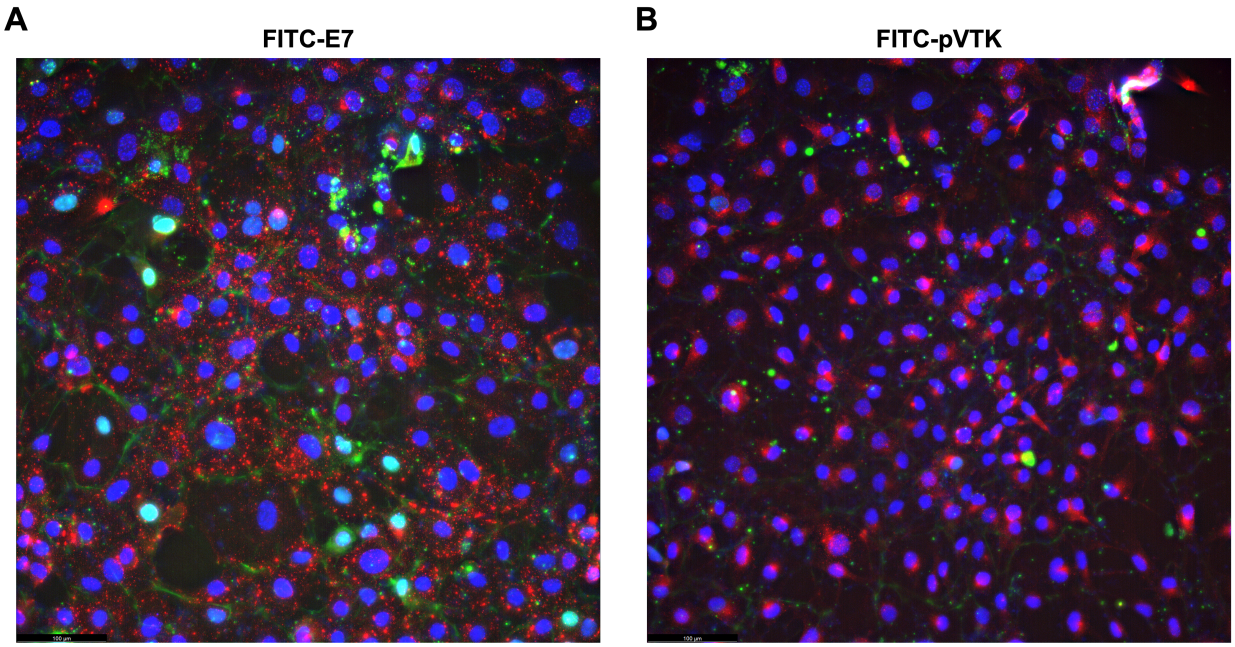


Figure 6.1 Immunofluorescence images of Rab-5 labelled vesicles and FITC-tagged peptides

MC3T3s incubated with FITC-E7 (A, green) or FITC-pVTK (B, green) for 1 hour and subjected to immunofluorescence staining to identify Rab5 (red) and histological staining to identify cell nuclei (blue). Representative images are maximum intensity projections of cell monolayers. Scale bars represent 100µm (bottom left).

6.5.3 References

1. Fujisawa R, Wada Y, Nodasak Y, Kuboki Y. Acidic amino acid-rich sequences as binding sites of osteonectin to hydroxyapatite crystals. Biochim Biophys Acta 1996;1292:53–60.

2. Fujisawa R, Mizuno M, Nodasaka Y, Kuboki Y. Attachment of Osteoblastic Cells to Hydroxyapatite by a Synthetic Peptide (Glu7-Pro-Arg-Gly-Asp-Thr) Containing Two Functional Sequences of Bone Sialoprotein. Matrix Biol 1997;16:21–8.

6.6 Appendix B: Mineralization Inhibition with Phosphorylated Peptide Variants

6.6.1 Methods

MC3T3s (murine calvarial pre-osteoblast cells) were plated at a density of 50,000 cells/cm^2 in 12-well tissue-coated polystyrene plate in growth media: αMEM (Gibco) with 10% fetal bovine serum (FBS; Gibco) and 1% penicillin-streptomycin (Gibco). After 24 hours, MC3T3s were switched to osteogenic media (growth media plus β-glycerophosphate (10mM, Sigma-Aldrich) and ascorbic acid (50μg/mL, Sigma-Aldrich)) with or without peptide (200 or 300 μM). The peptide variants tested were: VTKHLNQI(p)SQ(p)SY (VTK(pSpS)) and VTKHLNQISQS(p)Y (VTK(pY)). Each group was run in biological triplicate. Media was refreshed every 2 to 3 days for up to 12 days.

Mineralization was assessed via Alizarin red staining. MC3T3s were fixed in 10% neutral-buffered formalin for 10 minutes at room temperature, followed by 3 washes with distilled water. Then, fixed cell monolayers were incubated with 2% (w/v) Alizarin Red S solution (pH 4.2, Sigma-Aldrich) for 45 minutes at room temperature, protected from light. Stained monolayers were washed repeatedly with distilled water until the wash fluid ran clear. Then, monolayers were allowed to dry overnight prior to imaging.

To quantify positive Alizarin Red staining, the bound Alizarin Red S was extracted from the cell monolayers. Stained monolayers were incubated with a methanol-acetic acid solution (20% methanol, 10% acetic acid in double distilled water) for 45 minutes at room temperature protected from light. Then, the extraction solution was removed from the monolayers and quantified via colorimetric assay. A serial dilution of the original Alizarin Red S staining solution in the extraction solution as diluent was used for quantification of extracted Alizarin Red S. Samples were run in duplicate at a volume of 100μL and standards were run in duplicate

at the same volume. The plate was run at 450nm, and absorbance values were normalized using the serial dilution as the standard curve.

6.6.2 Figures

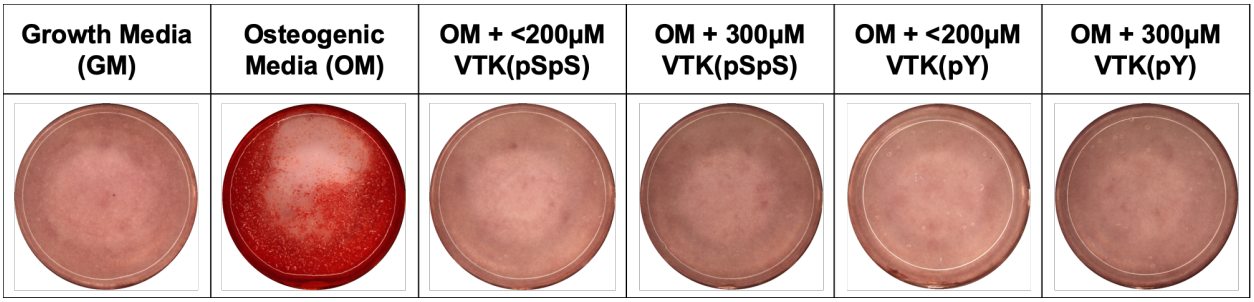


Figure 6.2 Alizarin Red staining of MC3T3s mineralized with different peptide variants

MC3T3s underwent a 12-day osteogenic differentiation scheme with phosphorylated VTK variants. The negative control was MC3T3s in growth media and the positive control was MC3T3s in osteogenic media without any added peptides. Each group was run in triplicate and representative images are presented above.

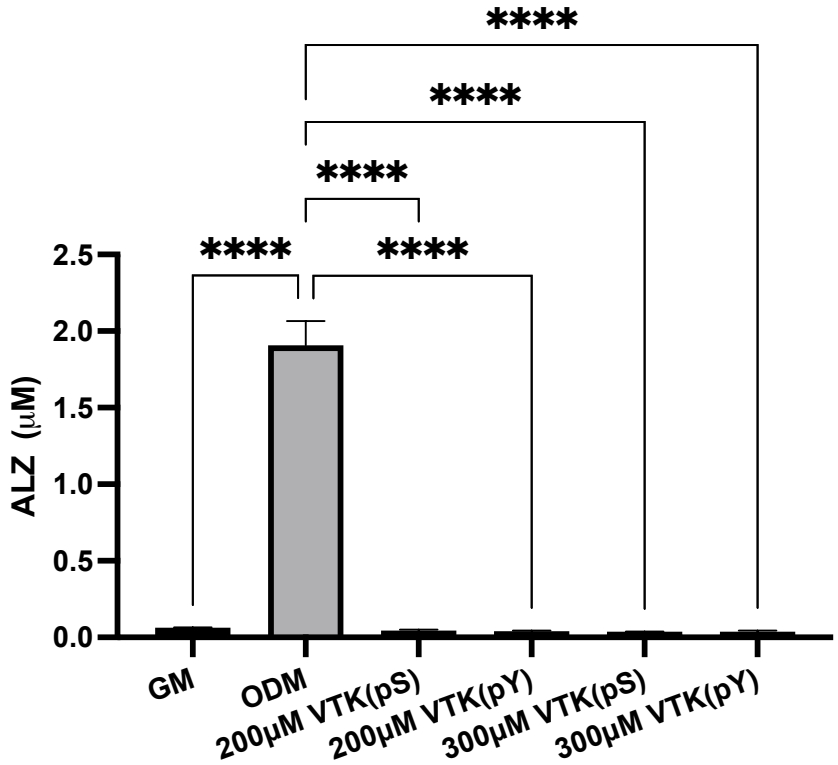


Figure 6.3 Quantification of Alizarin Red staining of MC3T3s mineralized with different peptide variants

Alizarin Red S was extracted from the mineralized MC3T3s and quantified using colorimetric assay compared to a serial dilution of the original staining solution. Each biological replicate (n = 3) was assayed in duplicate.